

Faculdade de Engenharia da Universidade do Porto



FEUP

**Developing Antimicrobial Collagen/Silk Fibroin
Biocomposites with Immobilized Phages**

IMA GHAEI

Dissertation submitted in fulfillment of the requirements for the degree of Doctor in
Biomedical Engineering by Faculdade de Engenharia da Universidade do Porto

Supervisor: Prof. Fernando Jorge Monteiro

January 2018

I, Ima Ghaeli, confirm that the work presented in this thesis is my own. Where information has been derived from other sources, I confirm that this has been indicated in the thesis.

Signed..... Date.....

ACKNOWLEDGMENTS

I would like to express my gratitude to my supervisor, Prof. Fernando Jorge Monteiro, for his continuous support to my Ph.D study, for his patience, motivation, and his expertise in scientific aspects. It's been a privilege to work with him.

Besides my supervisor, I would like to thank my advisors: Prof. Marisa Masumi Beppu, Prof. Alina Siokowska, Prof. Nathalie Tufenkji, and Prof. Corinne Hoesli, for allowing me to join their teams as intern and give me the access to their laboratories and research facilities. Without their support it would not be possible to conduct this research.

My sincere thanks also goes to Dr. Mariana Agostini de Moraes, Dr. Katarzyna Lewandowska, Dr. Adam J. Olsson, Dr. Natalie Fekete, Dr. Frederico Silva, and Prof. Zeinab Hosseinidoust, for their immense knowledge, insightful comments and encouragement, allowing me to widen my research from various perspectives.

Last but not the least, I would like to give special thanks to my parents and my brother that without their financial and spiritual support throughout this thesis and my life, it would not be possible to progress this research. Also, I thank my dearest friend, Mona Jabbari for her precious support and motivation in the last four years.

Resumo

As infeções associadas à presença de implantes podem ser um grave problema para pacientes que recebem próteses e implantes ortopédicos como é o caso das próteses articulares aplicados na anca ou no joelho.

Dado que a forma de tentar a cura de infeções associadas a implantes cirúrgicos é difícil e cara, é importante fazer a prevenção destas infeções. A disponibilidade de biomateriais que possam constituir revestimentos de implantes ou próteses e de estruturas de suporte (scaffolds) com atividade antimicrobiana para evitar estas infeções é de grande importância para este trabalho. Em termos gerais o objectivo deste trabalho é conceber novos compósitos biomédicos com propriedades antibacterianas.

A terapia baseada em fagos é o método escolhido para a prevenção de infeções bacterianas.

Os bacteriófagos são alternativas aos tradicionais antibióticos em virtude da resistência bacteriana aos antibióticos convencionais.

Biomateriais poliméricos, biocompatíveis e biodegradáveis são utilizados para desenvolver matrizes biológicas ou scaffolds não só para aplicação em engenharia de tecidos mas também para outras aplicações biomédicas que incluem, pensos para feridas, filtros de membrana e para dispositivos de libertação controlada de fármacos. O Colagénio e a fibroína da seda são biomateriais conhecidos e largamente utilizados em aplicações biomédicas.

A combinação destes dois materiais apresenta grandes vantagens em relação a cada um de per si. Provou-se que a combinação de colagénio/fibroína da seda melhora as propriedades mecânicas bem como a proliferação celular.

Foi objetivo deste trabalho imobilizar bacteriófagos na superfície de um biocompósito colagénio/ fibroína da seda como uma inovadora metodologia de combate antimicrobiano.

ABSTRACT

Implant-associated infection can be a serious problem for patients that receive orthopaedic implants such as hip or knee replacements. Because management of infections associated with surgical implants are both difficult and costly, prevention of such infections is important. Provision of biomaterial to produce coating of the implants to prevent the infections or of a scaffold with antimicrobial activity is of great interest to this work. Generally, the aim of this study is to design new biomedical composites presenting antimicrobial properties.

Phage therapy is the method chosen for prevention of bacterial infections. Bacteriophages are alternatives to traditional antibiotics considering the bacterial resistance to conventional antibiotics.

Biocompatible and biodegradable polymeric biomaterials are used to develop biological matrices or scaffolds not only for tissue engineering but also for various biomedical applications including, wound dressing, membrane filters and drug delivery. Collagen and silk fibroin are well know biomaterials widely used in biomedical applications. Blending of these two biomaterials has great advantages over each one. It has been proved that collagen/silk fibroin blending enhances the mechanical properties as well as cell proliferation.

The aim of this work is to immobilize bacteriophages on a collagen/silk fibroin biocomposite as a novel antimicrobial method.

Table of Contents

1. Chapter One: Introduction	1
1.1 Implant-associated infections:.....	1
1.3 Parameters influencing bacterial adhesion:.....	2
1.4 Pathogenic bacteria:	3
1.5 Biofilm formation and mechanism of bacterial resistance to antibiotics:	3
1.6 Antimicrobial surface treatment of implants.....	5
1.6.1 Development of anti-adhesive surfaces (passive surface modification):	6
1.6.2 Development of surface-associated with antimicrobial agents (active surface modification):.....	6
1.7 Alternative antibacterial agents to antibiotics	7
1.7.1 Bacterial cell wall hydrolases (BCWH):.....	7
1.7.2 Antimicrobial peptides (AMP).....	7
1.7.3 Bacteriophages	8
1.8 Phage therapy common antibacterial alternative to antibiotics:.....	8
1.8.1 Non-therapeutic applications of bacteriophages:	8
1.8.2 Clinical trials for bacteriophage therapy:	9
1.9 Bacteriophage isolation and the environment:	9
1.10 Bacteriophage classification and biology:	9
1.11 Bacteriophage life cycles:	10
1.12 Mechanism of phage adsorption and penetration into microbial cells:.....	11
1.13 Comparison of phages and antibiotics:	11
1.14 Interaction of phage and biofilm:	12
1.15 Delivery mechanisms of bacteriophages:.....	13
1.15.1 Parental delivery of bacteriophages:	13
1.15.2 Oral delivery of phages:	14
1.15.3 Local delivery of phages:	14

1.15.4	Dental phage administration:	14
1.15.5	Inhalation of bacteriophages:	15
1.16	Phage immobilization on the functionalized polymer surfaces:	15
1.17	Biopolymers used for phage immobilization	17
1.17.1	Collagen:	17
1.17.2	Silk fibroin:	19
1.17.3	Collagen/silk fibroin blends:	23
1.18	Thesis outline	24
1.19	References	25
2.	Chapter Two: Phase behaviour and miscibility studies of Collagen/Silk Fibroin macromolecular system in dilute solutions and solid state.....	32
2.1	Introduction	33
2.2	Experimental	35
2.2.1	Sample preparation	35
2.2.2	Ternary phase diagram and blend preparation	36
2.2.3	Miscibility and ζ -potential analysis.....	36
2.2.4	Light stereoscopic magnifier microscope	37
2.2.5	Structure of collagen/silk fibroin blended solutions and films after dialysis	37
2.3	Results.....	38
2.3.1	Miscibility study of collagen/silk fibroin.....	38
2.3.2	Phase change after collagen/silk fibroin dialysis	41
2.3.3	Structural characteristics of collagen/silk fibroin blend solutions and solid films.....	44
2.4	Discussion	48
2.5	Conclusion	50
2.6	References.....	51
3.	Chapter Three: A new label-free technique for analysing evaporation induced self-assembly of viral nanoparticles based on enhanced dark-field optical imaging.....	54

3.1	Introduction.....	55
3.2	Materials and Methods:.....	58
3.2.1	Bacteriophage propagation and purification	58
3.2.2	Experimental setup: Enhanced dark-field microscopy and monitoring of evaporation process	59
3.2.3	Particle Tracking and image analysis.....	59
3.3	Results and Discussion.....	60
3.3.1	Analysing the bacteriophage motion and its influence on phage assembly onto the glass coverslip	61
3.3.2	Analysing fluid flow through monitoring drying process and final dried patterns (macroscopic observations).....	65
3.4	Concluding Remarks.....	71
3.5	References:.....	72
4.	Chapter Four: Immobilization of Bacteriophages on glass and collagen surfaces: An approach to make antibacterial coatings	76
4.1	Introduction.....	77
4.2	Materials and Methods:.....	79
4.2.1	Sample preparation	79
4.2.2	Phage-based materials.....	79
4.2.3	Phage stability analysis	80
4.2.5	Bacteria culture and antibacterial activity of materials.....	80
4.2.6	Bacterial adhesion to the surfaces.....	80
4.2.7	Storage effect:	80
4.2.8	In vitro cytotoxicity.....	80
4.3	Results:.....	81
4.3.1	Immobilization of phages on glass coverslip.....	81
4.3.3	Phage stability and lysis analysis:	84
4.3.4	Storage effect on the phages infectivity	85

4.3.5	Mammalian cell adhesion on the phage-based surfaces.....	87
4.4	Discussion	90
4.5	Conclusion:	92
5.	Chapter Five: Antibacterial properties of phage-immobilized collagen/silk fibroin biocomposites	96
5.1	Introduction	97
5.2	Materials and methods:.....	98
5.2.1	Phage propagation and purification.....	98
5.2.2	Phage-based materials	98
5.2.3	In vitro antibacterial properties.....	99
5.2.4	Cytocompatibility of phage-immobilized surfaces.....	99
5.3	Results:	100
5.3.1	Antibacterial activity of immobilized and non-immobilized surfaces	100
5.3.2	In vitro cytocompatibility	105
5.4	Discussions:.....	106
5.5	Conclusion.....	108
5.6	References	109
6.	Chapter Six.....	111

1. Chapter One: Introduction

1.1 Implant-associated infections:

Biomaterial-based implants significantly impact the quality of patients' lives. However, infections related to medical devices as the result of biofilm growth, are a challenge in healthcare. Currently the only remedy is surgery to remove the implant, combined with long-term antibiotic therapies. Implant-associated infections mainly caused by *Staphylococcus epidermidis* and *Staphylococcus aureus*, result in chronic infections and rising costs [1-6]. In US, the medical device associated infections were estimated to cost around 60% of total costs of healthcare associated infections [3].

Infection-associated implant surgeries are divided into two groups. The first group is the early pre-operation infections in which the implant is contaminated by direct exposure to the dust particles in the air, gloves or surgical instruments. The second group contains the late post-operative infections, which are the results of haematogenous spread of bacteria from a distant focus [7, 8].

1.2 Mechanisms of Bacterial Adhesion to the implant:

The interaction between bacteria and the surface consists of two phases:

Phase 1) Non-specific interactions: Bacteria prefer to attach and grow on the surfaces rather than in the surrounding aqueous phase. They adhere to surfaces through physical forces such as van der Waals, Brownian motion, gravitational, electrostatic charges and hydrophobic interactions.

These interactions are divided into long-range ones where the distances between bacteria and surface are more than 50 nm and short-range interactions where these distances are below 5 nm. The forces in the former are mutually attractive forces that are a function of distance and free energy, while the forces in the latter derive from chemical bonding such as hydrogen bonding, ionic and dipole interactions and hydrophobic interactions.

Through this initial adhesion, the molecular or cellular attachment of bacteria to the surface is possible.

Phase 2) Specific interactions: In this phase, the adhesion of bacteria occurs through strong binding between the surface and the functional part of bacterial polymeric structures including capsules, fimbriae, or pili and slime. These functional groups in *s. epidermidis* can be several polysaccharide intercellular adhesin, of which the most important are: a galactose-rich capsular polysaccharide adhesion, a slime-associated antigen, a polysaccharide, and an accumulation associated protein [8-10].

1.3 Parameters influencing bacterial adhesion:

Three parameters influencing the bacterial adhesion are the environment, material surface characteristics and the properties of microorganisms, as shown in Table 1.1.

Temperature, exposure time, presence of antibiotics, flow conditions, and bacterial concentration are the environmental parameters affecting bacterial adhesion. The effect of fluid flow conditions on bacterial adhesion is of great importance, in such a way that parameters such as shear forces cannot only increase the bacterial attachment, but also enhance the possibility of bacterial colonization [11]. Furthermore, the electrolytes, such as KCl or NaCl, concentration and pH value affect bacterial adhesion.

Parameters influencing bacterial adhesion	Environment	Temperature Exposure time Antibiotics Flow conditions Bacterial concentration pH and salt
	Material Surface Characteristics	Charge Roughness Chemical Composition Physical configuration Hydrophobicity
	Bacterial Characteristics	Susceptibility to antibiotics Hydrophobicity Extracellular polysaccharide

Table 1.1: Parameters affecting bacterial adhesion

Surface characteristic parameters include surface charge and roughness, chemical composition, physical configuration, and hydrophobicity. Different material functional groups depending on material hydrophobicity and charge can change bacterial adhesion. Adsorption of a water layer to the material surface decreases the direct contact between bacteria and surface. Also, negative charge decreases bacterial adhesion. Surface modification with silver [12], synthetic antimicrobial peptides (AMPs) [13], poly (ethylene glycol) [14], plasma treatment [15] or diamond-like carbon (DLC) [16] hinder the bacterial adhesion.

Irregularities in polymeric surfaces enhance bacterial adhesion and biofilm deposition because roughness increases the surface area [17]. In the case of surface configuration, porous materials have high rate of infection because bacteria adhere and colonize in the substrate pores [18].

Hydrophobicity may be one of the most important factors in the initial attachment of bacteria to the surface. Hydrophobic bacteria prefer to attach to the hydrophobic surfaces. Material surface hydrophobicity plays a more important role than bacterial surface hydrophobicity [8, 9, 19]. Researchers showed that bacterial cell can sense the external environment changes and in turn change the major cell characteristics such as surface hydrophobicity [20].

Tissue proteins such as albumin, fibrinogen, laminin, collagen, fibronectin and others influence bacterial adhesion to surfaces. Fibronectin increases *S. aureus* adhesion to a surface while Albumin inhibits bacterial adhesion [21]. Adsorbed fibrinogen promotes bacterial attachment [22]. Thrombin enhances bacterial adhesion [23].

1.4 Pathogenic bacteria:

In an experimental research on poly-methyl-methacrylate and bone autografts, and after a survey on previous works, Jose Cordero et. al. proved that the susceptibility to infection in orthopaedic implants is not only dependent on the material but also on the bacteria [24]. For example, the metal-implanted bone is more susceptible to *S. Aureus*, while the bone implanted with a polymer is likely to be affected by *S. epidermidis* [24].

The most common bacteria causing infections are originated from the patient's skin where the biomaterial touches the skin [25, 26] or the hospital environment [27]. The most common pathogens related to the skin are Staphylococci (*Staphylococcus epidermidis* and *Staphylococcus aureus*) that are among gram-positive bacteria. Other environmental pathogens such as *Pseudomonas*, *E. coli*, and *Vibrio cholera* are among gram-negative bacteria that cause implant infections [28].

The number of resistant bacteria has increased in recent years. Methicillin-resistant *S. aureus* (MRSA) is one of these bacteria that is responsible for considerably increased nosocomial infections in hospitals. In 1994, a study reported that up to 60% of infections in hospitals were caused by MRSA [29]. It has been proved that the bacterial resistance to antimicrobial therapies will increase 10-100 times when they colonize onto the surfaces and form biofilm [30].

1.5 Biofilm formation and mechanism of bacterial resistance to antibiotics:

Biofilm is a surface-bound community of bacteria which can form on the surface of vital and inert structures. The biofilm protects bacteria from immune system and from antibiotics. It can be mono or polymicrobial and is the source of infection. Biofilm formation begins when the environmental conditions motivate bacterial transition to sessile to promote survival. Different environmental parameters such as

presence of oxygen or certain nutrients, temperature and pH influence biofilm formation. However, some bacteria such as *P. aeruginosa* and *P. fluorescens* form biofilm in any growing conditions, while others such as *Escherichia coli* K-12 and *Vibrio cholera* form biofilms in the presence of amino acids [31, 32].

Palmer et. al. [20], explained the initial stages of biofilm formation including cell-cell and cell-surface interactions. As shown in figure 1.1, this initial attachment is important for biofilm formation.

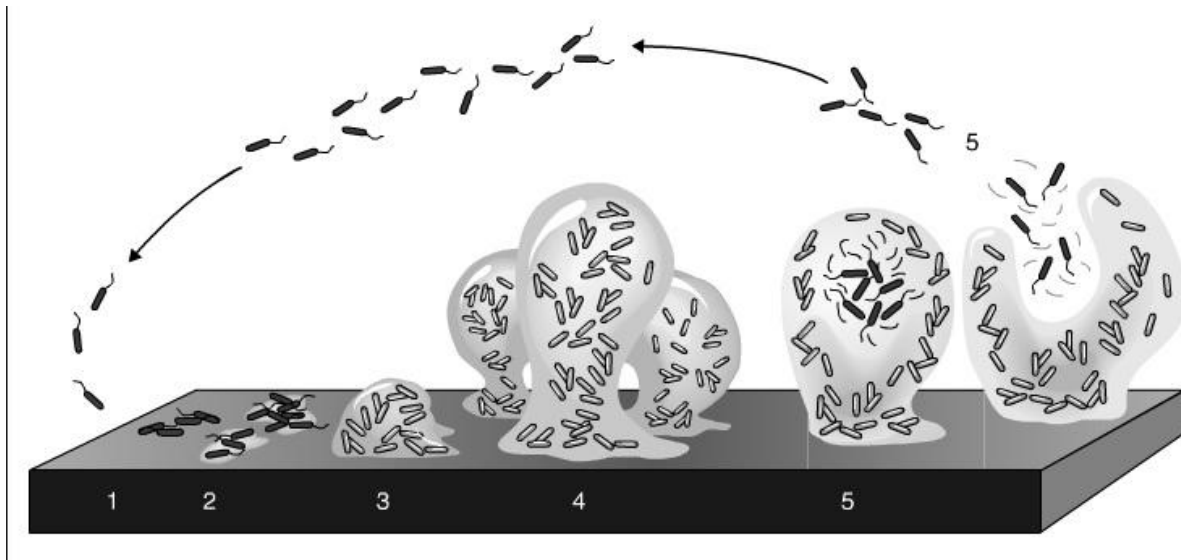


Figure 1.1: Five steps in biofilm formation. Step 1) Initial attachment, step 2) Irreversible attachment, step 3) the first maturation, step 4) fully mature biofilm, step 5) dispersion [20]

In the case of gram-negative bacteria, at the beginning, the planktonic bacteria float over the surface of the material to find an appropriate site of contact. Once the site has been found and surface contact is initiated, they continue to attach to the rest of surface. The bacteria attached to the surface increase the synthesis of the exopolysaccharide (EPS), causing decreased antibiotic susceptibility [33]. In the early stages, the microorganisms can move as a unit along the surface and interact with the surface and other bacteria. Several researchers proposed bacterial gene expression changes taking place during their attachment to the surfaces [34]. In the final stage of biofilm formation, some portion of biofilm detach from the matured biofilm [35]. Some researchers showed that the detachment occurs due to some starvation signals [36], while some others declared that the overexpression of alginate lyase could speed detachment [37]. In the study by Allison et. al. [38], they present the loss of EPS as the cause of detachment.

The biofilm-associated infections could be caused by gram-positive bacteria, as well as gram-negative ones [39]. The infections caused by biofilm formation from gram-positive bacteria such as *S. epidermis*, *S. aureus* and Enterococci, are difficult to treat with antibiotics, due to their high resistivity to antibiotics. The studies on *S. epidermidis* show that the subsequent steps after the initial cell-surface interactions, include

the cell-cell interactions along with polysaccharide intercellular adhesion (ICA) and formation of cell aggregates on the surface. The reports indicate the similarity between the early stages of bacterial attachment in *S. aureus* and *S. epidermidis* but there is lack of data on attachment of Enterococci [39].

Similarly to gram negative bacteria, gram positive bacteria produce extracellular polysaccharides (namely “slime”), while growing on a surface. Deighton et. al. [40], indicated that the increase of slime production of *S. epidermidis* is due to the iron limited medium at the initial steps of biofilm formation, and the lack of nutrients, at the later times.

All in all, the biofilm formation sequences could be categorized as 1) Initial adhesion and attachment, 2) Aggregation and colonization, and 3) Dispersion.

Most antibiotics only interfere with the structure of bacteria and cause no serious side effects.

Bacterial resistance is the result of mutation in nucleic acids [41]. In a person with an antibiotic resistance mutation, treatment with the resisted antibiotic will inhibit the non-resistant bacteria, while leaving the antibiotic-resistant bacteria to multiply. Transfer of the antibiotic-resistance to the other bacteria and contribution of the genetic material lead to increased spreading of the antibiotic-resistant bacteria.

The cost of controlling and monitoring antibiotic resistant bacteria in hospitals is estimated to be between \$100 million and \$30 billion, annually. In addition, other infections caused by other bacteria will increase the cost to several billion dollars [42, 43].

The most threatening aspect of resistant organisms is the spreading of existing ones through human microflora and emergence of new resistant strains by gene transfer. The resistant genes are not easily lost and become a stable part of a genome. In addition, other bacterial resistance may join them, expanding the multidrug resistance phenotype [44].

Multidrug resistant bacteria are a serious problem these days. Till now, the pharmaceutical industries try to solve the problem by modifying the existing antibiotics and developing new ones while their efforts are less effective.

The worldwide demands caused development of new antibacterial treatment alternatives for the implant-associated infections that could be divided into two categories of 1) antimicrobial surface treatment for implants and 2) the alternative antimicrobial agents, such as bacteriophages (phages), bacterial cell wall hydrolases (BCWH), and antimicrobial peptides (AMP) which are the most promising candidates.

1.6 Antimicrobial surface treatment of implants

According to a medical review on infections caused by medical devices, different methods such as removal of the infected device, antimicrobial therapy or other alternative procedures have been assessed to detect and prevent the infections associated with implants. In order to prevent medical device associated infections, inhibition of biofilm formation as well as minimizing local immune response should be

considered. The traditional antimicrobial procedures inhibit bacterial colonization rather than bacterial attachment. However, the current procedures focus on developing medical devices that are against bacterial adherence and colonization [45]. Thus, passive or active strategies have been applied to the polymer surface to prevent biofilm formation [46].

1.6.1 Development of anti-adhesive surfaces (passive surface modification):

Coating of substrates alters the physiochemical properties of the substrate and reduces the bacteria/substrate interaction, which is the initial step of bacterial adhesion to surfaces. Several researches on bacterial adhesion to the modified coated surfaces, represented reduction of bacterial adhesion between 70% and 95% compared to the untreated polymers [45, 47, 48]. These coatings are called passive because their capability is not due to the chemical or biological reactivity, rather due to the poor ability of microbes to attach to the surface. Surfaces could be modified using passive coatings with other polymers, e.g. polyethylene glycol, polyethylene oxide brushes and hydrophilic polyurethanes [49, 50]. The difficulty in producing the anti-adhesive material is that due to thermodynamic reasons, it is not feasible to create zero adhesion surfaces [45].

1.6.2 Development of surface-associated with antimicrobial agents (active surface modification):

The stabilization of antimicrobial agents on medical devices can be a proper method to prevent bacterial attachment. The base of these systems is that the antibacterial agent is bound superficially to the surface or incorporated into the surface coating. The initial release of the drug from such systems is high and according to the first order kinetics. However, it is not definite yet if the procedure inhibits the microbial adherence or if it is against the colonization of bacteria. Most studies have focused on the incorporation or surface coating of antimicrobials rather than chemical reaction with the surface [51-54]. Bacterial resistivity against antimicrobial agents is the risk of this approach [10].

The antibacterial agents alternative to antibiotics that are being used as active coatings are:

1.6.2.1 Quaternary ammonium compound coatings:

Quaternary ammonium coatings are immobilized onto surfaces by immersing the substrates in the respective solutions. The inhibition of initial bacterial adherence by octadecyl chain and the killing of cells by quaternary ammonium salts are two mechanisms of antimicrobial coating which results in delayed or reduced microbial growth [55].

1.6.2.2 Silver coating:

Silver is well known for its antimicrobial activities. Hydroxyl and amino groups of proteins, nucleophilic sulfhydryl, enzymes and membranes are easily bound to silver cations (Ag^+), causing cell membrane disruption and the loss of essential protein and enzyme functions and cell death [56]. Silver is

applied in urine catheter and in the management of wounds and burn wounds. Polymers containing silver are able to release this cation for more than three months [57, 58]. Silver ions can be incorporated into polyamide through a melt mix process.

1.7 Alternative antibacterial agents to antibiotics

1.7.1 Bacterial cell wall hydrolases (BCWH):

BCWHs are enzymes cause bacteriolysis by degradation of peptidoglycan which are the major components of bacterial walls. BCWH can degrade the cell wall by hydrolysis or by non-lytic mechanisms [59].

Hydrolysis occurs through two modalities: 1) binding to the cell wall and positioning in the right place and 2) cleaving specific peptidoglycan bonds. Sites of C-terminal and N-domain are the two main domains responsible for most of BCWH lysis activities.

The non-lytic mechanism is based on cationic and amphiphilic properties of BCWH which trigger membrane perturbation or activate the autolytic system of bacteria.

Several resistance mechanisms of gram positive bacteria have been reported for BCWH. Also, BCWH has no effect on gram negative bacteria due to the presence of the outer membrane. Additionally, virolysins that appear to be the most promising type of BCWH has the highest production costs. These disadvantages make BCWH less attractive as alternatives to antibiotics [59].

1.7.2 Antimicrobial peptides (AMP)

AMPs are a large family of naturally occurring peptides from different sources with different structures and functionalities. According to their origins they are divided into eukaryotic AMP, bacteriocins, and phage-encoded AMP [60].

Eukaryotic AMP: they are cationic peptides with molecular weight of 1-5 kDa and positive charge at physiological pH. In this condition the AMP can interact with the anionic cytoplasmic membrane. With their hydrophobic and hydrophilic segments, they form pores in the cytoplasmic membrane that increase the permeability of the membrane and loss of cell content [61].

Bacteriocins AMP: they are peptides produced by bacteria with narrow killing spectra and specific to bacterial strains closely related to the producing strain. 99% or all bacteria may produce at least one bacteriocin. Bacteriocins are categorized according to the producing strains, common resistance mechanisms, protein structure and mode of action [62].

Phage-encoded AMP: two types of phage-encoded AMP are phage-encoded lytic factors and the phage tail complexes. The lytic factors induce bacteriolysis at a programmed time and allow the phage particles to release into the environment. Phage tail complexes are large molecular peptides that can recognize and

attach to specific receptors on the bacterium surface, penetrate the outer membrane (in gram negative bacteria), induce lysis of peptidoglycan on their attachment place and inject the phage genes into the bacterium [63].

Although several natural and synthetic AMPs are used in clinical and preclinical applications, none of them has been approved by FDA yet because of different disadvantages such as: i) toxicity, ii) high cost of drug development and iii) lack of higher efficiency than the existing standard methods of care [59]. However, phage therapy remains the most efficient alternative treatment to antibiotics [64].

1.7.3 Bacteriophages

Bacteriophages, also called “phages” are viruses that infect and kill bacteria. It has been shown that there are more than 100 different phages with a populations that is ten time higher than bacteria. Also, it is estimated that there are about 3×10^9 phage particles in one tablespoon of non-polluted water and 10^{31} phage particles on earth. Phages are classified into 13 families based on their morphological characteristics, types of nucleic acid, shape, size and presence or absence of lipid envelope. The reports indicate that about 4950 out of 5100 phages integrate the tailed phage groups that are composed of icosahedral head and a tail [59, 65].

1.8 Phage therapy common antibacterial alternative to antibiotics:

shortly after being discovered in 1915 and 1917 by Fredrick Twort and Felix D`Herelle, bacteriophages were used to prevent and treat human and animal infections. After discovery of penicillin, phage therapy was replaced by antibiotic treatment in almost all the world, except some countries in Eastern Europe. With the increase of antibiotic resistant bacteria, the use of bacteria-specific viruses attracts interests again.

The early experiments on bacteriophages lacked controls, failed to provide information on size and spacing of doses or routes of administration, and provided no information on phage preparation. Since 1980, different studies were carried out on phage therapy and different detailed reviews on bacteriophage efficacy have been published.

One of the most extensive experiments on bacteriophage therapy was done in Tbilisi, Georgia from 1963 to 1964 using bacteriophage of *Shigella spp* for controlling dysentery in children [59, 66-68].

Up to know, bacteriophages have been applied in both non-therapeutic applications and clinical trials.

1.8.1 Non-therapeutic applications of bacteriophages:

Due to the long regulatory process of phage therapy in clinical use, many companies decided to study application in food safety, agriculture, industry and clinical diagnosis. Several companies could successfully develop phage-based products with EPA, USDA and FDA approval. The first example of the

product approved as Safe (GRAS) status from FDA was the phage cocktails targeted at *Listeria monocytogenes* that were designed to be used as sterilizing agent for processed foods [69].

1.8.2 Clinical trials for bacteriophage therapy:

As mentioned above, the clinical use of bacteriophage therapy requires rigorous trials to validate the safety and efficacy of the process. Some animal studies have been done on phage therapy against bacterial pathogens, such as *Pseudomonas aeruginosa*, *Staphylococcus aureus*, *Clostridium difficile*, and *Klebsiella pneumonia* [70-72].

In phase I trial that was completed at a wound care center in Lubbock, Texas with mixtures of bacteriophages targeting *P. aeruginosa*, *S. aureus* and *E. Coli*, revealed no increase in adverse reactions associated with application of phage cocktails [73]. In phase II trial, Wright et al., reported the decrease of *Pseudomonas* in adult with chronic external otitis by bacteriophage treatment [74]. This research produced a pioneering work for phage therapy in the phase III.

Recently, further research is being done on feasibility, efficacy, cost of bacteriophage therapy compared to antibiotic treatment, the bioavailability and pharmacokinetics of bacteriophage treatment and treatment of complex infections in humans [75].

1.9 Bacteriophage isolation and the environment:

Bacteriophages can be isolated from the environments populated by bacteria. The most abundant source of viruses is the sea. The coastal waters have more numbers of viruses than the oligotrophic open ocean. Also, researchers found a high source of phages in the soil. Different environments can be the source of phages. As shown in table 1.2, viruses can be varied according to their hosts.

Environment	Numbers
Sea water	10^6 - 10^7 tailed phage cm^{-3}
Soil	10^7 pfug $^{-1}$
Sewage	10^5 - 10^7 pfug $^{-3}$
Sewage (by electron microscopy)	10^8 - 10^{10} total phage particles
Human faeces	10^5 pfu cm^{-3}

Table1.2: the distribution of phages in the environment [76]

1.10 Bacteriophage classification and biology:

Bacteriophage characterization is based on the host range, physical properties of the free virion (such as capsid size, shape, resistance to organic solvents, structure, and genome size) and its nature (single or double stranded DNA or RNA).

Phage families are based on the nature of nucleic acid and particle morphology. Phage virions are classified into tailed, polyhedral, filamentous and pleomorphic. Most of capsids contain double stranded DNA. About 96.2% of the phages are tailed, while 3.7% are polyhedral, filamentous or pleomorphic [77].

1.11 Bacteriophage life cycles:

Most bacteriophages have dsDNA and some have ssDNA, dsRNA or ssRNA. Bacterial infection is different for different phages. Some phages infect bacteria through lytic cycle while others infect through lysogenic pathways.

During lytic infection, the phages multiply in bacterial cell and lyse the bacterial cell at the end of the cycle while releasing the new phage particles. In the lysogenic process, the phage genome replicates as part of the host genome and stays dormant in the bacterial host as a prophage for an extended period of time until being activated by adverse environmental conditions and turns to the lytic cycle.

The lysis steps as shown in figure 1.2 are identified as following:

- 1) Phage adsorption on the bacterial membrane through binding to the specific receptors.
- 2) Genome injection into the bacterial host
- 3) Expression of the early genes, and synthesis of early proteins
- 4) Replication of the phage genome
- 5) Expression of phage late proteins for the formation of new phage particles
- 6) Assembly of phage heads and tails and packaging of the genome.
- 7) Bacteriolysis and new phage release.

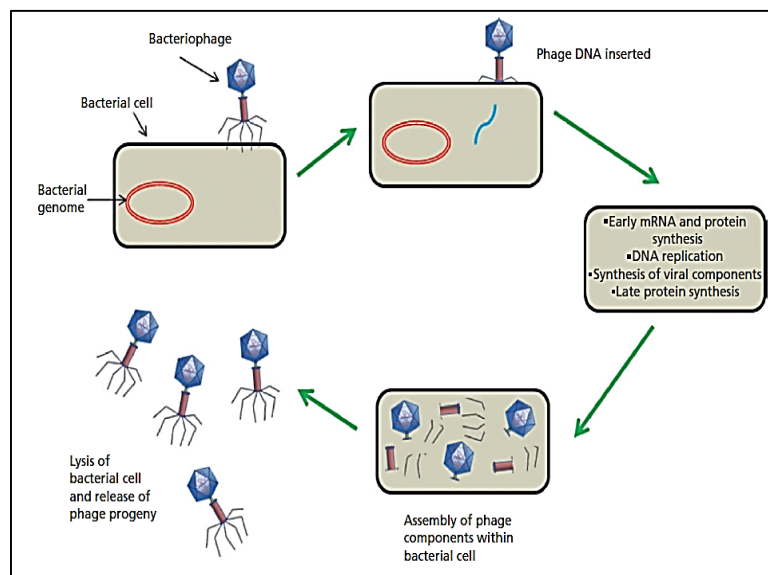


Figure1.2: Lysis cycle of bacteriophage [66]

1.12 Mechanism of phage adsorption and penetration into microbial cells:

The phage-bacteria interaction is a process with sequential stages: phage adsorption on the bacterial cell surface and injection of DNA into the cell, intracellular synthesis of virus components and assembly of phages, bacterial cell lysis and phage release.

The initial adsorption of phage onto the cell surface depends on the nature and structure of different receptors on bacterial cell surface, such as lipopolysaccharide (LPS), flagella, fimbriae and many other surface proteins. Also, the localization of receptors, their amount and density at various cell wall sites are important. Losing of the phage receptor on the bacterial surface, causes the bacterial resistivity to the phages [78, 79].

Bacteriophages do not have any specific structure for virion motion, so the adsorption process is the result of random phage-cell collision. Rate of adsorption is determined by different physicochemical factors such as pH, temperature, and presence of certain substances and ions in the media [80]. Phage adsorption onto the surface can be reversible or irreversible binding. It should be noted that interaction mechanism is specific for different phage systems. The process starts with the reversible attachment of long tail fibers to specific receptors on the surface of bacterial cell. For an attachment to be successful, it is better that three or more tail fibers might adsorb to the cell surface. After adsorption, conformational shape will occur and finally six short fibers can irreversibly adsorb to heptose moiety in LPS core. DNA penetration can be done just after irreversible adsorption and it depends on different factors such as electrochemical membrane potential, ATP molecules, etc [81-83].

Conformational alteration as the consequence of irreversible attachment, causes the contraction of tail sheaths. In order to break down the outer bacterial membrane, bacteriophages may use enzymes on the bacterial surfaces in a drill-like manner to reach the cell wall of the bacterium. Through enzymatic degradation of peptidoglycan, phages can penetrate easily and contact with phosphatidylglycerol of the inner membrane. Afterwards, through the electrochemical potential of inner membrane, DNA transports along the tail into the cell [83].

1.13 Comparison between phages and antibiotics:

Although both phages and antibiotics are similar in their significant antimicrobial activities, phages have some advantages over antibiotics. One advantage is that therapeutic phages have been reported to be more effective than antibiotics in some special infections. In one survey, *Staphylococcus aureus* phages and antibiotics have been used to treat the patients with purulent disease of the lungs and pleura. It showed an overall 82% recovery in the phage-treated patients while 64% recovery was seen in the antibiotic-treated ones. Table 1.3, shows other advantages of bacteriophages over antibiotics:

Bacteriophages	Antibiotics
Very specific affecting the targeted bacteria	Target both bacteria and normal microflora, that may lead to serious infections
Replicate in the site and so available whenever it is needed	Eliminated from the body and do not concentrate in the site of infection
No serious side effects	Multiple side effects such as intestinal disorder, allergies and secondary infections
Bacterial resistivity to the phages remains susceptible to other phages having a similar target range	Resistance to antibiotics is not limited to targeted bacteria
Selecting new phages is a rapid process	Developing new antibiotic is a time consuming process

Table 1.3: comparison between phage and antibiotic use [84]

Additionally, biofilm are resistance to antibiotics, due to the low oxygen limitations that restricts bacterial metabolic activity rather than restricted penetration from the extracellular matrix, while phage therapy can work against bacteria in specific conditions. For example, naturally occurring lytic phages show biofilm attacking properties in the presence of polysaccharide depolymerizing enzymes [85]. Several in vitro experiments have presented the ability of phage to infect biofilm cells with production of depolymerases and to penetrate in the inner layers of the biofilm by degrading biofilm exopolymeric matrix [86].

It is important to know that getting a specific phage with high lytic capability and expressing a relevant exopolymer degrading enzyme is quite difficult. In this case, genetically engineered phages can play an important role [87, 88].

1.14 Interaction of phage and biofilm:

Even though, phage-biofilm interactions are poorly understood, the common perception is mostly based on phage movement within biofilms, phage enzymatic impact, and the bacterial microcolony as the primary focus of phage exploitation. The overview of this interaction is shown in figure 1.3.

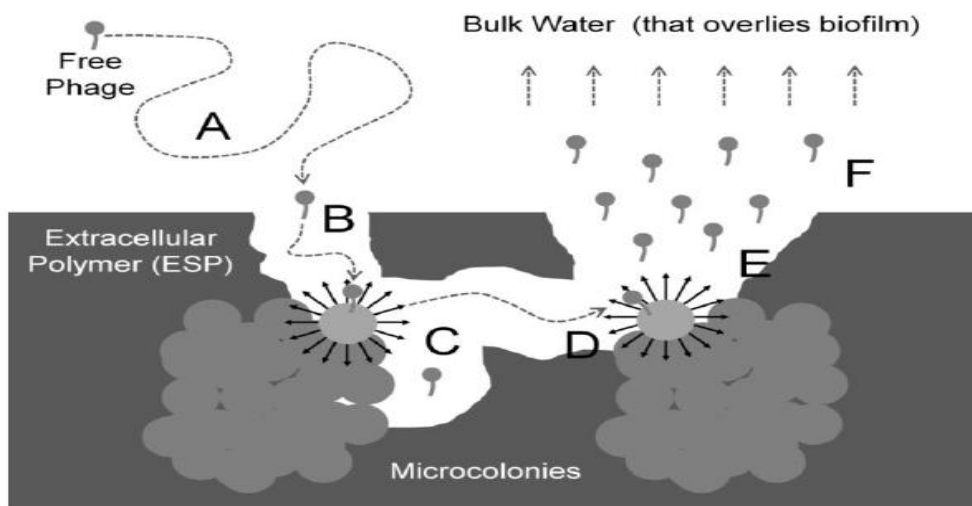


Figure 1.3: Overview of phage-biofilm interaction. (A) Free phage diffusion above biofilm. (B) Free phage encounter and digest EPS. (C) Phage progeny release while encountering the susceptible bacterium. (D) Phage encounters the near microcolony followed by infection and burst. (E) Burst precedes the path of released phages toward the biofilm surface. (F) Free-phage diffuses into bulk water toward subsequent biofilm [89].

The biofilm pores and water channels permit the access of the phages inside the structure. After adsorption of phage to the susceptible bacterial surface, the phage polysaccharide depolymerase has the capability of degrading the biofilm EPS [90]. The depolymerase enzyme is important for the phage release from the biofilm as well as the initial penetration and subsequent infection of cells. Increasing the thickness of biofilm causes the phage captures in the basal layer without any enzymatic function to release itself from the EPS [90].

1.15 Delivery mechanisms of bacteriophages:

In the last few years, several studies were done on the delivery routes of bacteriophages such as oral, parenteral, or directed towards local phage delivery and inhalation. Also, application of lytic bacteriophages on indwelling medical devices in order to prevent biofilm formation, has been considered.

1.15.1 Parental delivery of bacteriophages:

This method due to the distribution of phages in the systemic circulation has to be one of the most popular and successful of all delivery methods of bacteriophages. The specific sites of administration such as intramuscular (IM), subcutaneous (SC) or intraperitoneal (IP) have a significant influence on the success of phage therapy.

Additionally, the studies showed that higher concentrations of phages significantly influenced the protection against infection. It has been illustrated that optimum protection can be achieved by

administration of phages within 3 hours of bacterial inoculation at doses as high as 10^8 PFU/ml (PFU is the plaque-forming units) [66].

1.15.2 Oral delivery of phages:

This route has proven to be successful in the treatment of gastrointestinal infections and in some cases, systemic infections. Methods such as polymer microencapsulation can protect phages against highly acidic environment of the gastric and enhance the efficacy of orally administration. Without protection, bacteriophage might not survive in the gastric passages due to the acid sensitivity of individual phage.

The gut is the location of pathogenic bacteria and is accessible to orally applied phages. Some researches show that the phages may not only reside in the gut lumen but also pass the intestinal wall in a process similar to bacterial translocation. Phage passage can be affected by different factors such as phage concentration, specific sequences within the phage capsid proteins interacting with enterocyte receptors, and phage interactions with gut immune cells [66].

1.15.3 Local delivery of phages:

In the studies especially from former Soviet/Eastern Bloc countries, the local delivery of phages has proven very successful. Wound healing is one of the interesting therapeutic areas. Use of hydrogels and impregnated wound healing formulations enhanced the efficacy of phage therapy in topical applications [66].

One of the successful commercial products is Phagebioderm developed by Eliava Institute in Georgia which targets *P. aeruginosa*, *S. aureus* and *Streptococcus* spp. This product is a hydrogel containing a cocktail of bacteriophages and antibiotics [91-93].

In the study done by Donlan et. al. [94], immobilization of antimicrobial agents was done through filling each catheter segment with the phage culture and incubating at 37 °C for 1 hour within the catheter lumens before removal. Regrowth of biofilm on the phage treated catheters occurred between 24 and 48 hours, but supplemental treatment with phage at 24 hours significantly reduced biofilm regrowth. The results showed the potential ability of phage applications specially phage cocktails, to the surface of medical devices from alleviation of biofilm formation.

1.15.4 Dental phage administration:

Several researches assessed the effect of bacteriophages on the viability of bacteria in human dental roots. Before inoculation with phages, the crowns of the teeth were removed and canals were rinsed with sterile PBS and fully sterilized.

The substantial reduction in bacterial growth indicates the ability of phages to reduce the bacteria growth in tubules. The studies present phage therapy as an important alternative for the treatment of root canal infections [95].

1.15.5 Inhalation of bacteriophages:

The use of bacteriophages to combat bacterial lung infections can be done through the development of modern inhalation and process technologies. The studies using nebulizer delivery suggested that phages can be nebulized and delivered successfully [96-98]. The in-vitro delivery of bacteriophages using dry powder inhalation formulation is proven as a successful therapeutic approach for cystic fibrosis pulmonary infections [99].

Pulmonary delivery was determined by measuring the amount of powder delivered as a percentage of inhaler loads. The relevant studies showed the stability of phages at both 4 °C and 22 °C, over 3 months period [66].

1.16 Phage immobilization on the functionalized polymer surfaces:

Phage immobilization may provide the existence of phages near the surface that is being treated and prevent the excessive phage wastage. Immobilization of biologic materials is of great interest in industry and depends on the nature of the material and on the application. Bacteriophage adsorption has been investigated to detect, concentrate and identify target bacteria.

In several research works, the physical adsorption of filamentous and *Podovirida* phages on gold surface of plasmon resonance (SPR) sensors and glass substrates has been studied in order to recognize many targeted bacteria [100-102].

In another works, immobilization of *Salmonella*-specific phage on polystyrene can lead to the capture of *Salmonella* cells. Also phages chemically biotinylated have been used to immobilize on streptavidin-coated beads [103, 104].

Site specific immobilization is a method to orient the phages in such a way that their tail fibers be free and thus increase the capture of bacteria. Regarding phage orientation, the adequate orientation of genetically modified wild T4 phages onto cellulose membranes or streptavidin-coated magnetic beads, resulted in higher capture of *E. coli* cells [105].

Another mechanism of phage immobilization is through electrostatic interaction between the phage and the substrate. A negative net charge for most of viruses and the isoelectric point of close to 4 for the whole T4 phage (capsid, tail and fibers), have been reported. Also, the capsid charge is negative in pH above 4, while the tail fibers are positively charged [106]. Therefore, the inherent charge characteristics of phages can be responsible for the immobilizing them in the right orientation on the modified surfaces [107].

Griffiths et. al. [108], developed a novel method for the oriented immobilization of bacteriophage based on charge difference between bacteriophage head with negative charge and tail fibers with positive charge. So, the head has tendency to attach to the positively charged surfaces leaving the tail free to capture and lyse bacteria. They could successfully immobilize the cocktail of phages active against *Listeria* or *E. coli* on the modified surface of Cellulose with positive charge.

Van de Ven et. al. [109], studied the capture and deactivation of bacteria by incorporating of bacteriophages in the modified cellulose. Figure 1.4 shows the immobilization of T4 bacteriophage capsid on cellulose surface through carbohydrate-binding modules (CBMs). This CBM specifically binds to the amorphous and crystalline cellulose and also a range of mono and disaccharides. More than 800 copies of CBMs expressed on the capsid are responsible for the orientation and binding of phages to the cellulose. The free tail and fibers have the ability to move and capture the *E. coli* bacteria.

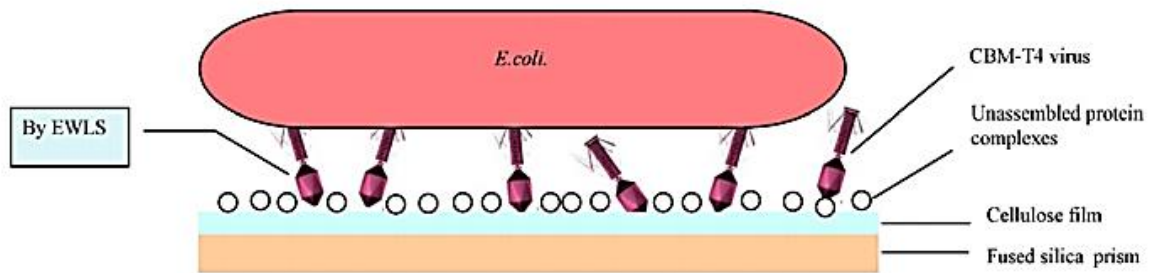


Figure 1.4: Immobilization of CBM-T4 onto cellulose surface [109]

Pearson et. al. [110], investigated the covalent attachment of T1 and Φ 11 phages onto surfaces on polytetrafluoroethylene (PTFE) and ultra-high molecular weight of polyethylene (UHMWPE) while trying to maintain the biological activity of bacteriophages. As shown in figure 1.5, the polymeric substrate is initially modified with reactive acid groups using clean microwave plasma reaction in the presence of maleic anhydride. Afterwards, T1 bacteriophages are covalently attached via acid amine reactions leading to amide linkages. In the presence of bacteria, phages linked onto the substrate, attached specifically to the external structure of bacteria (e.g. lipopolysaccharide or protein) and injected their DNA into the target.

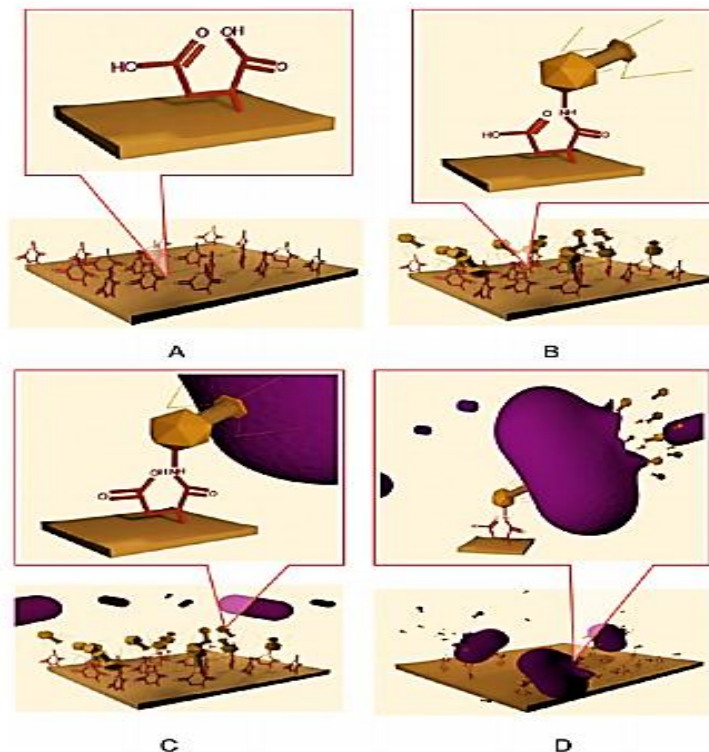


Figure 1.5: (A) modification of the polymeric surface with covalent attachment of acid groups, (B) acid group reaction with NH_2 groups of T1, (C) bacteria-phage interaction and injection of DNA, (D) destruction of bacteria through replication of DNA [110]

The attempt of this work is to investigate the bacteriophages immobilization onto collagen/silk fibroin biocomposites. So in the following sections properties and characteristics of each biopolymer as well as their mixing methods, have been assessed.

1.17 Biopolymers used for phage immobilization

1.17.1 Collagen:

Role of collagen and its structure: Collagen is abundant in many tissues representing about 25% of the total body protein of mammals. The triple helix structure of collagen provides the major structural support of all vertebrate tissues. There are about 20 different types of collagen in various tissues of the same individual and all of them contain the same monomeric structures consisting at least 32 individual polypeptide α -chains.

As shown in figure 1.6, a single collagen molecule called tropocollagen has a rodlike shape with the length of 300 nm, a width of 1.5 nm and a molecular mass of 285 kD. This molecule composed of three left handed α -helices twisted together around a central axis to form a right handed superhelical structure. Each α -chain has a distinctive amino acid sequence that consists repeating Gly-X-Y triplets. X is often Pro and Y is often Hyp. The stabilization of collagen triple helix is due to the hydrogen bonds between Gly residues

and Pro residues. Diversity of antigenic determinants influences the complex structure of collagen and its precursor procollagen. At least 5 distinct groups of antigenic determinants have been recognized. Two of these groups belong to precursor and are located at both ends of the molecule. The helical determinants are located in the triple helical body of the protein and are dependent on the intact triple helical conformation.

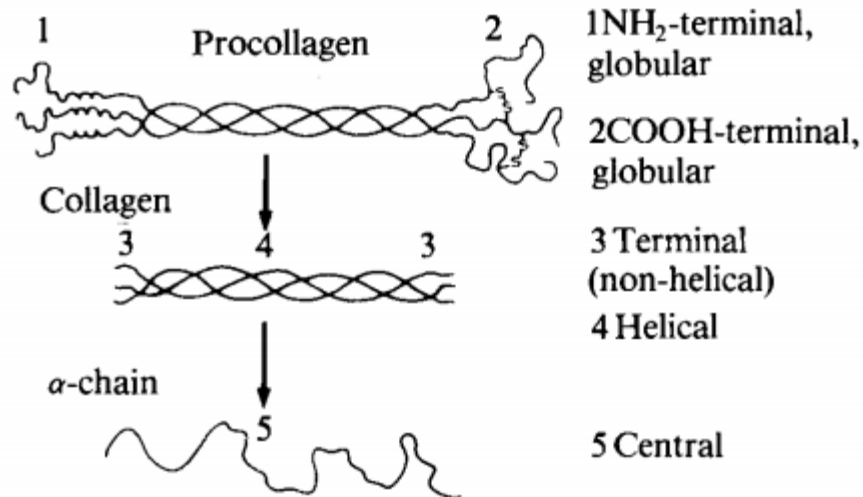


Figure 1.6: collagen structure and the localization of the 5 antigenic determinant groups

Collagen is synthesized within the cell as soluble procollagen and can be transformed into the collagen monomer by specific enzymatic cleavage of terminal peptide and consequently form fibrils [111-113].

The interactions between collagen molecules take place through electrostatic or hydrophobic forces. Parallel fibril assemblies can form fibers or lamellae at micron level in tendon, bone and other tissues.

Collagen degradation and denaturation: Collagen degradation occurs through MMPs, specifically collagenase and phagocytosis without any toxic residues. The site of implantation influences the rate of degradation.

Collagen denaturation occurs through physical treatment (e.g., UV) or by heating which causes the conformation change of triple helix to random coil. Collagen denaturation depends on the degree and origin of collagen assembly. The mammalian collagens denature at about 40 °C, while aggregated fibers denature at about 65 °C.

Collagen denaturation can be detected by FTIR analysis where the peaks of specific bands (e.g., amide I, II) shift to lower frequencies indicating the triple helix-random coil transition.

Collagen advantages come from its unique structural, biochemical and biological properties.

Low immunogenicity: Compared to proteins that are completely immunogenic, collagens are poor immunogens which is due to the small quantities of non-collagenous proteins presented in some of the materials. Another source of immunogenicity is the presence of denatured collagen because individual chains are more immunogenic than intact helical molecules.

Cell matrix interactions: It is well known that collagen can enhance the growth of different cell types and various research works demonstrates the use of collagen substrates, especially collagen type I for culture of a variety of cell types. Cell-collagen interaction mechanism depends on cell type and can occur through specific receptors. Additionally, collagen substrate can also promote subsequent growth, differentiation and migration of cells. These properties of collagen are not found in synthetic polymers and collagen coating have been developed for non-biological materials in order to enhance their performance characteristics.

Mechanical properties: Inherent strength of collagen is an important characteristic of tissue collagen and it can provide a variety of mechanical demands for different tissues. For example in tendons, the collagen is almost all type I, which is aligned along the tendon length in the direction of the force, while in skin, the collagen fibers are arranged randomly [113].

Biodegradability and collagenases: The wide biological application of collagen is due to the biocompatibility of this material and the possibility of its degradation through human collagenases. The degradation rate can be regulated by crosslinking. Different collagenases such as MMP-1, MMP-2, MMP-8, MMP-13 and MMP-14 can hydrolyze collagen type I to II.

Collagen based biomaterials may be a proper substitute for natural damaged bone. Scaffolds for bone tissue engineering rely on hardening of a collagen biomaterial by mineralization with calcium phosphate. Sheet like collagen scaffolds cultured with or without autologous cells can be used to fill osteochondral defects [114].

Influence of pH and salt on isoelectric point of collagen: The importance of pH and ionic strength has been investigated by several authors. Also, the thermal stability of collagen I is dependent on salt type and solution pH. Additionally, the acid base behavior of collagen I was found to be strongly influenced by ionic strength in KCl and in CaCl₂ solutions. For example, the thermal stability of collagen in CaCl₂ and in physiological pH decreases with the increasing of salt concentration, while thermal stability was reported to enhance with increasing salt concentration from 0.4 to 1 M at pH of 2.3 [115]. Werner et. al. [116], showed that increasing ionic strength in the KCl systems will lead to more acidic (negatively charged) collagen molecules, whereas, an increase of the ionic strength in the CaCl₂ system will lead to a more basic (positively charged) collagen molecule.

1.17.2 Silk fibroin:

Introduction to silk: Silk is a natural fiber produced by more than 3000 species of spider and several types of worms including mites, butterflies and moths in the form of continuous filament. Silk fibroin has several interesting properties such as excellent toughness and stiffness combined with low density. High mechanical strength along with biodegradability and environmental stability attracted researchers to work with silk fibroin.

Of all the silk spinning insects, the silkworm *Bombyx mori* (*B. Mori*) and the spider *Nephila Clavipes* are extensively studied because of the possibility of silk production in commercial quantities.

The tensile strength of *B. Mori* silk is 0.6 GPa and the stiffness is 7 GPa. These high mechanical characteristics cause silk fiber to be used in many technologically important applications in several areas other than textiles. Silkworm silk has been used in a variety of different biomaterials.

Silk fiber consists of two proteins, the core structural protein called fibroin and the gummy sheath protein called sericin.

Fibroin structure: Silk fibroin belongs to the class of fiber forming structural proteins. It is a protein consisting of a chain of amino acids, with three groups of amine (NH₂), carboxyl (COOH) and hydrogen (H) that are common in all amino acids and are bound to a carbon molecule called α -carbon. The fourth group is the side chain group of "R" that can vary in shape, size, charge and chemical reactivity.

The major amino acid residues in fibroin chains are 42.9% glycine (G), 30% alanine (A), 12.2% serine (S), 4.8% tyrosine (Y), 2.5% valine (V) and 7.6% other remaining amino acids. The heavy (H) and light (L) chains in fibroin are linked to each other by disulfide bonds.

The crystalline regions of fibroin are responsible for the secondary structure of fibroin (β -sheets). Also, it is clear that crystalline domains of fibroin are responsible for the high strength properties of silk fibers whereas the amorphous regions are in charge of silk flexibility. Figure 1.7, shows the structure of heavy and light chains in fibroin chains.

The end blocks in the hydrophilic chains are N-terminus and C-terminus. Under the pH conditions existing in the silk spinning process, the N-terminus is negatively charged (its isoelectric point is 4.6), while the C-terminus is positively charged (its isoelectric point is 10.5). The charge distribution results in the isoelectric pH of 3.9-4 for fibroin [117, 118].

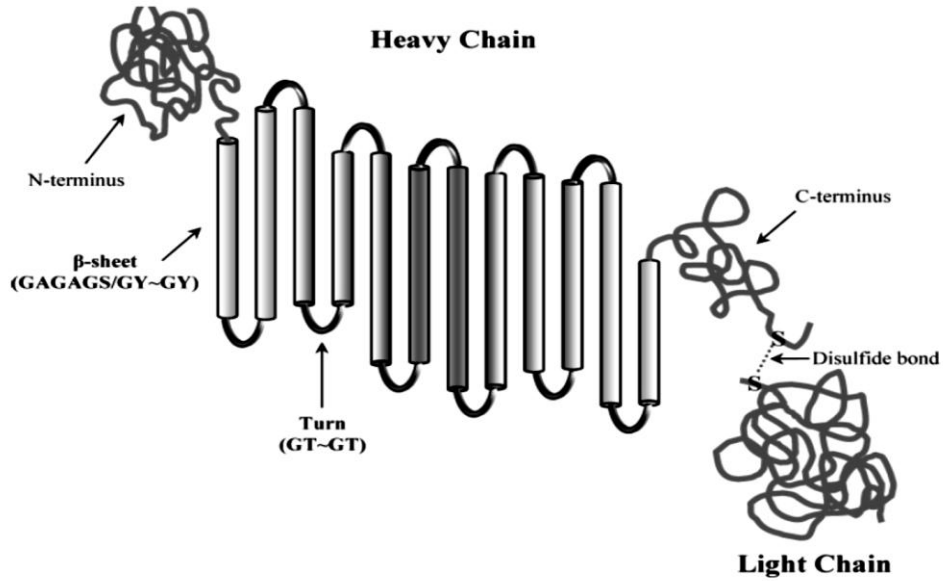


Figure 1.7: Schematic representation of heavy-light chains in fibroin.

Matusmoto et. al. [119], showed that changing pH from neutral to acidic causes protonation of the carboxyl group on the side chains that decreases the charge repulsions and increases hydrophobicity of the fibroin. As shown in figure 1.8, alteration of pH from neutral to basic in the range of 6 to 9, results to the both carboxylic and amino groups being charged. Above pH 9, the basic amino groups and the acidic carboxyl groups start deprotonating.

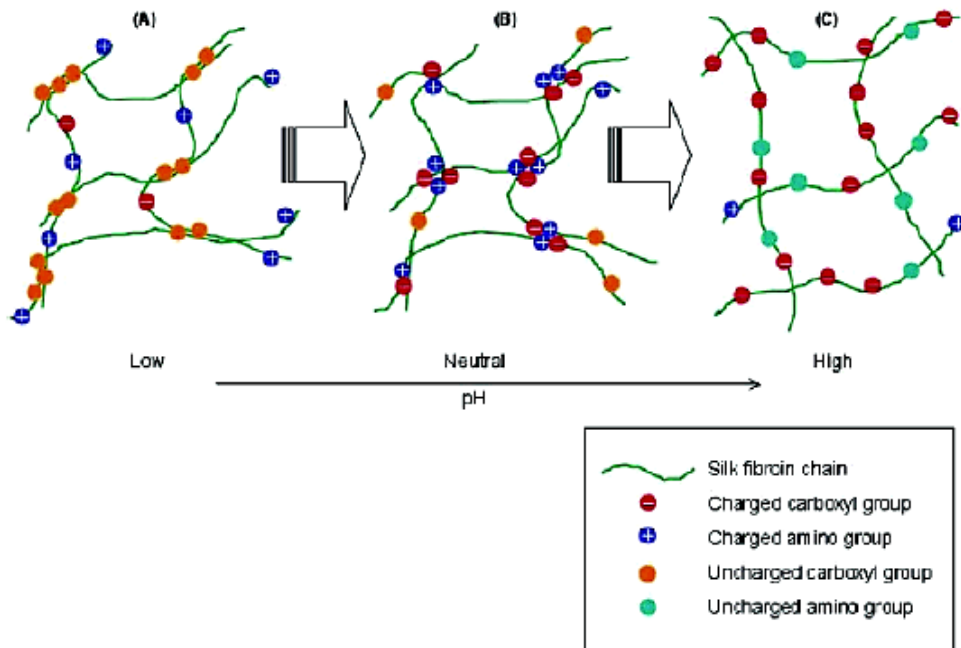


Figure 1.8: Fibroin interaction chains depend on pH [119]

Mechanical properties: GAGAGS and GAGAGY abundance in fibroin promote folding of the crystalline region of the protein into an anti-parallel β -sheet secondary structure, enhancing the mechanical properties of silk fibers. The combination of strength and toughness in fibroin is not found in other biopolymers. For example, in comparison with collagen with higher elasticity than fibroin, the tensile strength of collagen is several orders of magnitude less than that of silk fibroin.

High mechanical compression along with biocompatibility and slow degradation rate are properties, making fibroin suitable for biomedical applications. Table 1.4 shows the comparison of silk fibroin properties with other polymers.

Material	UTS (MPa)	Elastic Modulus (Gpa)	% Strain at break
<i>B. Mori</i> silk (w/sericin)	500	5-12	19
<i>B. Mori</i> silk (W/O sericin)	610-690	15-17	4-16
Spider silk	875-972	11-13	17-18
Collagen	0.9-7.4	0.0018-0.0146	24-68
Bone	160	20	3
Kevlar	3600	130	2.7
Synthetic rubber	50	0.001	850

Table 1.4: Mechanical properties of silk and other polymers [120, 121]

Biocompatibility and degradation: The immune response of body to silk is due to the presence of sericin and some wax-like materials. Studies have shown that the complete removal of sericin allows the fabrication of this biomaterial as scaffolds with immunological responses similar to those of other widely used biomaterials.

It has been shown that the fibroin molecule degradation *in vitro*, occurs through proteolytic enzymes such as chymotrypsin that cleave the less crystalline linker regions of the molecule. It should be noted that a wide range of factors such as physiological health, implantation site, shape, size and animal model influence the degradation rate of silk fibroin biomaterials *in vivo* [122].

Tissue engineering: Numerous researches have been done on the adsorption and proliferation of cells to the fibroin scaffolds. The results show that fibroin biomaterials with different geometries can support cell adhesion and proliferation. Comparison of silk fibroin and collagen scaffolds, illustrated the same cell adhesion and proliferation on both.

The crosslinking occurs through covalent bond between the amino terminus of the peptide and activated carboxylate groups in silk fibroin. Peptide binding to silk fibroin matrices has been shown to enhance cellular proliferation similarly to levels found on collagen matrices [123, 124].

1.17.3 Collagen/silk fibroin blends:

As mentioned in previous sections, silk fibroin has unique mechanical properties. Also, collagen plays an essential role in providing a scaffold for cellular support and affecting cell attachment, migration and proliferation. However, collagen derived from animals has practical problems such as risk of infectious disease transmission and provoking immunological reactions.

In a research by Hu et. al. [125], animal derived collagen was blended with fibroin to enhance the hydrophilicity of the film. They showed the excellent biocompatibility of human-like recombinant collagen (RHLC) and fibroin along with the improvement of the fibroin film elasticity due to the RHLC in the blend film. The mixture was prepared by adding different amounts of RHLC gel into the aqueous silk fibroin solution and heated up to 50-60 °C. The blend film was formed with casting of the aqueous solution on polystyrene petri dishes and dried at 70 °C. They showed that hepatocyte cells cultured on the blend films adhered and grew better than on pure fibroin films.

In another work done by Yeo et. al. [126], collagen/silk fibroin blend solution was electrospun in order to enhance biological reactions with cells and speed up tissue regeneration. Also, for after-treatment of electrospun matrix, the collagen/silk fibroin matrix has been cross linked by treatment with glutaraldehyde and water vapor. Cytocompatibility test showed the capability of blend scaffolds with ratio of 50:50 for better attachment and spreading of normal human keratinocytes than the pure ones.

Qiang et. al. [127], investigated on fibroin/collagen hydrogel stiffness by adding crosslinking 1-ethyl-3-(3-dimethylaminopropyl) (EDC). They showed higher mechanical strength for these hydrogels than that of previously reported protein based hydrogels. Also, the crosslinked hydrogels can maintain their configuration above 80 °C, proving their increased thermal stability. The cross linking has no negative effect on the biocompatibility of blend hydrogels due to the growth of vascular smooth muscle cells. The scaffolds were prepared by adding collagen gel into fibroin solution and heated to 40 °C with mild stirring until the collagen gel dissolved in fibroin solution. During this process, all the collagen gel denatured and dissolved in fibroin solution at 60 °C. Various concentrations of EDC were added to the blend solution and freeze dried once the hydrogel was formed. They showed the highest mechanical strength for these hydrogels.

In another work, the effect of pH on the formation of fibroin/collagen scaffolds was investigated. In the range of pH from 4 to 8.5, the fibroin/collagen scaffolds were prepared with good porous structures. The mechanical assessment proved that the scaffolds prepared at several pH values had better mechanical

properties. The fibroin/collagen blend has been prepared by adding collagen gel into fibroin aqueous solutions and heated up to 50-60 °C until the collagen gel dissolved in fibroin solutions. Afterwards, the pH was adjusted to 4, 5.5, 7 and 8.5 by adding some content of 1 mol/L HCl or 1 mol/L NaOH and freeze dried [128, 129].

1.18 Thesis outline

This thesis covers aspects related to the designing of phage immobilized collagen/silk fibroin biocomposites films and the potential antibacterial activity of such surfaces.

Chapter 1 is an introduction to the parameters influencing on bacterial adhesion and biofilm formation, antibiotic resistant bacteria, phage therapy as an alternative to antibiotics, methods of phage immobilization and stabilization onto the biomedical surfaces, biopolymers, silk fibroin and collagen properties, including biodegradability and biocompatibility, and the literature review on the methods to mix these two biomaterials.

Chapter 2 introduces a strategy to mix collagen and silk fibroin aiming at preserving their natural structure. This method focuses on preparing miscible mixtures of two biomaterials using salt ions and obtaining biocomposite films after removing salts ions through dialysis procedure. The physicochemical properties of the mixture solutions and films have been analyzed by several methods. From this chapter, the following manuscript has been published as journal article:

I Ghaeli, MA de Moraes, MM Beppu, K Lewandowska, A Sionkowska, F Ferreira-da- Silva, MP Ferraz, FJ Monteiro, “Phase behaviour and miscibility studies of collagen/silk fibroin macromolecular system in dilute solutions and solid state”, *Molecules*, 22(8) (2017), 1368.

Chapter 3 describes a designing method to immobilized bacteriophage T4 onto the surface of glass coverslip. This method is based on the drying induced self assembly of viral nanoparticles onto the glass substrates. The drying procedure has been analyzed under darkfield enhanced microscope, phage nanoparticles movement inside the suspensions has been tracked and the drying parameters have been analyzed on the final dried patterns. From this chapter, the following manuscript has been published as journal article:

I Ghaeli, Z Hosseinidoust, H Zolfagharnasab, FJ Monteiro, “A new label free technique for analysing evaporation induced self-assembly of viral nanoparticles based on enhanced darkfield optical imaging”, *Nanomaterials*, 8 (1), 1, 2018.

Chapter 4 contains results concerning the antibacterial and cytocompatibility of the phage immobilization technique onto the surfaces of collagen and glass coverslip. The planktonic growth and biofilm formation have been measured individually to assess the bioactivity of resulted phage immobilized surfaces. Storage effect was analyzed on the obtained materials and the results of *in vitro* studies with mesenchymal stem cells have been reported.

Chapter 5 presents the antibacterial activity of phage immobilized collagen, silk fibroin and mixture films, based on the immobilization technique introduced in Chapter 3. Similar to Chapter 4, antibacterial activity has been analyzed through planktonic growth and biofilm formation and the cytocompatibility analysis has been assessed using mesenchymal stem cells.

Chapter 6 presents the main results and conclusions of the research reported in this thesis.

1.19 References

1. Gao, G., et al., *Antibacterial surfaces based on polymer brushes: investigation on the influence of brush properties on antimicrobial peptide immobilization and antimicrobial activity*. Biomacromolecules, 2011. **12**(10): p. 3715-27.
2. Harding, J.L. and M.M. Reynolds, *Combating medical device fouling*. Trends Biotechnol, 2014. **32**(3): p. 140-6.
3. Salwiczek, M., et al., *Emerging rules for effective antimicrobial coatings*. Trends Biotechnol, 2014. **32**(2): p. 82-90.
4. Hadesfandiari, N., et al., *Polymer brush-based approaches for the development of infection-resistant surfaces*. Journal of Materials Chemistry B, 2014. **2**(31): p. 4968-4978.
5. Mack, D., et al., *Staphylococcus epidermidis in Biomaterial-Associated Infections*, in *Biomaterials Associated Infection: Immunological Aspects and Antimicrobial Strategies*, T.F. Moriarty, S.A.J. Zaat, and H.J. Busscher, Editors. 2013, Springer New York: New York, NY. p. 25-56.
6. Hidron, A.I., et al., *NHSN annual update: antimicrobial-resistant pathogens associated with healthcare-associated infections: annual summary of data reported to the National Healthcare Safety Network at the Centers for Disease Control and Prevention, 2006-2007*. Infect Control Hosp Epidemiol, 2008. **29**(11): p. 996-1011.
7. Vogelyl, H.C., et al., *The infected orthopaedic implant. An animal model to study the mechanisms of haematogenous infection of cementless implant materials*. European Journal of Orthopaedic Surgery & Traumatology, 1996. **6**(2): p. 91-95.
8. An, Y.H. and R.J. Friedman, *Animal models of orthopedic implant infection*. J Invest Surg, 1998. **11**(2): p. 139-46.
9. Katsikogianni, M. and Y.F. Missirlis, *Concise review of mechanisms of bacterial adhesion to biomaterials and of techniques used in estimating bacteria-material interactions*. Eur Cell Mater, 2004. **8**: p. 37-57.
10. von Eiff, C., et al., *Infections associated with medical devices: pathogenesis, management and prophylaxis*. Drugs, 2005. **65**(2): p. 179-214.

11. Lecuyer, S., et al., *Shear stress increases the residence time of adhesion of Pseudomonas aeruginosa*. Biophys J, 2011. **100**(2): p. 341-50.
12. Wassall, M.A., et al., *Adhesion of bacteria to stainless steel and silver-coated orthopedic external fixation pins*. J Biomed Mater Res, 1997. **36**(3): p. 325-30.
13. Riool, M., et al., *Antimicrobial Peptides in Biomedical Device Manufacturing*. Front Chem, 2017. **5**: p. 63.
14. Park, K.D., et al., *Bacterial adhesion on PEG modified polyurethane surfaces*. Biomaterials, 1998. **19**(7): p. 851-859.
15. Lorenzetti, M., et al., *Hydrothermal and plasma treatments drastically reduce bacterial adhesion to Ti-based materials used in medicine*. Frontiers in Bioengineering and Biotechnology.
16. Liu, C., et al., *Reduction of bacterial adhesion on modified DLC coatings*. Colloids and Surfaces B: Biointerfaces, 2008. **61**(2): p. 182-187.
17. Yoda, I., et al., *Effect of surface roughness of biomaterials on Staphylococcus epidermidis adhesion*. BMC Microbiol, 2014. **14**: p. 234.
18. Hsu, L.C., et al., *Effect of Micro- and Nanoscale Topography on the Adhesion of Bacterial Cells to Solid Surfaces*. Applied and Environmental Microbiology, 2013. **79**(8): p. 2703-2712.
19. Renner, L.D. and D.B. Weibel, *Physicochemical regulation of biofilm formation*. MRS bulletin / Materials Research Society, 2011. **36**(5): p. 347-355.
20. Palmer, J., S. Flint, and J. Brooks, *Bacterial cell attachment, the beginning of a biofilm*. J Ind Microbiol Biotechnol, 2007. **34**(9): p. 577-88.
21. Bisognano, C., et al., *Induction of fibronectin-binding proteins and increased adhesion of quinolone-resistant Staphylococcus aureus by subinhibitory levels of ciprofloxacin*. Antimicrob Agents Chemother, 2000. **44**(6): p. 1428-37.
22. Herrmann, M., et al., *Fibronectin, fibrinogen, and laminin act as mediators of adherence of clinical staphylococcal isolates to foreign material*. J Infect Dis, 1988. **158**(4): p. 693-701.
23. Baumgartner, J.N. and S.L. Cooper, *Influence of thrombus components in mediating Staphylococcus aureus adhesion to polyurethane surfaces*. J Biomed Mater Res, 1998. **40**(4): p. 660-70.
24. Cordero, J., L. Munuera, and M.D. Folgueira, *Influence of bacterial strains on bone infection*. J Orthop Res, 1996. **14**(4): p. 663-7.
25. Arciola CR, C.D., Gamberini S, Donati ME, Pirini V, Visai L, Speziale P, Montanaro L, *Antibiotic resistance in exopolysaccharide-forming Staphylococcus epidermidis clinical isolates from orthopaedic implant infections*. Biomaterials, 2005. **26**(33): p. 6530-6535.
26. Vuong, C. and M. Otto, *Staphylococcus epidermidis infections*. Microbes Infect, 2002. **4**(4): p. 481-9.
27. Bagnall, N.M., S. Vig, and P. Trivedi, *Surgical-site infection*. Surgery (Oxford), 2009. **27**(10): p. 426-430.
28. Weigelt, J.A., et al., *Surgical site infections: Causative pathogens and associated outcomes*. Am J Infect Control, 2010. **38**(2): p. 112-20.
29. Boyce, J.M., et al., *Methicillin-resistant Staphylococcus aureus (MRSA): a briefing for acute care hospitals and nursing facilities*. The AHA Technical Panel on Infections Within Hospitals. Infect Control Hosp Epidemiol, 1994. **15**(2): p. 105-15.
30. Nickel, J.C., et al., *Tobramycin resistance of Pseudomonas aeruginosa cells growing as a biofilm on urinary catheter material*. Antimicrob Agents Chemother, 1985. **27**(4): p. 619-24.
31. Pratt, L.A. and R. Kolter, *Genetic analysis of Escherichia coli biofilm formation: roles of flagella, motility, chemotaxis and type I pili*. Mol Microbiol, 1998. **30**(2): p. 285-93.
32. Watnick, P.I., K.J. Fullner, and R. Kolter, *A role for the mannose-sensitive hemagglutinin in biofilm formation by Vibrio cholerae El Tor*. J Bacteriol, 1999. **181**(11): p. 3606-9.

33. Khan, W., et al., *Aminoglycoside resistance of Pseudomonas aeruginosa biofilms modulated by extracellular polysaccharide*. *Int Microbiol*, 2010. **13**(4): p. 207-12.
34. Whiteley, M., et al., *Gene expression in Pseudomonas aeruginosa biofilms*. *Nature*, 2001. **413**(6858): p. 860-4.
35. Bester, E., E.A. Edwards, and G.M. Wolfaardt, *Planktonic cell yield is linked to biofilm development*. *Can J Microbiol*, 2009. **55**(10): p. 1195-206.
36. O'Toole, G.A. and R. Kolter, *Flagellar and twitching motility are necessary for Pseudomonas aeruginosa biofilm development*. *Mol Microbiol*, 1998. **30**(2): p. 295-304.
37. Boyd, A. and A.M. Chakrabarty, *Role of alginate lyase in cell detachment of Pseudomonas aeruginosa*. *Appl Environ Microbiol*, 1994. **60**(7): p. 2355-9.
38. Allison, D.G., et al., *Extracellular products as mediators of the formation and detachment of Pseudomonas fluorescens biofilms*. *FEMS Microbiol Lett*, 1998. **167**(2): p. 179-84.
39. Heilmann, C. and F. Götz, *Cell–Cell Communication and Biofilm Formation in Gram-Positive Bacteria*, in *Bacterial Signaling*. 2010, Wiley-VCH Verlag GmbH & Co. KGaA. p. 7-22.
40. Deighton, M. and R. Borland, *Regulation of slime production in Staphylococcus epidermidis by iron limitation*. *Infect Immun*, 1993. **61**(10): p. 4473-9.
41. Woodford, N. and M.J. Ellington, *The emergence of antibiotic resistance by mutation*. *Clin Microbiol Infect*, 2007. **13**(1): p. 5-18.
42. United, S., *Impacts of antibiotic-resistant bacteria: Thanks to penicillin-- He will come home*. *Impacts of antibiotic resistant bacteria*. 1995, Washington, DC: Office of Technology Assessment, Congress of the U.S. : For sale by the U.S. G.P.O., Supt. of Docs. ix, 183 p.
43. Wright, G.D., *Bacterial resistance to antibiotics: enzymatic degradation and modification*. *Adv Drug Deliv Rev*, 2005. **57**(10): p. 1451-70.
44. Džidić, S., J. Šušković, and B. Kos, *Antibiotic Resistance Mechanisms in Bacteria: Biochemical and Genetic Aspects*. *Food Technol Biotechnol*, 2008. **46**: p. 11-21.
45. Gallo, J., M. Holinka, and C.S. Moucha, *Antibacterial Surface Treatment for Orthopaedic Implants*. *International Journal of Molecular Sciences*, 2014. **15**(8): p. 13849-13880.
46. Romano, C.L., et al., *Antibacterial coating of implants in orthopaedics and trauma: a classification proposal in an evolving panorama*. *J Orthop Surg Res*, 2015. **10**: p. 157.
47. Rojo, L., et al., *Intrinsically Antibacterial Materials Based on Polymeric Derivatives of Eugenol for Biomedical Applications*. *Biomacromolecules*, 2008. **9**(9): p. 2530-2535.
48. Campoccia, D., L. Montanaro, and C.R. Arciola, *A review of the biomaterials technologies for infection-resistant surfaces*. *Biomaterials*, 2013. **34**(34): p. 8533-54.
49. Zhang, F., et al., *Silk-functionalized titanium surfaces for enhancing osteoblast functions and reducing bacterial adhesion*. *Biomaterials*, 2008. **29**(36): p. 4751-9.
50. Kaper, H.J., H.J. Busscher, and W. Norde, *Characterization of poly(ethylene oxide) brushes on glass surfaces and adhesion of Staphylococcus epidermidis*. *J Biomater Sci Polym Ed*, 2003. **14**(4): p. 313-24.
51. Antoci, V., Jr., et al., *Vancomycin covalently bonded to titanium alloy prevents bacterial colonization*. *J Orthop Res*, 2007. **25**(7): p. 858-66.
52. Schmidmaier, G., et al., *Prophylaxis and treatment of implant-related infections by antibiotic-coated implants: a review*. *Injury*, 2006. **37 Suppl 2**: p. S105-12.
53. Fei, J., et al., *Preparation, release profiles and antibacterial properties of vancomycin-loaded Ca–P coating titanium alloy plate*. *Journal of materials science: Materials in medicine*, 2011. **22**(4): p. 989-995.
54. Neut, D., et al., *A gentamicin-releasing coating for cementless hip prostheses—Longitudinal evaluation of efficacy using in vitro bio-optical imaging and its wide-spectrum antibacterial efficacy*. *Journal of Biomedical Materials Research Part A*, 2012. **100A**(12): p. 3220-3226.

55. Gozzelino, G., et al., *Antibacterial activity of reactive quaternary ammonium compounds in solution and in nonleachable coatings*. J Food Prot, 2011. **74**(12): p. 2107-12.
56. Jung, W.K., et al., *Antibacterial Activity and Mechanism of Action of the Silver Ion in Staphylococcus aureus and Escherichia coli*. Applied and Environmental Microbiology, 2008. **74**(7): p. 2171-2178.
57. Moreno, I., et al., *Modulation of bactericidal action in polymer nanocomposites: light-tuned Ag+ release from electrospun PMMA fibers*. RSC Advances, 2016. **6**(81): p. 78036-78042.
58. Reidy, B., et al., *Mechanisms of Silver Nanoparticle Release, Transformation and Toxicity: A Critical Review of Current Knowledge and Recommendations for Future Studies and Applications*. Materials, 2013. **6**(6): p. 2295.
59. Parisien, A., et al., *Novel alternatives to antibiotics: bacteriophages, bacterial cell wall hydrolases, and antimicrobial peptides*. J Appl Microbiol, 2008. **104**(1): p. 1-13.
60. Bahar, A.A. and D. Ren, *Antimicrobial peptides*. Pharmaceuticals (Basel), 2013. **6**(12): p. 1543-75.
61. Gaiser, R.A., P. López, and L. Rivas, *Production of eukaryotic antimicrobial peptides by bacteria A review*. 2011, Formatex.
62. Sang, Y. and F. Blecha, *Antimicrobial peptides and bacteriocins: alternatives to traditional antibiotics*. Anim Health Res Rev, 2008. **9**(2): p. 227-35.
63. Roach, D.R. and D.M. Donovan, *Antimicrobial bacteriophage-derived proteins and therapeutic applications*. Bacteriophage, 2015. **5**(3): p. e1062590.
64. Waters, E.M., et al., *Phage therapy is highly effective against chronic lung infections with Pseudomonas aeruginosa*. Thorax, 2017.
65. Skurnik, M. and E. Strauch, *Phage therapy: Facts and fiction*. International Journal of Medical Microbiology, 2006. **296**(1): p. 5-14.
66. Ryan, E.M., et al., *Recent advances in bacteriophage therapy: how delivery routes, formulation, concentration and timing influence the success of phage therapy*. J Pharm Pharmacol, 2011. **63**(10): p. 1253-64.
67. Mathur, M.D., S. Vidhani, and P.L. Mehndiratta, *Bacteriophage therapy: an alternative to conventional antibiotics*. J Assoc Physicians India, 2003. **51**: p. 593-6.
68. A, S., *The challenges of bacteriophage therapy*. European Industrial Pharmacy, 2011. **10**(14-18).
69. Sillankorva, S.M., H. Oliveira, and J. Azeredo, *Bacteriophages and Their Role in Food Safety*. International Journal of Microbiology, 2012. **2012**: p. 13.
70. Debarbieux, L., et al., *Bacteriophages can treat and prevent Pseudomonas aeruginosa lung infections*. J Infect Dis, 2010. **201**(7): p. 1096-104.
71. Alemayehu, D., et al., *Bacteriophages ϕ MR299-2 and ϕ NH-4 Can Eliminate Pseudomonas aeruginosa in the Murine Lung and on Cystic Fibrosis Lung Airway Cells*. mBio, 2012. **3**(2).
72. Smith, H.W. and M.B. Huggins, *Successful treatment of experimental Escherichia coli infections in mice using phage: its general superiority over antibiotics*. J Gen Microbiol, 1982. **128**(2): p. 307-18.
73. Rhoads, D.D., et al., *Bacteriophage therapy of venous leg ulcers in humans: results of a phase I safety trial*. J Wound Care, 2009. **18**(6): p. 237-8, 240-3.
74. Wright, A., et al., *A controlled clinical trial of a therapeutic bacteriophage preparation in chronic otitis due to antibiotic-resistant Pseudomonas aeruginosa; a preliminary report of efficacy*. Clin Otolaryngol, 2009. **34**(4): p. 349-57.
75. Lu, T.K. and M.S. Koeris, *The next generation of bacteriophage therapy*. Curr Opin Microbiol, 2011. **14**(5): p. 524-31.
76. Sharp, R., *Bacteriophages: biology and history*. Journal of Chemical Technology & Biotechnology, 2001. **76**(7): p. 667-672.
77. Ackermann, H.W., *Tailed bacteriophages: the order caudovirales*. Adv Virus Res, 1998. **51**: p. 135-201.

78. Pelkonen, S., J. Aalto, and J. Finne, *Differential activities of bacteriophage depolymerase on bacterial polysaccharide: binding is essential but degradation is inhibitory in phage infection of K1-defective Escherichia coli*. Journal of Bacteriology, 1992. **174**(23): p. 7757-7761.
79. Pelkonen, S., J. Pelkonen, and J. Finne, *Common cleavage pattern of polysialic acid by bacteriophage endosialidases of different properties and origins*. J Virol, 1989. **63**(10): p. 4409-16.
80. Jonczyk, E., et al., *The influence of external factors on bacteriophages--review*. Folia Microbiol (Praha), 2011. **56**(3): p. 191-200.
81. Crawford, J.T. and E.B. Goldberg, *The effect of baseplate mutations on the requirement for tail-fiber binding for irreversible adsorption of bacteriophage T4*. Journal of Molecular Biology, 1977. **111**(3): p. 305-313.
82. Montag, D., et al., *Receptor-recognizing proteins of T-even type bacteriophages. Constant and hypervariable regions and an unusual case of evolution*. J Mol Biol, 1987. **196**(1): p. 165-74.
83. Rakhuba, D.V., et al., *Bacteriophage receptors, mechanisms of phage adsorption and penetration into host cell*. Pol J Microbiol, 2010. **59**(3): p. 145-55.
84. Sulakvelidze, A., Z. Alavidze, and J.G. Morris, *Bacteriophage Therapy*. Antimicrobial Agents and Chemotherapy, 2001. **45**(3): p. 649-659.
85. Hughes, K.A., et al., *Bacteriophage and associated polysaccharide depolymerases--novel tools for study of bacterial biofilms*. J Appl Microbiol, 1998. **85**(3): p. 583-90.
86. Stengel, D., et al., *Systematic review and meta-analysis of antibiotic therapy for bone and joint infections*. Lancet Infect Dis, 2001. **1**(3): p. 175-88.
87. Wu, S., et al., *Phage Therapy: Future Inquiries*. Postdoc journal : a journal of postdoctoral research and postdoctoral affairs, 2013. **1**(6): p. 24-35.
88. Azeredo, J. and I.W. Sutherland, *The use of phages for the removal of infectious biofilms*. Curr Pharm Biotechnol, 2008. **9**(4): p. 261-6.
89. Abedon, S., *Bacteriophages and biofilms*, in *Biofilms: Formation, Development and Properties*. 2011, Nova Science Publishers, Inc.
90. Sutherland, I.W., et al., *The interaction of phage and biofilms*. FEMS Microbiol Lett, 2004. **232**(1): p. 1-6.
91. Kutter, E. and A. Sulakvelidze, *Bacteriophage therapy in humans*, in *Bacteriophages: Biology and Applications* 2004, CRC Press. p. 381-436.
92. Markoishvili, K., et al., *A novel sustained-release matrix based on biodegradable poly(ester amide)s and impregnated with bacteriophages and an antibiotic shows promise in management of infected venous stasis ulcers and other poorly healing wounds*. Int J Dermatol, 2002. **41**(7): p. 453-8.
93. Jikia, D., et al., *The use of a novel biodegradable preparation capable of the sustained release of bacteriophages and ciprofloxacin, in the complex treatment of multidrug-resistant Staphylococcus aureus-infected local radiation injuries caused by exposure to Sr90*. Clin Exp Dermatol, 2005. **30**(1): p. 23-6.
94. Curtin, J.J. and R.M. Donlan, *Using bacteriophages to reduce formation of catheter-associated biofilms by Staphylococcus epidermidis*. Antimicrob Agents Chemother, 2006. **50**(4): p. 1268-75.
95. Khalifa, L., et al., *Phage therapy against Enterococcus faecalis in dental root canals*. J Oral Microbiol, 2016. **8**: p. 32157.
96. Semler, D.D., et al., *Aerosol phage therapy efficacy in Burkholderia cepacia complex respiratory infections*. Antimicrob Agents Chemother, 2014. **58**(7): p. 4005-13.
97. Kutateladze, M. and R. Adamia, *Phage therapy experience at the Eliava Institute*. Med Mal Infect, 2008. **38**(8): p. 426-30.

98. Golshahi, L., et al., *Toward modern inhalational bacteriophage therapy: nebulization of bacteriophages of Burkholderia cepacia complex*. J Aerosol Med Pulm Drug Deliv, 2008. **21**(4): p. 351-60.
99. Golshahi, L., et al., *In vitro lung delivery of bacteriophages KS4-M and PhiKZ using dry powder inhalers for treatment of Burkholderia cepacia complex and Pseudomonas aeruginosa infections in cystic fibrosis*. J Appl Microbiol, 2011. **110**(1): p. 106-17.
100. Balasubramanian, S., et al., *Lytic phage as a specific and selective probe for detection of Staphylococcus aureus--A surface plasmon resonance spectroscopic study*. Biosens Bioelectron, 2007. **22**(6): p. 948-55.
101. Handa, H., et al., *Recognition of Salmonella Typhimurium by Immobilized Phage P22 Monolayers*. Surf Sci, 2008. **602**(7): p. 1392-1400.
102. Nanduri, V., et al., *SPR biosensor for the detection of L. monocytogenes using phage-displayed antibody*. Biosens Bioelectron, 2007. **23**(2): p. 248-52.
103. Bennett, A.R., et al., *The use of bacteriophage-based systems for the separation and concentration of Salmonella*. J Appl Microbiol, 1997. **83**(2): p. 259-65.
104. Sun, W., L. Brovko, and M. Griffiths, *Use of bioluminescent Salmonella for assessing the efficiency of constructed phage-based biosorbent*. J Ind Microbiol Biotechnol, 2001. **27**(2): p. 126-8.
105. Tolba, M., et al., *Oriented Immobilization of Bacteriophages for Biosensor Applications*. Applied and Environmental Microbiology, 2010. **76**(2): p. 528-535.
106. Archer, M.J. and J.L. Liu, *Bacteriophage T4 Nanoparticles as Materials in Sensor Applications: Variables That Influence Their Organization and Assembly on Surfaces*. Sensors (Basel, Switzerland), 2009. **9**(8): p. 6298-6311.
107. Serwer, P. and S.J. Hayes, *Agarose gel electrophoresis of bacteriophages and related particles. I. Avoidance of binding to the gel and recognizing of particles with packaged DNA*. ELECTROPHORESIS, 1982. **3**(2): p. 76-80.
108. Anany, H., et al., *Biocontrol of Listeria monocytogenes and Escherichia coli O157:H7 in meat by using phages immobilized on modified cellulose membranes*. Appl Environ Microbiol, 2011. **77**(18): p. 6379-87.
109. Li, Z., et al., *Effect of unassembled phage protein complexes on the attachment to cellulose of genetically modified bacteriophages containing cellulose binding modules*. Colloids Surf B Biointerfaces, 2010. **76**(2): p. 529-34.
110. Pearson, H.A., et al., *Phage-bacterium war on polymeric surfaces: can surface-anchored bacteriophages eliminate microbial infections?* Biomacromolecules, 2013. **14**(5): p. 1257-61.
111. Kühn, K., *Structure and biochemistry of collagen*. Aesthetic Plastic Surgery, 1985. **9**(2): p. 141-144.
112. Gelse, K., E. Pöschl, and T. Aigner, *Collagens—structure, function, and biosynthesis*. Advanced Drug Delivery Reviews, 2003. **55**(12): p. 1531-1546.
113. Ramshaw, J.A., J.A. Werkmeister, and V. Glattauer, *Collagen-based biomaterials*. Biotechnol Genet Eng Rev, 1996. **13**: p. 335-82.
114. Du, C., et al., *Formation of calcium phosphate/collagen composites through mineralization of collagen matrix*. J Biomed Mater Res, 2000. **50**(4): p. 518-27.
115. Bianchi, E., et al., *The role of pH, temperature, salt type, and salt concentration on the stability of the crystalline, helical, and randomly coiled forms of collagen*. J Biol Chem, 1967. **242**(7): p. 1361-9.
116. Freudenberg, U., et al., *Electrostatic interactions modulate the conformation of collagen I*. Biophys J, 2007. **92**(6): p. 2108-19.
117. Vepari, C. and D.L. Kaplan, *Silk as a biomaterial*. Progress in Polymer Science, 2007. **32**(8-9): p. 991-1007.

118. Asakura, T., et al., *Heterogeneous structure of silk fibers from Bombyx mori resolved by ¹³C solid-state NMR spectroscopy*. J Am Chem Soc, 2002. **124**(30): p. 8794-5.
119. Matsumoto, A., et al., *Mechanisms of silk fibroin sol-gel transitions*. J Phys Chem B, 2006. **110**(43): p. 21630-8.
120. Zhou, C.Z., et al., *Silk fibroin: structural implications of a remarkable amino acid sequence*. Proteins, 2001. **44**(2): p. 119-22.
121. Pérez-Rigueiro, J., et al., *Mechanical properties of single-brin silkworm silk*. Journal of Applied Polymer Science, 2000. **75**(10): p. 1270-1277.
122. Arai, T., et al., *Biodegradation of Bombyx mori silk fibroin fibers and films*. Journal of Applied Polymer Science, 2004. **91**(4): p. 2383-2390.
123. Minoura, N., et al., *Attachment and growth of cultured fibroblast cells on silk protein matrices*. Journal of Biomedical Materials Research, 1995. **29**(10): p. 1215-1221.
124. Inouye, K., et al., *Use of Bombyx mori silk fibroin as a substratum for cultivation of animal cells*. J Biochem Biophys Methods, 1998. **37**(3): p. 159-64.
125. Hu, K., et al., *Biocompatible Fibroin Blended Films with Recombinant Human-like Collagen for Hepatic Tissue Engineering*. Journal of Bioactive and Compatible Polymers, 2006. **21**(1): p. 23-37.
126. Yeo, I.-S., et al., *Collagen-Based Biomimetic Nanofibrous Scaffolds: Preparation and Characterization of Collagen/Silk Fibroin Bicomponent Nanofibrous Structures*. Biomacromolecules, 2008. **9**(4): p. 1106-1116.
127. Lv, Q., et al., *Fibroin/collagen hybrid hydrogels with crosslinking method: preparation, properties, and cytocompatibility*. J Biomed Mater Res A, 2008. **84**(1): p. 198-207.
128. Lu, Q., et al., *Preparation of three-dimensional fibroin/collagen scaffolds in various pH conditions*. J Mater Sci Mater Med, 2008. **19**(2): p. 629-34.
129. Lv, Q., et al., *Preparation of insoluble fibroin/collagen films without methanol treatment and the increase of its flexibility and cytocompatibility*. Journal of Applied Polymer Science, 2008. **109**(3): p. 1577-1584.

2. Chapter Two

Phase behaviour and miscibility studies of Collagen/Silk Fibroin macromolecular system in dilute solutions and solid state

*Ima Ghaeli 1,2,3,**, *Mariana A. de Moraes 4,5*, *Marisa M. Beppu 4*, *Katarzyna Lewandowska 6*,
Alina Sionkowska 6, *Frederico Ferreira-da-Silva 1,7*, *Maria P. Ferraz 8* and *Fernando J. Monteiro 1,2,3,**

¹ i3S—Instituto de Investigação e Inovação em Saúde, Universidade do Porto, Rua Alfredo Allen, 208, 4200-135 Porto, Portugal; ffsilva@ibmc.up.pt

² INEB—Instituto de Engenharia Biomédica, Universidade do Porto, Rua Alfredo Allen, 208, 4200-135 Porto, Portugal

³ FEUP, Faculdade de Engenharia, Departamento de Engenharia Metalurgia e Materiais, Universidade do Porto, 4200-465 Porto, Portugal

⁴ School of Chemical Engineering, University of Campinas, 13083-852 Campinas, Brazil; mamoraes@unifesp.br (M.A.d.M.); beppu@feq.unicamp.br (M.M.B.)

⁵ Department of Chemical Engineering, Federal University of São Paulo, 09913-030 Diadema, Brazil

⁶ Nicolaus Copernicus University in Toruń, Faculty of Chemistry, Department of Chemistry of Biomaterials and Cosmetics, ul. Gagarina 7, 87-100 Toruń, Poland; reol@chem.umk.pl (K.L.); as@chem.umk.pl (A.S.)

⁷ IBMC—Instituto de Biologia Molecular e Celular, Universidade do Porto, Rua Alfredo Allen, 208, 4200-135 Porto, Portugal

⁸ FP-ENAS/CEBIMED, University Fernando Pessoa Energy, Environment and Health Research Unit/Biomedical Research Center, 200-150 Porto, Portugal; mpferraz@ufp.edu.pt

*Correspondence: ema.ghaeli@gmail.com (I.G.); fjmont@fe.up.pt (F.J.M.); Tel.: +351-220-408-800 (F.J.M.)

Received: 18 July 2017; Accepted: 16 August; Published: 18 August 2017

Abstract

Miscibility is an important issue in biopolymer blends for analysis of the behavior of polymer pairs through the detection of phase separation and improvement of the mechanical and physical properties of the blend. This study presents the formulation of a stable and one-phase mixture of collagen and regenerated silk fibroin (RSF), with the highest miscibility ratio between these two macromolecules, through inducing electrostatic interactions, using salt ions. For this aim, a ternary phase diagram was experimentally built for the mixtures, based on observations of phase behavior of blend solutions with various ratios. The miscibility behavior of the blend solutions in the miscible zones of the phase diagram was confirmed quantitatively by viscosimetric measurements. Assessing the effects of biopolymer mixing ratio and salt ions, before and after dialysis of blend solutions, revealed the importance of ion-specific interactions in the formation of coacervate-based materials containing collagen and RSF blends that can be used in pharmaceutical, drug delivery, and biomedical applications. Moreover, the conformational change of silk fibroin from random coil to beta sheet, in solution and in the final solid films, was detected by circular dichroism (CD) and Fourier transform infrared spectroscopy (FTIR), respectively. Scanning electron microscopy (SEM) exhibited alterations of surface morphology for the biocomposite films with different ratios. Surface contact angle measurement illustrated different hydrophobic properties for the blended film surfaces. Differential scanning calorimetry (DSC) showed that the formation of the beta sheet structure of silk fibroin enhances the thermal stability of the final blend films. Therefore, the novel method presented in this study resulted in the formation of biocomposite films whose physico-chemical properties can be tuned by silk fibroin conformational changes by applying different component mixing ratios.

Keywords: biopolymers; protein-protein interaction; silk fibroin; miscibility; coacervation

2.1 Introduction

Miscible blending of two biopolymers with different physicochemical characteristics is an interesting route to produce new biomaterials with unique properties that may present the advantages of each single polymer and compensate the disadvantages over each one. The films prepared from blends of natural polymers can potentially be used in wound healing and skin tissue engineering applications [1, 2]. The presence of proteins as natural macromolecules in blends may improve cell adhesion, due to the presence of more protein binding sites [3]. However, native physical structures of proteins such as collagen with linear triple helix, limits its possible intra- and interchain interactions in blends [4, 5]. The forces found in protein interactions are electrostatic, Van der Waals, hydrogen bonds, hydrophobic and steric interactions, of which the electrostatic interactions are predominant [6]. Parameters such as pH and ionic strength may

affect electrostatic interactions, whereas, temperature may have influence on hydrophobic and hydrogen bindings [7, 8]. However, temperature induces protein denaturation. For example, heating collagen induces the cleavage of the intermolecular hydrophobic and hydrogen bonds, transforming collagen triple helix into a randomly coiled form, allowing fibril formation and interactions with other proteins [9]. This work has been focused on blending of collagen and silk fibroin as two relevant biomaterials showing high potential to be used for producing protein-based biocomposite films.

Collagen as a biomaterial is a key player in biomedical applications. Collagen acts as a natural scaffold for cells proliferation and has adequate mechanical strength, good biocompatibility, biodegradability, and ability to promote cellular attachment and growth. In addition, different functional groups along the collagen backbone may promote incorporation growth factors and other biological molecules [10]. Preservation of collagen native structure in biomedical applications may be of importance, since the collagen triple helix network may withstand the mechanical stresses through transmitting the forces and dissipating energy [11]. Moreover, the triple helix characteristics such as high stability in biological environment, binding ligands for cell surface receptors and essential signals to influence cell activity [12, 13], highlights the importance of protecting such conformational integrity for functional applications.

On the other hand, silk fibroin presents several interesting properties such as excellent toughness and stiffness combined with low density. The high mechanical strength of silk fibroin attracted the attention of several researchers. The crystalline structure of native silk fibroin gives it a very hydrophobic character. Even though silk fibroin has good mechanical properties, the biomedical applications require other desired properties such as high water retention capability and biodegradability which are absent in the native silk fibroin. Hence, it is adequate to increase the amount of amorphous structure of fibroin molecules by dissolving fibers, disrupting the hydrogen interactions and inducing the transitions of fibroin to random coil conformation that results in regenerated silk fibroin solution (RSF) [14]. Solubility of native silk fibroin depends on the organic salts which participate in the disruption of hydrogen bonds. Foo et al. [15], revealed that the hydrophilic parts of silk fibroin stabilized by Ca^{2+} or other ions, cause the aggregation of fibroin molecules into hydrophilic regions, forming a gel through ionic cross links. Water molecules absorbed by hydrophilic regions restrain the premature crystallization of the hydrophobic domains. The highly concentrated salt solutions of silk fibroin have to be dialyzed in order to remove the salts and make it adequate for preparation of SF-based materials [16].

The mechanism of fibroin self-assembly during dialysis has been described by several researchers [17, 18], and the influence of various parameters such as concentration [19], temperature [20] and ethanol content [21] on RSF self-assembly, have been analyzed. Jin et al. [17] suggested a micellar structure pattern for silk fibroin chains in water in which the small hydrophilic parts of silk fibroin remain hydrated, while the large termini hydrophilic parts are located at the outer edge of micelles and the hydrophobic parts are

placed between those two hydrophilic blocks [17]. Hence, the regenerated silk fibroin solution after dialysis is water-soluble and metastable until the hydrophobic parts of micelles join together and eventually form gels. Even though RSF is a promising material with specific biological and functional characteristics, its partially amorphous structure, along with its limited solubility, restrain the applications of this biomaterial. Hence, blending with other biomaterials is a useful way to improve the properties of RSF [19].

Several studies on collagen/silk fibroin blends showed not only the improvement in mechanical properties of the final materials, but also favourable environment of the mixtures for cell attachment and proliferation. Nevertheless, the blends were restricted to low collagen concentration or COL/RSF ratios, or to be able to incorporate higher collagen ratios, high temperatures are required that denature collagen triple helix and facilitate the hydrogen bonding between the two biopolymers [21-27]. However, inducing electrostatic interactions between these two biopolymers, which has not been used up to now, may avoid the risk of the undesirable denaturation of collagen as the result of increasing the temperature. Hence, dialysis procedure can be an appropriate approach to obtain the electrostatic binding of the two polymers through salt diffusion during dialysis. Incorporation of other molecules in the dialysis tube containing silk fibroin may induce hydrophobic or electrostatic interactions to occur, depending on the structure and net charge of the other compounds. Gradual release of salt ions existing among silk fibroin chains yields to the reduction of silk fibroin chain dissociation during dialysis. Hence, depending on the electrical or hydrophobic properties of the incorporated molecules, the hydrogen or electrostatic interactions may occur between silk fibroin chains and the mixed molecules. Aiming at preserving the collagen natural structure, this study tries to present a new method based on electrostatic interactions, for templating protein-protein interactions between collagen and regenerated silk fibroin macromolecules, in dilute solutions and in solid thin films. Considering the importance of salt for electrostatic interactions, three single-phase compositions of COL/RSF with 75/25, 50/50, and 25/75 volume ratios (V/V) before dialysis, were prepared according to their phase diagram and dialyzed against distilled water. Different blends were obtained and physico-chemically characterized after dialysis.

2.2 Experimental

2.2.1 *Sample preparation*

Collagen solution was prepared by dissolving type I bovine collagen (Bovine Achilles tendon, Sigma-Aldrich, St. Louis, Missouri, USA) in 0.5 mol/L acetic acid to the final concentration of 0.5% (w/v%) and stirring with high speed Turrax (T25D, IKA®, Janke and Kunkel IKA-Labortechnik, Staufen, Germany) at 10,000 rpm and 4 °C for 2-3 hours.

B. mori silk fibroin was prepared by initially degumming process through boiling silkworm cocoons in Na₂CO₃ solution at 1 g/L for 30 min at 85 °C. This procedure was repeated two times and at last, the cocoons

were boiled in distilled water for 30 min in order to separate the glue-like sericin from fibroin. After adequate washing with distilled water, the obtained silk fibroin fibers were dried at room temperature. Finally, silk fibroin agglomerates were milled to facilitate their dissolution process. Silk fibroin was dissolved in solution of ternary solvent containing $\text{CaCl}_2:\text{CH}_3\text{CH}_2\text{OH}:\text{H}_2\text{O}$ (1:2:8 molar ratio), at 85 °C in order to obtain the final concentration of 0.5% (w/v%). The fibroin solution was dialyzed against distilled water for 72 h.

2.2.2 Ternary phase diagram and blend preparation

Considering the key role of salt ions in ternary solvent for inducing the ionic interactions between protein chains in solvent, the ternary phase diagram of collagen, RSF and ternary solvent at 4 °C (in order to prevent collagen denaturation) was analysed. Aiming at obtaining different Col/RSF ratios of 100/0, 75/25, 50/50, 25/75 and 0/100, collagen/RSF/ternary solvent blends were prepared by selecting the relevant points in single phase region of ternary phase diagram. Identifying volume fractions of each component ($X_{\text{component}}=V_{\text{component}}/V_{\text{total}}$), the single phase blends were prepared, at 4 °C. Later, the blended solutions were dialyzed against distilled water for three days. The resultant solutions were dried in polystyrene dishes at room temperature to obtain the blended films in the solid state.

2.2.3 Miscibility and ζ -potential analysis

In order to assess the miscibility, the viscosity behaviour of mixtures in the single-phase region of ternary phase diagram, was analysed at 25 ± 0.1 °C by Ubbelohde capillary viscometer (NCU Laboratory, Toruń, Poland). According to the intended blend ratios, different mass fractions of each polymer solution have been mixed. The intrinsic viscosity and the viscosity interaction parameter of each polymer solution as well as the ternary systems (collagen/RSF/ternary solvent) were obtained and used to estimate the miscibility of polymer mixtures through classical dilution method. Thus, each solution was prepared and diluted with NaCl (0.1 mol/L) to yield lower concentrations. The relative viscosities of blends were obtained by dividing solutions flow times by the value found for pure solvent (NaCl 0.1 mol/L). The intrinsic viscosity, the interaction parameter and Huggins coefficient values were determined according to Huggins equation using solutions of several concentrations.

The values of experimental interaction parameter for all the blends, using diluted regime with solutions of 5 concentrations, were obtained from the plot of η_{sp}/c vs c (mass concentration, in g/mL) using Equation (1).

$$\frac{(\eta_{sp})_m}{c_m} = [\eta]_m^{exp} + b_m^{exp} c_m \quad (1)$$

Where, $(\eta_{sp})/c$ is the reduced viscosity b_m^{exp} is the experimental viscosity interaction parameter of polymer mixture, $[\eta]_m^{exp}$ is the experimental intrinsic viscosity of the polymer blends and c_m is the total concentration of solution.

The ideal values in this study were determined according to the Krigbaum and Wall [28], and Garcia [29] techniques. The ideal interaction parameter of b_m^{id} have been determined by Krigbaum and Wall through Equation (2).

$$b_m^{id*} = b_A w_A^2 + b_B w_B^2 + 2b_{AB}^{id} w_A w_B \quad (2)$$

Where w_A and w_B are the weight fractions of polymers A and B, respectively, and b_A and b_B are the interaction parameters of each individual polymer which were obtained from the slope of the plots of the reduced viscosity versus concentration. b_{AB} , the interspecific interaction parameter that was obtained by Equation (3).

$$b_{AB}^{id} = b_A^{1/2} b_B^{1/2} \quad (3)$$

The ideal interaction parameter by Garcia et al. [29], was calculated through Equation (4).

$$b_m^{id**} = b_A w_A^2 + b_B w_B^2 \quad (4)$$

The polymer mixture is miscible if $\Delta b_m = b_m^{exp} - b_m^{id} \geq 0$ and immiscible if $\Delta b_m = b_m^{exp} - b_m^{id} < 0$.

This viscometry analysis was done for all the mixtures after dialysis procedure. Thus, the solutions after dialysis have been passed through the gas and vacuum filters. The remaining solutions after filtration have been passed through two calibrated markers of the Ubbelohde viscometer, and the time has been measured.

The ζ -potential analysis was done for all solutions before and after dialysis through measuring electrophoretic mobility by ZetaPALS (Brookhaven Instruments Corporation, Holtsville, NY, USA), as temperature was maintained at 25 °C.

2.2.4 Light stereoscopic magnifier microscope

The blend mixtures after dialysis procedure were observed and optical images were collected from the Leica EC3 stereo microscope equipped with Leica LAS Software (Leica, Wetzlar, Germany). The mixtures in their containers were placed on a stage with a dark base and the pictures of the blend solutions were captured using the digital camera zoomed onto the solutions as closely as possible.

2.2.5 Structure of collagen/silk fibroin blended solutions and films after dialysis

The structures of blended solutions after dialysis, were analysed by circular dichroism (CD) using a J-815 (Jasco, Tokyo, Japan) spectrometer. Far-UV CD spectra were recorded between 190 and 260 nm using a 1 mm path length cuvette. CD spectra were acquired with a scanning speed of 100 nm/min, integration time of 1 s, and using a bandwidth of 1 nm. The spectra were averaged over eight scans and corrected by subtraction of the buffer signal. Spectra of silk fibroin in the mixtures were obtained by subtraction of pure

collagen (Col/RSF 100/0 blend) spectrum from the mixture spectra. The results are expressed as the mean residue ellipticity Θ_{MRW} , defined as Equation (5).

$$\Theta_{MRW} = \Theta_{obs}(0.1MRW)/(lc) \quad (5)$$

Where Θ_{obs} is the observed ellipticity (mdeg), MRW is the mean residue weight (g/mol), c is the concentration (mg/ml), l is the light path length (cm) and Θ_{MRW} is the mean residue ellipticity (deg.cm²/dmol). MRW was calculated from data (MW and number of aminoacids) in the UniProt database as 76.1 for Silk Fibroin and 94.9 for collagen.

The structures of blended films were assessed by scanning electron microscopy (SEM), contact angle measurements, Fourier transform infrared spectroscopy (Perkin-Elmer 2000 FTIR spectrometer, Hopkinton, MA, USA), and differential scanning calorimetry (Setaram DSC 131, Caluire-et-Cuire, France). For scanning electron microscopy (SEM), samples were coated with an Au/Pd thin film, by sputtering, using an SPI module sputter coater. The SEM analysis was performed using a high resolution (Schottky) environmental scanning electron microscope (FEI Quanta 400 FEG ESEM, Hillsboro, OR, USA). In order to analyze surface hydrophobicity, contact angle measurements were done using a digital imaging capture system (OCA 15, DataPhysics Instruments GmbH, Filderstadt, Germany). For this reason, the sessile drop method with distilled water at 25 °C was used and the contact angle was calculated using software version SCA 20. Thermal analysis of the prepared films has been performed using a Setaram DSC 131, from 25–450 °C at a scan rate of 10 °C/min with nitrogen flow of 50 mL/min. Moreover, FTIR analysis were carried out in the spectral range of 400–4000 cm⁻¹ using a Perkin Elmer FTIR spectrophotometer model 2000, equipped with an ATR diamond cell accessory.

2.3 Results

2.3.1 Miscibility study of collagen/silk fibroin

In this study, ternary solvent containing salt ions was used in order to induce electrostatic interactions between collagen and RSF chains and obtain miscible or semi-miscible blends.

The borderline mixing ratio points of collagen/RSF/ternary solvent, were obtained by blending the different volumes of component, and the points were plotted in the ternary phase diagram as shown in Figure 1. The miscible solutions can be identified in the single phase region, while phase-separated solutions (which can be easily visually observed as the fibrils start to be formed) are indicated as the two phase region.

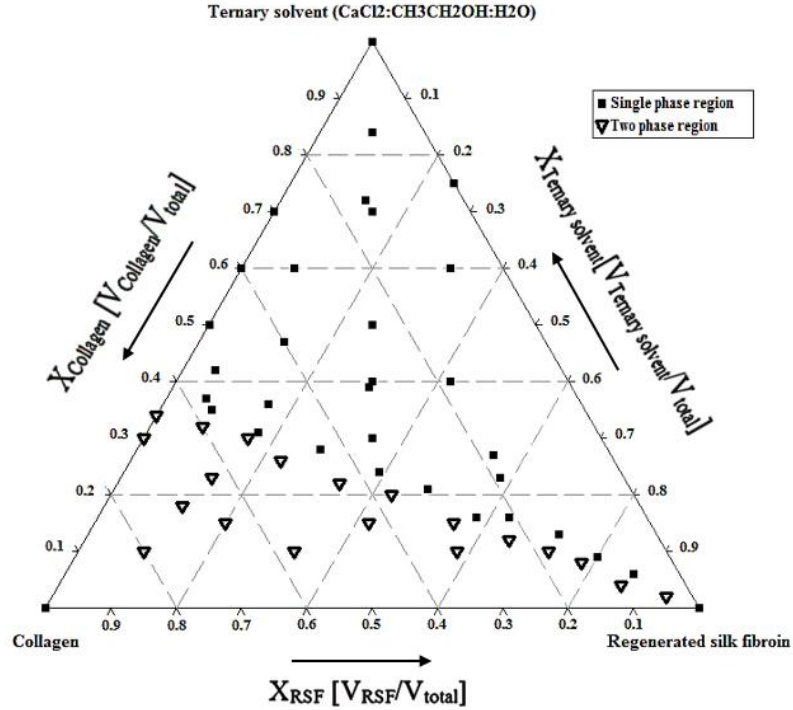


Figure 2.1: Ternary phase diagram of collagen/RSF/ternary solvent at 4 °C.

Regarding the polyelectrolyte nature of the involving proteins in this research, the electrostatic interaction between cationic amino groups of collagen and anionic groups of silk fibroin, and high calcium content, are the main cause of polyelectrolyte complex (PEC) formation.

The ζ potential measurements brought detailed understanding into the composition of charged groups in the mixture blends. Therefore, solutions with different mixing ratios according to the single phase region in ternary phase diagram were measured and the results are shown in Table 2.1.

The net charge of all blends in the single phase region, is around zero, corresponding to almost electroneutrality of the solutions due to high amount of salt. As shown in Table 2.1, the amount of ζ potential is negative for solutions containing more silk fibroin, which is attributed to higher amounts of silk chains with negative groups.

Sample	Zeta potential (mV)
Collagen solution in acetic acid (0.5%)	39.06
Col/SF: 75/25	1.41
Col/SF: 50/50	3.12
Col/SF:25/75	-0.497

Table 2.1: ζ potential of collagen/RSF blends.

The quantitative analysis of miscibility by viscosimetry has been done by calculating the miscibility parameter (Δb_m) as well as relative and reduced viscosities, both theoretically (by methods of Krigbaum and Wall [28], and Garcia [29]), and experimentally and plotted against solution concentration.

The theoretical and experimental values for pure collagen and silk fibroin and their blends are shown in Table 2.2. The positive miscibility parameter for all the blends indicates good miscibility for all prepared blends which is due to the electrostatic interactions between chains and calcium ions, making the whole mixture more stable.

$W_{\text{Collagen}}(0.5\%)$	$[\eta]_m^{\text{exp}}$ (dL/g)	$[\eta]_m^{\text{id}}$ (dL/g)	$\Delta[\eta]_m$	b_m^{exp} (dL/g) ²	$b_m^{\text{id}*}$ (dL/g) ²	Δb_m^*	$b_m^{\text{id}**}$ (dL/g) ²	Δb_m^{**}
1($W_{\text{silk fibroin}} : 0$)	2.48			38.44				
0.75	6.47	2.06	4.41	72.41	30.04	42.37	21.64	50.77
0.5	3.54	1.94	1.6	75.91	20.87	55.04	9.67	66.24
0.25	1.78	1.23	0.55	39.54	10.94	28.6	2.54	37.0
0($W_{\text{silk fibroin}} : 1$)	0.81			0.2433				

$b_m^{\text{id}*}$: determined according to Krigbaum and Wall [28]. $b_m^{\text{id}**}$: determined according to Garcia et al. [29]

Table 2.2: Theoretical (by Krigbaum [28] and Garcia [29] methods) and experimental values for pure collagen, pure silk fibroin and the mixtures

In a highly soluble polyelectrolyte mixture containing high amount of salt, the individual chains of each polyelectrolyte are separated from each other, with salt ions placed among them that yields to the rising of solution viscosity [30]. Increasing salt concentration in the complex system leads to the screening of the electrostatic interactions between two macromolecules, as well as the rearrangement of the polymer chains that may raise the viscosity of solution [31].

Figure 2.2 shows the reduced viscosity versus the concentration for pure collagen, pure silk fibroin and their blends. Silk fibroin in ternary solvent has the lowest viscosity of all the solutions due to the solvation of fibroin chains by calcium ions of the ternary solvent. The viscosity of the primary mixtures with 25%, 50% and 75% of collagen (without adding the dilution solvent), is higher than the viscosity of pure silk fibroin and pure collagen.

Mixtures with more collagen content, have higher ionic strength and viscosity. Therefore, initial mixtures with 75% and 50% collagen were more viscous than the others. Besides, the reduced viscosities

of mixtures with 50% and 75% collagen show close values, both above the values for other solutions, illustrating the high ionic strength in these solutions.

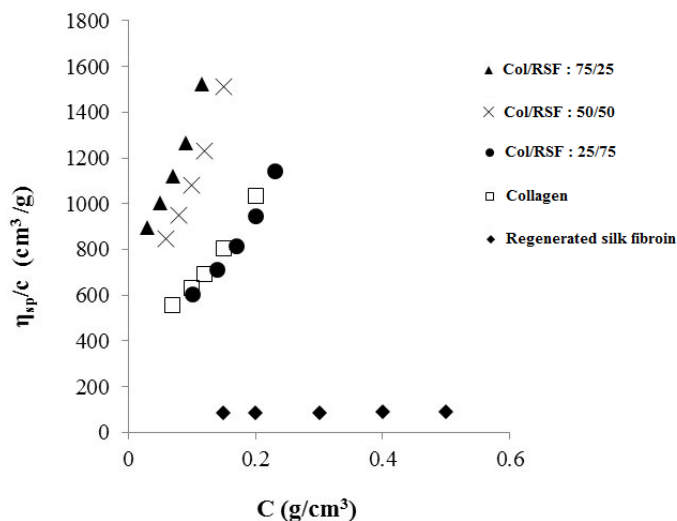


Figure 2.2: Reduced viscosity versus concentrations of collagen/RSF solutions.

However, introducing NaCl solution as the diluting solvent to the aqueous system of proteins containing high calcium ions increases the probability of gradual precipitation after second time dilution. The imbalance of salt concentration among protein chains and the outside medium through dilution causes the calcium diffusion towards the medium by osmotic pressure. Moreover, the likelihood of Ca^{2+} ions displacement by Na^{+1} , in the sites requiring the ions in a dehydrated state, alters the conformation of binding sites, which is due to the Kosmotropic behaviour of NaCl, together with the prevention of binding sites by calcium ions [32]. In view of these considerations, the precipitation caused by dilution can be controlled by careful selection of the added volume of the NaCl solution.

2.3.2 Phase change after collagen/silk fibroin dialysis

Slow diffusion of calcium salt through dialysis procedure, during 3 days, changes the phase behaviour of mixtures from a homogeneous solution to a coacervate or a precipitate, depending on the degree of neutralization. The phase behaviour after the last day of dialysis, when only residual salt amount may be present, shows a liquid-solid phase separation through formation of white solid complex coacervates or precipitates, for all the mixtures, which could be easily identified by naked-eye and optical microscope. This solid-liquid phase separation occurs because the removal of salt ions through the dialysis membrane increases the interaction of proteins COO^{-} and NH_3^{+} ionic groups.

Figure 2.3 shows optical stereoscopic microscope images of blend mixtures after dialysis for 3 days. It should be noted that all the mentioned ratios correspond to those before dialysis procedure. As shown in Figure 2.3, the aggregates size increases with increasing amount of silk fibroin, while fibril formation occurred in all the mixtures.

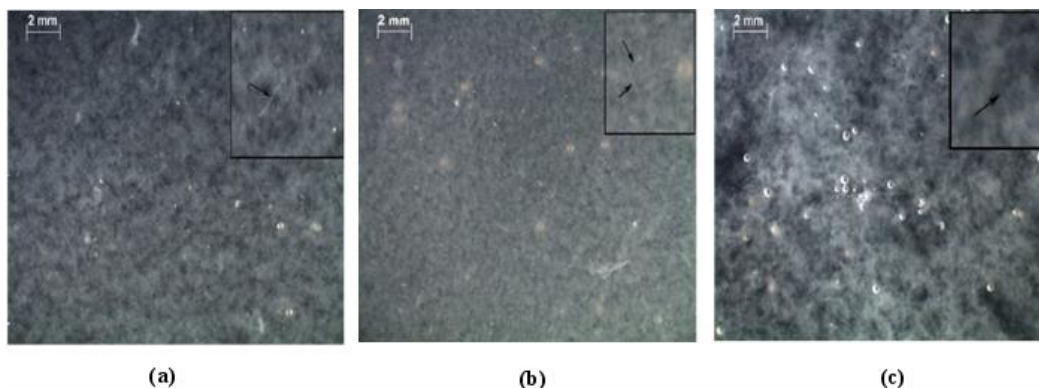


Figure 2.3: Optical microscope images of blend solutions after dialysis with the starting ratios (before dialysis) of, (a) Col/RSF: 75/25, (b) Col/RSF: 50/50, (c) Col/RSF: 25/75. Arrows indicates fibril formation in the system

To study the effect of dialysis (salt removal) on coacervate complexes, ζ potential has been used, and the results for the solutions after dialysis are presented in Table 2.3. The results show that dialysis procedure increased the charge density of solutions, leading to stronger attractive interactions among oppositely charged polyelectrolytes. The positive charge density for all the mixtures indicates the excess of NH_3^+ groups, which increases with increasing the collagen ratio. However, the ζ potential for silk fibroin rich mixture is lower than the other ones, which can be related to higher amount of silk fibroin negative charges in the mixture.

Sample	Zeta potential (mV)
Silk fibroin after dialysis	-5.96
Col/RSF: 75/25 (after dialysis)	10.26
Col/RSF:50/50 (after dialysis)	9.03
Col/RSF:25/75 (after dialysis)	5.36

Table 2.3: ζ potential of collagen/RSF blends after dialysis (the ratios are those before dialysis)

The ζ potential results are in agreement with optical images (Figure 2.3), proving that blend solutions of 75% and 50% collagen with high charge densities (Figures 2.3-a and 2.3-b), contain aggregates possessing charge-charge repulsion which inhibits their assembly. However, lower charge density of solution with higher silk fibroin ratio yields less repulsion and more aggregate assembly through hydrophobic interactions (Figure 2.3-c).

Finally, in order to confirm that the coacervate particles contain the complex of proteins, all the mixtures after dialysis procedure (as shown in Figure 2.3) have been passed through the gas and vacuum filters. Thereafter, the remaining solutions after filtration have been passed through two calibrated markers of the Ubbelohde viscosimeter, and the time has been measured. The RSF solution after dialysis with the reduced concentration from 0.5% to 0.17%, due to the dilution during 3 days of dialysis, showed a passing time of 111.16 (s) (without any filtration). Table 2.4 shows that, during 3 days of dialysis, all the aqueous solutions remaining after filtration, present a passing time (s) close to that of distilled water, illustrating that the coacervate particles remaining behind the filters were protein complexes.

Dialysis days	Col/RSF:75/25	Col/RSF:50/50	Col/RSF: 25/75	Water
Day 1	49.22 (s)	50.94 (s)	51.38 (s)	46.58 (s)
Day 2	48.59 (s)	49.32 (s)	49.95 (s)	46.58 (s)
Day 3	47.21 (s)	48.26 (s)	49.65 (s)	46.58 (s)

Table 2.4: Passing time (s) of the collagen/RSF solutions after filtrations (all the ratios are those before dialysis)

Slightly higher amount of solutions passing time than that of water may be due to the presence of remaining calcium ions in solution after interaction of collagen/RSF. Studies on the effect of lithium ions on silk fibroin films [33] confirmed that even after 72 days of dialysis, the salt ions cannot be removed completely. The passing time is higher for the 1th day and decreases on the 2nd and 3rd days, respectively. After release of high salt levels during the 1th day, the gradual release during the 2nd and 3rd days is a combination of concentration gradient and the result of gradual electrostatic and hydrophobic interactions between the two polymers as well as the fibroin fibrillation. Due to the not-fully neutralized coacervates, these calcium ions may be electrostatically weakly bonded to the opposite charged free residues of the proteins inside the dialysis tube and therefore have more tendency to stay inside the dialysis tube rather than being removed to the water bath. However, more detailed studies are required to assess the amount of salt and non-mixed proteins in the remaining solutions after filtration.

2.3.3 Structural characteristics of collagen/silk fibroin blend solutions and solid films

After preparation of the blended films through drying of solutions at room conditions, their structures were analyzed via SEM, FTIR, DSC, and contact angle.

As can be seen in Figure 2.4, SEM images show a rough surface for collagen (Figure 2.4a) while a smooth surface for RSF (Figure 2.4e). According to the Col/SF ratios, significant changes in film surface morphology could be observed upon mixing RSF with collagen. Blended film with more collagen (Figure 2.4b) showed a surface similar to the collagen film (Figure 2.4a). However, the surface of the blended film with more silk fibroin (Figure 2.4d) has less roughness than the other ones. The fibrous-like structure could be observed for Col/RSF: 50/50 (Figure 2.4c), which confirms the previous results of optical microscopy (Figure 2.3).

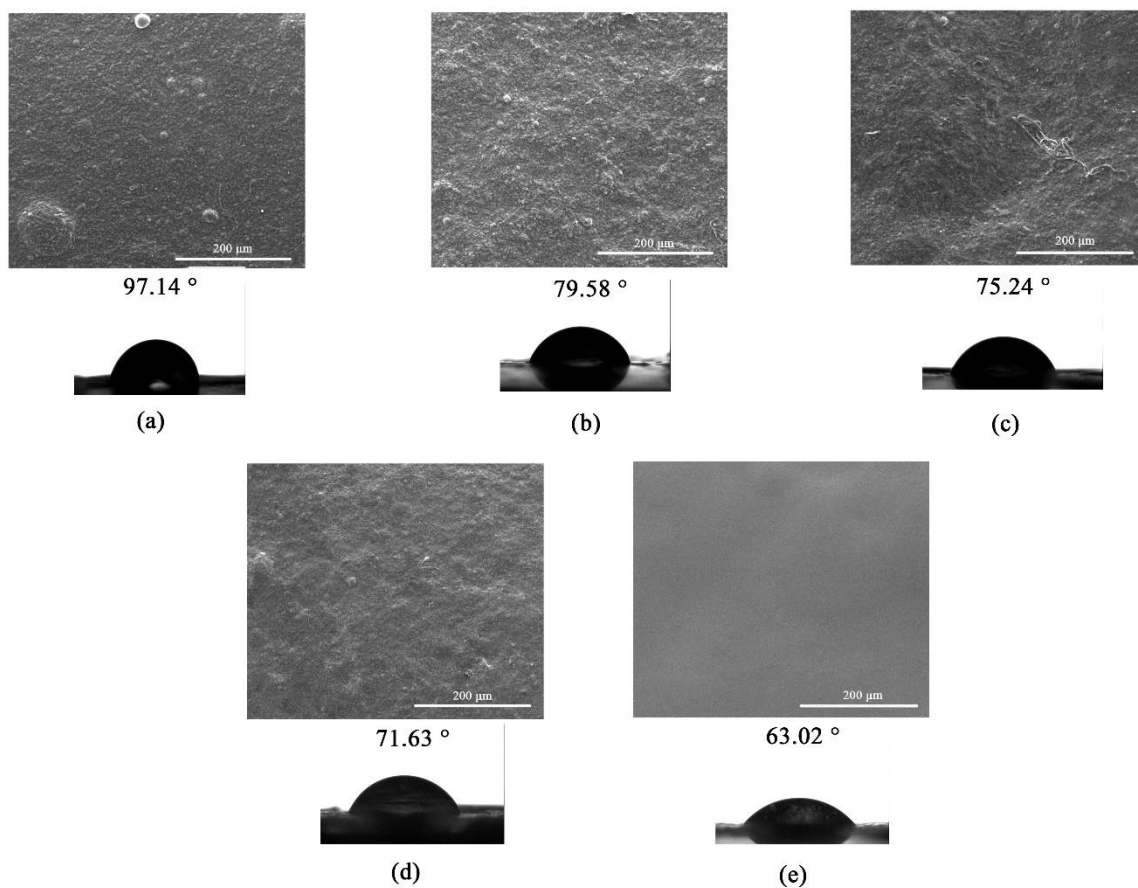


Figure 2.4: Scanning electron microscopy (SEM) and water contact angle images of blended films: (a) Collagen; (b) Col/RSF: 75/25; (c) Col/RSF: 50/50; (d) Col/RSF: 25/75; and (e) RSF at 500× magnification.

Moreover, the contact angle measurements of the films' surfaces shown in Figure 2.4 revealed that the RSF film had the highest hydrophilicity, and the hydrophilicity of blended films were in the range between

pure silk fibroin and pure collagen. The results indicated that the hydrophilicity of the blended films improved with increasing the regenerated silk fibroin proportions. The observation demonstrated that the regenerated silk fibroin has significant influence on the wettability of the blended surfaces, which can be explained by the entanglement of RSF molecules and the exposure of their hydrophilic groups, which may be arranged on the surface of RSF chains [34].

Figure 2.5 present the DSC curves of the prepared films. Collagen presents an endothermic peak at around 57 °C, attributed to the evaporation of unbounded water molecules and the denaturation of collagen fibrils [35]. However, the very small endothermic peak at around 308 °C corresponds to the breaking of hydrogen bonds between alpha chains and to collagen transformation from triple helix to random coil structure [36]. Regenerated silk fibroin presents a tiny endothermal peak at around 62 °C, that is related to the loss of unbound water molecules. The second endothermal peak is at around 330 °C, attributed to the thermal degradation of silk fibroin chains.

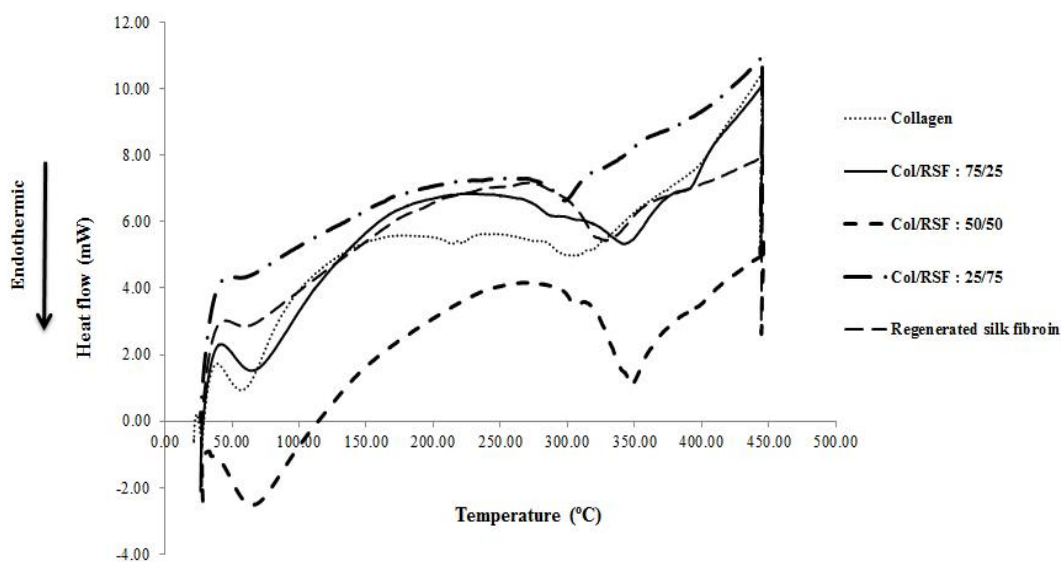


Figure 2.5: DSC curve of collagen/RSF blend films

The absence of denaturation peak in the blend film containing higher silk fibroin ratio, shows the persistence of silk fibroin beta sheet structure in protection of collagen from denaturation through presumable covering of collagen chains while limiting the space for collagen triple helix motion. However, the existence of denaturation peak for other mixtures indicated that the collagen triple helix structure is maintained in those blend films. Thermal denaturation peaks in such blends shifted towards higher temperatures (65-67 °C) compared to collagen sample, demonstrating higher stability of collagen triple

helix. Thermal degradation of collagen/RSF mixtures with ratios of 75/25, 50/50 and 25/75 occurred at 342 °C, 348 °C (sharp peak), and 298 °C (small peak), respectively. The sample with higher silk fibroin ratio shows a tiny endothermic peak which is attributed to the molecular motions of alpha helix chains within the small amorphous regions. However, the absence of degradation peaks illustrates dominating silk fibroin beta sheet conformation. Nevertheless, mixtures with 50% and 75% collagen, show larger decomposition peak at higher temperatures, indicating that thermal decomposition is the sum of heat adsorbed to degrade the hydrogen bonds in both collagen triple helix and the beta sheet structure of silk fibroin. In addition to the decomposition at higher temperature for the mixture with 50% collagen, the large observed decomposition peak may be the proof of existence of more amorphous regions with alpha helix structures. Overall, decomposition of mixtures at higher temperatures than that of silk fibroin can be due to the beta sheet structures of silk fibroin in the blend films that is along with higher thermal stability.

Figure 2.6 shows FTIR spectra of Collagen/RSF blend films as well as the individual polymer films. As reported in the literature, the spectral properties of silk fibroin showed two different structures of silk I and silk II, which are known to be rich in helical and beta-sheets, respectively. The spectral ranges of amide I (C=O and C-N stretching), amide II (N-H bending) and amide III (C-N stretching) are reported as 1655-1660 cm^{-1} , 1531-1542 cm^{-1} , and 1230 cm^{-1} for silk I, 1620-1630 cm^{-1} , 1515-1530 cm^{-1} and 1240 cm^{-1} for silk II, and 1640-1648 cm^{-1} , 1535-1545 cm^{-1} , 1235 cm^{-1} for random coil structure [37, 38]. Collagen amide I has been separated into three component peaks including 1628-1633 cm^{-1} for hydroxyproline [39]. Besides, the amide II bands [40] are presented at around 1550 cm^{-1} , and amide III bands [41] at around 1240 cm^{-1} .

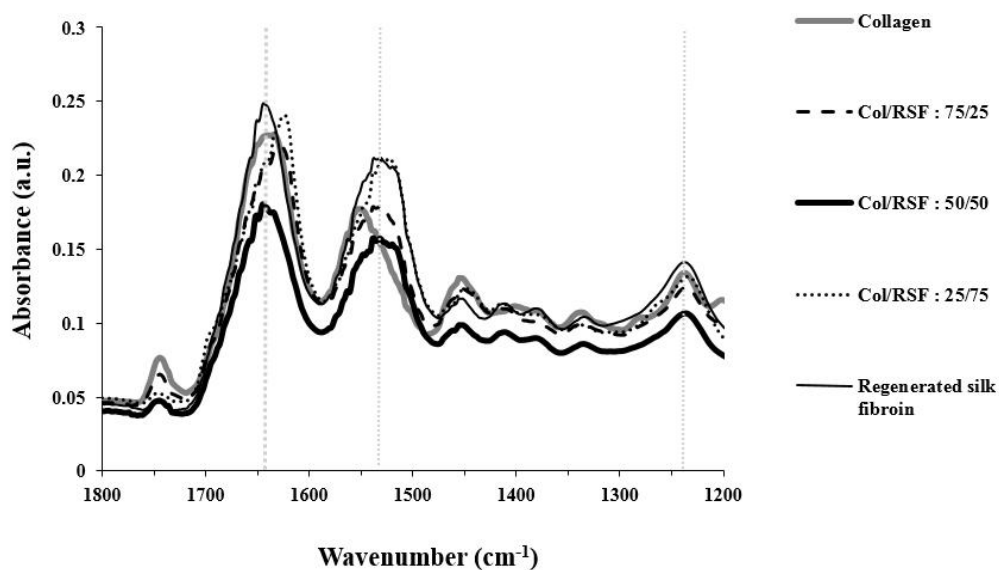


Figure 2.6: FTIR spectra of Collagen/RSF films

Amide I is the important peak in characterizing conformational changes. As shown in Figure 2.6, the position of amide I peaks of sample with 50/50 ratio remained unchanged for the fibroin molecules in the amide I region, showing predominant contribution of silk fibroin with random coil chains in the mixture. Increasing collagen to 75% contribution, induced silk fibroin β -sheet structure as the amide I peak shifted to 1626 cm^{-1} . However, the unchanged position of amide II at 1531 cm^{-1} , is consistent with the existence of some alpha helix structure of silk fibroin in the mixture. Blends with higher amount of silk fibroin showed the amide I peak at 1623 cm^{-1} , while the amide II peak appeared near 1525 cm^{-1} , indicating that the blended films contain mostly crystalline beta sheets that may be attributed to the fibrillogenesis of silk fibroin. Table 2.5, summarizes the assignment of the major IR peaks for each polymer and their blend films.

	Wavenumber (cm^{-1})		
	Amide I	Amide II	Amide III
Collagen	1634	1551	1238
Col/RSF : 75/25	1626	1531	1236
Col/RSF : 50/50	1644	1531	1237
Col/RSF : 25/75	1623	1525	1234
RSF	1644	1531	1237

Table 2.5. The FTIR band assignments of collagen/RSF blends

Circular dichroism (CD) analysis was performed in order to investigate and affirm conformational transition of silk fibroin in the blended solutions after dialysis. As shown in Figure 2.7, CD spectrum of pure silk fibroin after dialysis showed typical random coil structure with a negative peak near 195 nm, while for pure collagen that has been subjected to the blending process it was observed the collagen triple helix characteristic spectrum with a large negative peak near 197 nm as well as a small positive peak centered at 220 nm.

Considering the persistence of natural collagen structure in the mixtures that was confirmed by DSC analysis and in order to obtain the spectra for regenerated silk fibroin when blended with collagen, the spectrum of the later was subtracted from the spectra measured for the blended solutions. As shown in Figure 2.7, the spectra of silk fibroin in the mixtures show a negative peak between 210 and 220 nm and a positive peak between 195 and 200 nm, characteristic features of a beta sheet spectrum [42]. This indicates that silk fibroin structure changes toward beta sheet conformations upon interaction with collagen.

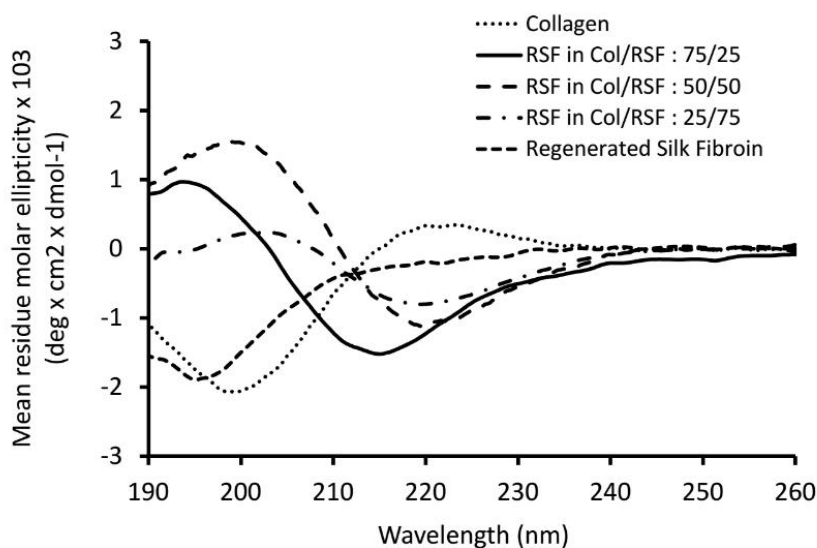


Figure 2.7. Circular dichroism (CD) spectrum of collagen/RSF mixtures after dialysis

2.4 Discussion

Direct mixing of collagen and silk fibroin solutions resulted in phase separation, possibly due to the different pH values of silk fibroin solution (with pH of 7.17) and collagen solution (with pH of 2.74). The low collagen solution pH causes the protonation of carboxyl groups on silk fibroin to their non-ionic form, and amine groups to their cationic form. This is along with increasing the hydrophobicity of uncharged carboxyl groups with subsequent induction of silk fibroin morphological changes in the solution from the spherical micelles to nanofibrils. Additionally, conformational transition from random coil to β -sheet may occur [36, 43-45]. Using higher temperatures (50–60 °C) as a way to prompt the interactions of collagen with other proteins through denaturing collagen molecules [22] is not the aim of this study, since the aim is the preservation of the collagen's native structure. Hence, collagen and RSF solutions were mixed, using calcium salt ions of the ternary solvent for inducing electrostatic interaction between biopolymer chains.

The chaotropic behavior of divalent calcium ions, under a phenomenon called “salting in”, causes more ion-protein interactions than protein-protein interactions in the blend system, yielding a homogenous mixture [46]. The stability of the mixtures in the single-phase region is due to the quasi-equilibrium between oppositely-charged proteins (collagen and fibroin) and the introduction of a ternary solvent containing high amounts of salt which acts both as the third component of the phase diagram and a simple electrolyte.

In a system containing oppositely-charged proteins (considering their polyelectrolyte nature), increasing the ionic strength through adding salt to some extent, enhances the attraction between the oppositely-charged residues and causes a transition of an overcharged polyelectrolyte complex (PEC) to a neutral or uncharged complex [47, 48]. Moreover, calcium ions with a radius of 4.1 Å in the hydrated state

fit well to the distance of $\sim 14 \text{ \AA}$ between adjacent triple helical molecules of collagen, probably interacting with the negatively-charged Asp or Glu side chains, forming salt bridges, and increasing the ionic strength of the solution [49-51].

Slow salt diffusion through the dialysis procedure changes the phase behavior of mixtures and causes coacervation or precipitation. Based on the results obtained from optical microscope images (Figure 2.3) and ζ potential analysis of the mixtures after dialysis, and considering the influence of proteins conformational structures on the aggregate formation, we hypothesized a model for mixtures with different ratios of collagen/silk fibroin (Figure 2.8).

In the mixtures containing collagen, it has been proved that the counterions were released to the media upon complexation with collagen [52]. Hence, in this research, at low ionic strength, the water and counterions may be released to the media upon the formation of hydrophobic and hydrogen bonds between the SF and collagen chains. Moreover, according to previous studies on silk fibroin mixtures [53], beta sheet conformation of silk fibroin showed by CD and FTIR analysis in this research may be due to the fact that upon complexation with collagen, silk fibroin chains may use collagen chains as a mold plate to stretch themselves. Through the process of the nucleation-dependent aggregation mechanism, once the beta sheet nucleus is formed, further growth of beta sheet units and beta sheet aggregation [54] will occur (Figure 2.8c).

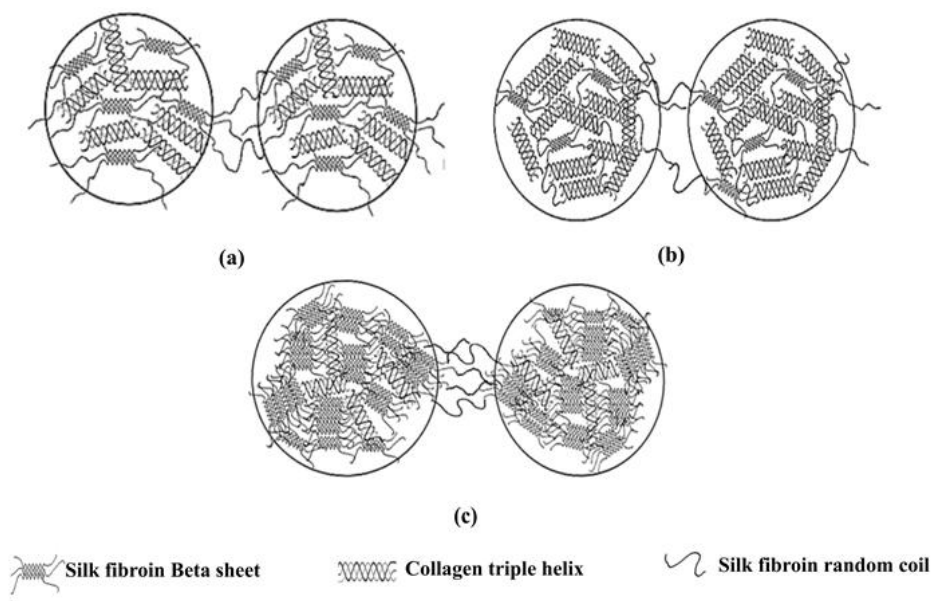


Figure 2.8. Schematic diagram of a hypothesized model for protein conformational changes in the two adjacent coacervate aggregates of Collagen/RSF mixtures after dialysis with different starting ratios of: (a) Col/RSF: 75/25, (b) Col/RSF: 50/50, (c) Col/RSF:25/75

On the other hand, the replacement of salt ions by water molecules (hydration) during dialysis causes the assembly of free collagen molecules, which probably happened in the mixtures with higher amounts of collagen (Figure 2.8b). Due to the specific hydroxyproline (Hyp) groups of collagen chains, the water molecules order around and between the collagen chains in a way that the triple helixes' organization forms a crystal packing. In these crystals, the triple helixes are bridged by ordered water molecules, causing the collagen assembly that induces collagen molecules aggregation or fibrillogenesis [55].

Overall, the characterization methods used in this study are simple techniques for primary assessment of phase behavior in collagen/silk fibroin blends. Further investigation can be done on ternary phase diagram of collagen/RSF/ternary solvent in order to obtain a boundary of miscibility/coacervate/precipitate, through application of other methods such as turbidimetry and potentiometric titration. Additionally, the size, shape, and inner composition characteristics of the precipitates can be further studied by small angle X-ray technique (SAXS) or WAXS (wide angle X-ray).

2.5 Conclusion

In this work, we studied the influence of salt ions on the phase behavior of collagen and silk fibroin mixtures. The results showed that ternary solvent containing calcium ions, as the third component in the ternary phase diagram, has a significant effect on the miscibility of mixtures. Its influence on implementing net charge density close to zero, making an almost electroneutral blend solution, was confirmed through the analysis of the observed ζ potential values. In such a system, the chains of collagen and silk fibroin should be in their most individual separated state with a high concentration of salt ions being placed among their chains. Moreover, the viscosity analysis reaffirmed the influence of ternary solvent to obtain high miscibility for all the blends. However, the maximum values were obtained for the mixture with the highest collagen ratio, due to the high ionic strength resulting from the higher amount of salt used in this mixture.

Removal of salt after the dialysis procedure yielded to complex coacervations (precipitation) with positive charge densities, demonstrating the importance of protein charge density and conformational structure. The protein-protein coacervate aggregates were formed as the oppositely charged protein chains got closer to each other and, after primary weak electrostatic interaction, the hydrogen and hydrophobic bonds were formed, leading to silk fibroin conformational changes from random coil to beta sheet. The conformational change of silk fibroin was reassured through CD spectra analysis of the solution after dialysis, as well as SEM, contact angle, DSC, and FTIR assessment of formed films after drying of dialyzed solutions.

Considering the physico-chemical changes of blended films, analyzed by SEM, contact angle, and DSC, it can be stated that the obtained blended films have tunable properties by varying the blend ratio.

Overall, such preparation procedure for collagen/silk fibroin blends is a promising method for engineering of protein-protein interactions, which is important for the development of a wide range of biopharmaceutical applications of these materials, from drug delivery, to wound healing and tissue engineering.

2.6 References

1. Paichit, I., et al., *Effects of the blended fibroin/aloë gel film on wound healing in streptozotocin-induced diabetic rats*. Biomedical Materials, 2012. **7**(3): p. 035008.
2. Gu, Z., et al., *Preparation of chitosan/silk fibroin blending membrane fixed with alginate dialdehyde for wound dressing*. Int J Biol Macromol, 2013. **58**: p. 121-6.
3. Silva, S.S., et al., *Physical properties and biocompatibility of chitosan/soy blended membranes*. J Mater Sci Mater Med, 2005. **16**(6): p. 575-9.
4. Katz, E.P. and C.W. David, *Energetics of intrachain salt-linkage formation in collagen*. Biopolymers, 1990. **29**(4-5): p. 791-8.
5. Katz, E.P. and C.W. David, *Unique side-chain conformation encoding for chirality and azimuthal orientation in the molecular packing of skin collagen*. Journal of Molecular Biology, 1992. **228**(3): p. 963-969.
6. Walker-Taylor, A. and D.T. Jones, *Computational Methods for Predicting Protein-Protein Interactions*, in *Proteomics and Protein-Protein Interactions: Biology, Chemistry, Bioinformatics, and Drug Design*, G. Waksman, Editor. 2005, Springer US: Boston, MA. p. 89-114.
7. Zhang, J., *Protein-protein interactions in salt solutions*, *Protein-protein Interactions – Computational and Experimental Tools*. Biochemistry, Genetics and Molecular Biology. 2012.
8. Ross, P.D. and M.V. Rekharsky, *Thermodynamics of hydrogen bond and hydrophobic interactions in cyclodextrin complexes*. Biophysical Journal, 1996. **71**(4): p. 2144-2154.
9. Rochdi, A., L. Foucat, and J.P. Renou, *Effect of thermal denaturation on water-collagen interactions: NMR relaxation and differential scanning calorimetry analysis*. Biopolymers, 1999. **50**(7): p. 690-6.
10. Gelse, K., E. Pöschl, and T. Aigner, *Collagens—structure, function, and biosynthesis*. Advanced Drug Delivery Reviews, 2003. **55**(12): p. 1531-1546.
11. Silver, F.H. and W.J. Landis, *Viscoelasticity, Energy Storage and Transmission and Dissipation by Extracellular Matrices in Vertebrates*, in *Collagen: Structure and Mechanics*, P. Fratzl, Editor. 2008, Springer US: Boston, MA. p. 133-154.
12. Knight, C.G., et al., *The collagen-binding A-domains of integrins alpha(1)beta(1) and alpha(2)beta(1) recognize the same specific amino acid sequence, GFOGER, in native (triple-helical) collagens*. J Biol Chem, 2000. **275**(1): p. 35-40.
13. Yannas, I.V., et al., *Biologically active collagen-based scaffolds: advances in processing and characterization*. Philos Trans A Math Phys Eng Sci, 2010. **368**(1917): p. 2123-39.
14. Sah, M. and K. Pramanik, *Regenerated silk fibroin from B. mori silk cocoon for tissue engineering applications*. International Journal of Environmental Science and Development, 2010. **1**: p. 404-408.
15. Foo, C.W.P., et al., *Role of pH and charge on silk protein assembly in insects and spiders*. Applied Physics A, 2006. **82**(2): p. 223-233.
16. Sashina, E.S., et al., *Structure and solubility of natural silk fibroin*. Russian Journal of Applied Chemistry, 2006. **79**(6): p. 869-876.

17. Jin, H.-J. and D.L. Kaplan, *Mechanism of silk processing in insects and spiders*. Nature, 2003. **424**(6952): p. 1057-1061.
18. Ochi, A., et al., *Rheology and Dynamic Light Scattering of Silk Fibroin Solution Extracted from the Middle Division of Bombyx mori Silkworm*. Biomacromolecules, 2002. **3**(6): p. 1187-1196.
19. Yang, G., et al., *Structure and microporous formation of cellulose/silk fibroin blend membranes: Part II. Effect of post-treatment by alkali*. Journal of Membrane Science, 2002. **210**(2): p. 379-387.
20. Tang, Y., et al., *Study on the preparation of collagen-modified silk fibroin films and their properties*. Biomed Mater, 2006. **1**(4): p. 242-6.
21. Chomchalao, P., et al., *Fibroin and fibroin blended three-dimensional scaffolds for rat chondrocyte culture*. Biomed Eng Online, 2013. **12**: p. 28.
22. Lu, Q., et al., *Preparation of three-dimensional fibroin/collagen scaffolds in various pH conditions*. J Mater Sci Mater Med, 2008. **19**(2): p. 629-34.
23. Hu, K., et al., *Biocompatible Fibroin Blended Films with Recombinant Human-like Collagen for Hepatic Tissue Engineering*. Journal of Bioactive and Compatible Polymers, 2006. **21**(1): p. 23-37.
24. Lv, Q., et al., *Preparation of insoluble fibroin/collagen films without methanol treatment and the increase of its flexibility and cytocompatibility*. Journal of Applied Polymer Science, 2008. **109**(3): p. 1577-1584.
25. Lv, Q., et al., *Fibroin/collagen hybrid hydrogels with crosslinking method: preparation, properties, and cytocompatibility*. J Biomed Mater Res A, 2008. **84**(1): p. 198-207.
26. Lv, Q., et al., *Three-dimensional fibroin/collagen scaffolds derived from aqueous solution and the use for HepG2 culture*. Polymer, 2005. **46**(26): p. 12662-12669.
27. Zhou, J., et al., *Electrospinning of silk fibroin and collagen for vascular tissue engineering*. International Journal of Biological Macromolecules, 2010. **47**(4): p. 514-519.
28. Krigbaum, W.R. and F.T. Wall, *Viscosities of binary polymeric mixtures*. Journal of Polymer Science, 1950. **5**(4): p. 505-514.
29. García, R., et al., *Viscometric study on the compatibility of polymer–polymer mixtures in solution*. European Polymer Journal, 1999. **35**(1): p. 47-55.
30. Wang, Q. and J.B. Schlenoff, *The Polyelectrolyte Complex/Coacervate Continuum*. Macromolecules, 2014. **47**(9): p. 3108-3116.
31. van der Gucht, J., et al., *Polyelectrolyte complexes: bulk phases and colloidal systems*. J Colloid Interface Sci, 2011. **361**(2): p. 407-22.
32. Cramer, G.R., A. Läuchli, and V.S. Polito, *Displacement of Ca(2+) by Na(+) from the Plasmalemma of Root Cells : A Primary Response to Salt Stress?* Plant Physiology, 1985. **79**(1): p. 207-211.
33. Yang, Y., H.W. Kwak, and K.H. Lee, *Effect of Residual Lithium Ions on the Structure and Cytotoxicity of Silk Fibroin Film*. International Journal of Industrial Entomology, 2013. **27**(2): p. 265-170.
34. Yin, Z., et al., *A silk fibroin hydrogel with reversible sol-gel transition*. RSC Advances, 2017. **7**(39): p. 24085-24096.
35. Tiktopulo, E.I. and A.V. Kajava, *Denaturation of type I collagen fibrils is an endothermic process accompanied by a noticeable change in the partial heat capacity*. Biochemistry, 1998. **37**(22): p. 8147-52.
36. Bozec, L. and M. Odlyha, *Thermal Denaturation Studies of Collagen by Microthermal Analysis and Atomic Force Microscopy*. Biophysical Journal, 2011. **101**(1): p. 228-236.
37. Hu, X., D. Kaplan, and P. Cebe, *Determining Beta-Sheet Crystallinity in Fibrous Proteins by Thermal Analysis and Infrared Spectroscopy*. Macromolecules, 2006. **39**(18): p. 6161-6170.
38. Chen, H., X. Hu, and P. Cebe, *Thermal properties and phase transitions in blends of Nylon-6 with silk fibroin*. Journal of Thermal Analysis and Calorimetry, 2008. **93**(1): p. 201-206.
39. Lazarev, Y.A., B.A. Grishkovsky, and T.B. Khromova, *Amide I band of IR spectrum and structure of collagen and related polypeptides*. Biopolymers, 1985. **24**(8): p. 1449-78.

40. Rabotyagova, O.S., P. Cebe, and D.L. Kaplan, *Collagen Structural Hierarchy and Susceptibility to Degradation by Ultraviolet Radiation*. Mater Sci Eng C Mater Biol Appl, 2008. **28**(8): p. 1420-1429.
41. Susi, H., J.S. Ard, and R.J. Carroll, *The infrared spectrum and water binding of collagen as a function of relative humidity*. Biopolymers, 1971. **10**(9): p. 1597-604.
42. Iizuka, E. and J.T. Yang, *Optical rotatory dispersion and circular dichroism of the beta-form of silk fibroin in solution*. Proceedings of the National Academy of Sciences of the United States of America, 1966. **55**(5): p. 1175-1182.
43. Ayub, Z., M. Arai, and K. Hirabayashi, *Mechanism of the Gelation of Fibroin Solution*. Bioscience, Biotechnology, and Biochemistry, 1993. **57**(11): p. 1910-1912.
44. Zhou, P., et al., *Effects of pH and Calcium Ions on the Conformational Transitions in Silk Fibroin Using 2D Raman Correlation Spectroscopy and ¹³C Solid-State NMR*. Biochemistry, 2004. **43**(35): p. 11302-11311.
45. Matsumoto, A., et al., *Mechanisms of silk fibroin sol-gel transitions*. J Phys Chem B, 2006. **110**(43): p. 21630-8.
46. Curtis, R.A., J.M. Prausnitz, and H.W. Blanch, *Protein-protein and protein-salt interactions in aqueous protein solutions containing concentrated electrolytes*. Biotechnology and Bioengineering, 1998. **57**(1): p. 11-21.
47. Laos, K., G.J. Brownsey, and S.G. Ring, *Interactions between furcellaran and the globular proteins bovine serum albumin and β -lactoglobulin*. Carbohydrate Polymers, 2007. **67**(1): p. 116-123.
48. Seyrek, E., et al., *Ionic Strength Dependence of Protein-Polyelectrolyte Interactions*. Biomacromolecules, 2003. **4**(2): p. 273-282.
49. Bianchi, E., et al., *The role of pH, temperature, salt type, and salt concentration on the stability of the crystalline, helical, and randomly coiled forms of collagen*. J Biol Chem, 1967. **242**(7): p. 1361-9.
50. Freudenberg, U., et al., *Electrostatic interactions modulate the conformation of collagen I*. Biophys J, 2007. **92**(6): p. 2108-19.
51. Li, S.T. and E.P. Katz, *An electrostatic model for collagen fibrils. The interaction of reconstituted collagen with Ca⁺⁺, Na⁺, and Cl*. Biopolymers, 1976. **15**(8): p. 1439-60.
52. Chung, E.J., A.E. Jakus, and R.N. Shah, *In situ forming collagen-hyaluronic acid membrane structures: mechanism of self-assembly and applications in regenerative medicine*. Acta Biomater, 2013. **9**(2): p. 5153-61.
53. Chen, X., W. Li, and T. Yu, *Conformation transition of silk fibroin induced by blending chitosan*. Journal of Polymer Science Part B: Polymer Physics, 1997. **35**(14): p. 2293-2296.
54. Li, G., et al., *The natural silk spinning process. A nucleation-dependent aggregation mechanism?* Eur J Biochem, 2001. **268**(24): p. 6600-6.
55. Bella, J., B. Brodsky, and H.M. Berman, *Hydration structure of a collagen peptide*. Structure, 1995. **3**(9): p. 893-906.

3. Chapter Three

A new label-free technique for analysing evaporation induced self-assembly of viral nanoparticles based on enhanced dark-field optical imaging

Ima Ghaeli^{1,2,3,*}, *Zeinab Hosseinidoust*⁴, *Hooshiar Zolfagharnasab*⁵ and *Fernando Jorge Monteiro*^{1,2,3,*}

¹ i3S-Instituto de Investigação e Inovação em Saúde, Universidade do Porto, Portugal

² INEB, Instituto de Engenharia Biomédica, Porto, Portugal

³ FEUP, Faculdade de Engenharia, Universidade do Porto, Departamento de Engenharia Metalurgia e Materiais, Porto, Portugal

⁴ Department of Chemical Engineering, McMaster University, Hamilton, ON, Canada,

⁵ FEUP, Faculdade de Engenharia, Universidade do Porto, Departamento de Engenharia Eletrotécnica e de Computadores, Porto, Portugal

*Correspondence: ema.ghaeli@gmail.com (Ima Ghaeli), fjmont@fe.up.pt (Fernando J. Monteiro)

Abstract

Nanoparticles self-assembly is a complex phenomenon, the control of which is complicated by the lack of appropriate tools and techniques for monitoring the phenomenon with adequate resolution in real-time. In this work, a label-free technique based on dark-field microscopy was developed to investigate the self-assembly of nanoparticles. A bio-nanoparticle with complex shape (T4 bacteriophage) that self-assembles on glass substrates upon drying was developed. The fluid flow regime during the drying process as well as the final self-assembled structures were studied using dark-field microscopy, while phage diffusion was analysed by tracking of phage nanoparticles in the bulk solutions. The concentrations of T4 phage nanoparticles and salt ions were identified as the main parameters influencing fluid flow, particle motion, and consequently, the resulting self-assembled structure. This work demonstrates the utility of enhanced dark-field microscopy as a label-free technique for observation of drying-induced self-assembly of bacteriophage T4. This technique provides the ability to track the nano-sized particles in different matrices and serves as a strong tool for monitoring self-assembled structures and bottom-up assembly of nano-sized building blocks in real-time.

Keywords: Nanoparticle self-assembly; T4 phage nanoparticle suspension; Enhanced dark-field microscopy; Nanoparticle tracking analysis; Label-free technique; Drying-induced self-assembly.

3.1 Introduction

Viral nanoparticles (VNPs) can be used as building blocks for developing advanced, functional material such as bioactive surfaces, flexible optics and electronics, biosensors, and drug/gene delivery vehicle for biomedical engineering [1-4].

Various structures, shapes, sizes and properties of viruses as well as their amino acid groups increase their benefits for the potential use as the precursors to create inorganic nanostructures. Wang et al. [5], summarized the studies on the self-assembly of different types of viruses to design and fabricate biomimetic nanostructures for sensor applications. VNPs can self-assemble into two- or three-dimensional macrostructures. The patterning of virus-based nanomaterials on a substrate (surface-specific virus assembly) as a requirement for advanced engineering applications such as nanowires and catalysis, has been reviewed by Lee et. al. [6]. The interfacial and biological methods through implementing of biological recognition (selectively immobilized viruses), mechanical and interfacial forces, have been reported for such patterning. Both substrate properties and surface characteristics of the viruses are influential on the formation of top virus layers onto the solid substrates [6]. Even though, specific affinities of viruses to the

substrate might be helpful for a targeted patterning, the specific interaction might result in higher binding energies, causing more defects in virus assembled structures. Besides, the specific interactions may limit to one substrate material. Hence, unspecific virus assembly on solid substrates is of concern [7].

Unspecific assembly of VNPs on solid surfaces can be achieved through methods such as Langmuir-Blodgett technique, convective assembly, and droplet evaporation [8-11], thus resulting in the bottom-up assembly of the nanoparticles into 2-dimensional films that exhibit various degrees of structure such as honeycomb, coffee rings, and nanocrystal superlattices [12]. A tuneable crack-free ultrathin film with highly-ordered assembly of nanoparticles into superlattices could be obtained through a controlled evaporation-induced self-assembly procedure [13, 14].

Several researchers have investigated the 2-dimensional ordered structures formed by droplet evaporation self-assembly of VNPs [2, 3, 15, 16], mainly focusing on icosahedral or rod-shaped viruses because of their simpler geometry. Fully dehydrated suspensions (if stored in a humidity and temperature controlled environment) are static and fairly stable because the self-organization process is complete. At this point, more invasive endpoint methods such as scanning electron microscopy (SEM) [17, 18], X-ray crystallography, and atomic force microscopy (AFM) [19, 20] can be safely applied, all of which can result in to high resolution endpoint data. Although some of these techniques (namely SEM and AFM) can, in theory, be carried out in the liquid mode, these techniques require meticulous sample preparation, which is invasive and will interfere with the self-organization process [21] making real-time, non-invasive visualization of VNPs (and nanoparticles in general) in a fluid matrix a challenging task. Optical methods such as light scanning microscopy (LSM) [22], incident light microscopy [23], fluorescence microscopy [17, 24], and confocal laser scanning microscopy [25-27], have proven useful to various degrees for non-invasive, real-time monitoring of nanoparticle suspensions. Optical methods are by far the simplest and less invasive techniques for this purpose; however, being very small in size, with ultra-weak polarization forces and low dielectric constants, it is difficult to discriminate the nanoparticles from the surrounding medium using optical methods [28]. Fluorescence labelling allows for real-time imaging of nanoparticles with reasonable resolution in a wide range of matrices; however, this method is invasive and is challenged by limitations of fluorescence emission lifetime and photo-bleaching [29-31]. Moreover, the Brownian motion of fluorescent micro- and nanoparticles causes the particles to tumble and blink irregularly, decreasing signal to noise ratio in fluorescence microscopy [32].

Recently, several attempts have been made to develop label-free, real-time, sensitive and low cost techniques for visualizing VNPs and other nanoparticles directly in the liquid matrix [33-37]. These methods are mainly based on elastically scattered light from the viral capsid [32, 36-38]. In contrast to the bright-field microscopy, dark-field microscopy is a well-known technique for clear nanoparticle identification, through reduction of visual noise and allowance of the bright crystalline contrast, in order to

differentiate the nanoparticles from remainder of the environment [39]. The dark-field microscopy has the advantage of detection of nanoparticles in complex media, including wastewaters or biological media [40].

Nanoparticle visualization via dark-field microscopy was demonstrated for gold nanoparticles based on their plasmonic spectra [41]. Total internal reflection dark-field microscopy (TIRDFM) was also demonstrated successfully for label- visualization of the influenza viruses [42]. It is noteworthy that most attempts to visualize VNPs with dark-field microscopy rely on other labelling approaches, such as using quantum dots or gold nanoparticles, for real-time visualization [43]. These methods can track nanoparticles for longer timescales compared to fluorescence methods. However, they still have some limits. The limitation of gold nanoparticle concentration for detection and the noise introduced from background scattering, such as dust in the imaging chamber in most dark-field detection methods, poses a challenge for real-time detection [40]. Using dark-field microscopy to detect elastically scattered light improves the detection sensitivity by reducing the background intensity [37].

In this work, we propose a new technique for label-free visualization and real time, in situ imaging of VNPs based on enhanced dark-field optical microscopy. A CytoViva® enhanced dark-field optical microscope was used to detect observe nanosized particles by detection of elastically scattered light, without the use of any labels. The hollow cone of light in CytoViva allows no light to be transmitted through the microscope objective in the absence of a scattering source therefore only scattered light may be imaged (Figure 3.1). CytoViva's patented dark-field condenser illuminates the sample more precisely than the standard microscope condenser by focusing fixed-geometry, highly collimated light at oblique angles on the sample, improving the signal-to-noise ratio up to seven times and enabling resolution beyond diffraction limits [38]. This study aims at visualizing and analyzing the two-dimensional self-assembly of bacteriophage T4 using an enhanced dark-field optical microscope. Tracking of VNPs was performed through image analysis of videos recorded exclusively from the scattered light originating from the virus nanoparticles.

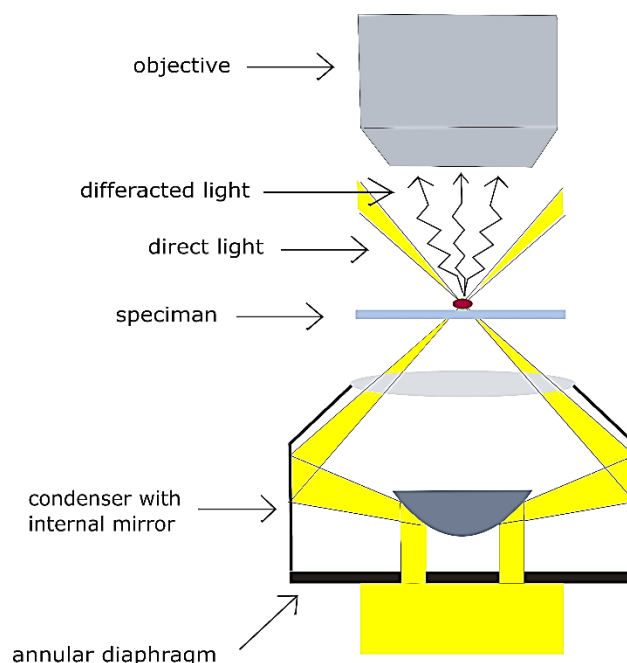


Figure 3.1. Scheme of nanoparticle illustration under CytoViva enhanced dark-field microscope with hollow cone condenser. Only diffracted rays are collected by the objective.

3.2 Materials and Methods:

3.2.1 Bacteriophage propagation and purification

Escherichia coli BL21 (5 mL each) was grown overnight in Luria broth (LB) at 37 °C. A 5 mL aliquot of this culture was added to 200 mL of sterilized LB and incubated with under shaking for 3 hrs. Another 5 mL aliquot was inoculated with 100 µL of bacteriophage T4 stock (10^{12} PFU/mL, plaque forming units per mL), incubated for 15 min at room temperature, and added to the first 3-hr culture and incubated while shaking overnight at 37 °C.

The phage suspension was purified based on PEG8000/NaCl aqueous two phase technique (ATPS) [44], and according to methods described in the literatures [45]. Briefly, the overnight cultures were centrifuged at 6000 RPM (RC-6, Sorvall) for 20 min, the supernatant was recovered and sterile-filtered. The supernatant was treated with nuclease solutions (final concentration of 1 µg/mL, 30 min at room temperature). The supernatant was subsequently mixed with 1M NaCl and PEG 8000 (10 v/w%) and stirred overnight at 4 °C to precipitate phage particles. The precipitated phage were spun down by centrifugation (14000 RPM, 10 °C, for 3 hrs). Finally, the phage suspension was purified using ultracel 100k filters (Amicon Ultra centrifugal filters, Millipore). The precipitated phage were re-suspended in SM buffer (containing 5.8 g/L NaCl, 120 mg/L MgSO₄, 50 mL of 1 M Tris-HCl, pH 8) and sterile filtered. This method resulted in a phage titer of 10^{10} - 10^{12} PFU (Plaque Forming Units)/mL. To determine the phage titer,

ten-fold serial dilutions were prepared and after mixing with overnight host bacteria, the solutions were added to molten soft agar, which was spread over the plates. The plates were incubated overnight at 37 °C and the number of plaques were enumerated. To remove excess salt, bacteriophage suspension was dialyzed against distilled water for 24 hrs (Using regenerated Cellulose membranes with MWCO: 14000), followed by sterile filtration and phage titer count.

3.2.2 Experimental setup: Enhanced dark-field microscopy and monitoring of evaporation process

An optical Olympus BX51 polarizing microscope (10× UPlan, NA-0.3) equipped with an integrated dark-field illumination system (CytoViva™) was used to observe phage droplet evaporation on a borosilicate glass coverslips. The glass substrates were cleaned by acid washing and rinsing with ethanol 70%, prior to the experiments and mounted in the microscope holder. Aqueous droplet of 0.5 µL containing T4 phage nanoparticles was gently pipetted and placed onto the clean glass coverslip. The droplet was left at room temperature, to evaporate until it dried completely. The drying procedure was monitored with 10×, 20× and 40× microscope objectives and acquired as 1280 × 720 resolution videos, captured with a digital Carl Zeiss camera (12 MP, f/2.8, 1.77 µm per pixel size) that was mounted onto the ocular lens. The captured movies were analysed by image processing using MATLAB software for tracking phage particles.

3.2.3 Particle Tracking and image analysis

For particle tracking analysis, the captured movies were converted into still frames and each frame was processed using Mean-Shift tracking algorithm.

The tracking procedure was initiated by defining a local feature (i.e. the brightness level of a phage particle) around the object to be tracked. In the first frame, a small window was located around the particle. While the particle was changing its location through consecutive frames, the tracking algorithm shifted the window to keep its centre on the defined feature.

To reinforce the tracking when particles were moving side by side to each other, a series of features instead of one could be taken into consideration instead of one. These features can vary from a simple pixel brightness, to more complex ones such as distribution of pixel normal vectors. In this work, a combination of two features, brightness level and elliptical diameters, insured that the particles were distinguishable from each other in situations where particles were too close to each other. The brightness level of each particle is obtained by averaging all the intensity values belonging to a particle phage. Note that since particles were captured as bright spots in all the frames, static thresholding technique was applied to segment them from dark background. Therefore, having segmented them, it was then possible to fit an ellipse to them in order to find approximated elliptical diameters.

The mean-shift methodology has been adopted from the code implemented by Bernhardt [46]. However, the code has been slightly modified in order to fulfil the requirements of the current research. The modifications included reinforcement of particle features, and evaluation of particles trajectory.

The initial location of each phage particle was manually identified; the algorithm then automatically traced the location of that particle in subsequent frames. Conventional mean square displacement (MSD) was plotted against time lapses and the resulting curves were used to calculate the diffusion coefficient of phage particles in each suspension. Each analysis was performed on a dataset consisting of 3 to 5 particles (randomly selected) for each suspension. For each particle the analysis was carried out on 150-450 frames with time lapses of 0.2s, 1s, and 2s (corresponding to time lags of $\tau=50, 10, 5$, respectively). Both tracking and MSD computation were performed using Mathworks MATLAB R2015a. Further information on data acquisition and MSD computation, available in the Supplementary File S, together with MATLAB code, are provided in the Supplementary Software File.

3.3 Results and Discussion

Assembling viruses on surfaces may lead to novel structures with high functionality in various areas such as energy storage (as rechargeable batteries and solar cells), and bioengineering (as novel extracellular matrices and sensitive colour sensors) [47, 48]. Drying induced assembly of viruses is a simple method to fabricate such functional structures. Gaining a fundamental understanding of drying process and how it affects the assembly of viruses (and final dried pattern) will affect our ability to control the self-assembly of VNPs.

During the drying process, particles undergo two types of motion, fluid flow-driven transport and particle self-diffusion, both being space and time-dependent [49]. Fluid flow transfers nanoparticles towards the free spaces, while particle self-diffusion decreases concentration gradients. These two parameters ultimately determine the shape of the self-assembled structure [50, 51].

In this work, we used dark-field microscopy to visualize the drying process, and analyse the virus motion and fluid flow during drying of phage-suspensions. Dark-field microscopy allowed to monitor the phage nanoparticle motion in real-time, enabling the tracking of the nanoparticles motions without disturbance of secondary agents (e.g., fluorphores) and enabled real-time investigation of the drying dynamics. We tracked VNPs in movies captured using the microscope software under various conditions and analysed evaporation-driven fluid flow and evaporation driven effects.

Furthermore, the effects of salt and phage concentration on virus motion and fluid flow have been assessed by drying salt-free phage suspensions at low and high phage concentrations, as well as phages in physiological salt concentrations, as an additional control.

3.3.1 Analysing the bacteriophage motion and its influence on phage assembly onto the glass coverslip

Virus motion was assessed through quantification of phage nanoparticle diffusion coefficient in various suspensions. The diffusion of phage nanoparticle was quantified by monitoring particle trajectories during the drying process. It is known that the particle motion during drying process accelerates towards the contact line. Hence, the diffusion coefficient was calculated through tracking method, when the fluid flow is slow enough, and compared with the standard diffusion coefficient of phage T4 at the same temperature, as reported in the literature [52-54]. VNP tracking was performed by processing captured movies obtained during evaporation procedure using a Mean-Shift algorithm of Kernel-based object tracking. Figure 3.2 (a-e) shows the image sequences of phage T4 movement (as motions of bright spots on a dark background) near the contact lines (the white line), while Figure 3.2 (f) illustrates the distance of randomly selected phage nanoparticles (near the contact line) from the liquid-solid contact line vs time, within 3-5 min after droplet contact to the glass coverslip. It should be noticed that the study on the phage diffusion behaviour in this study was limited to the conditions under slow fluid motion. This decreased the dynamics of VNP motion and increased the quality of the signal obtained from individual VNPs, allowing for better visibility.

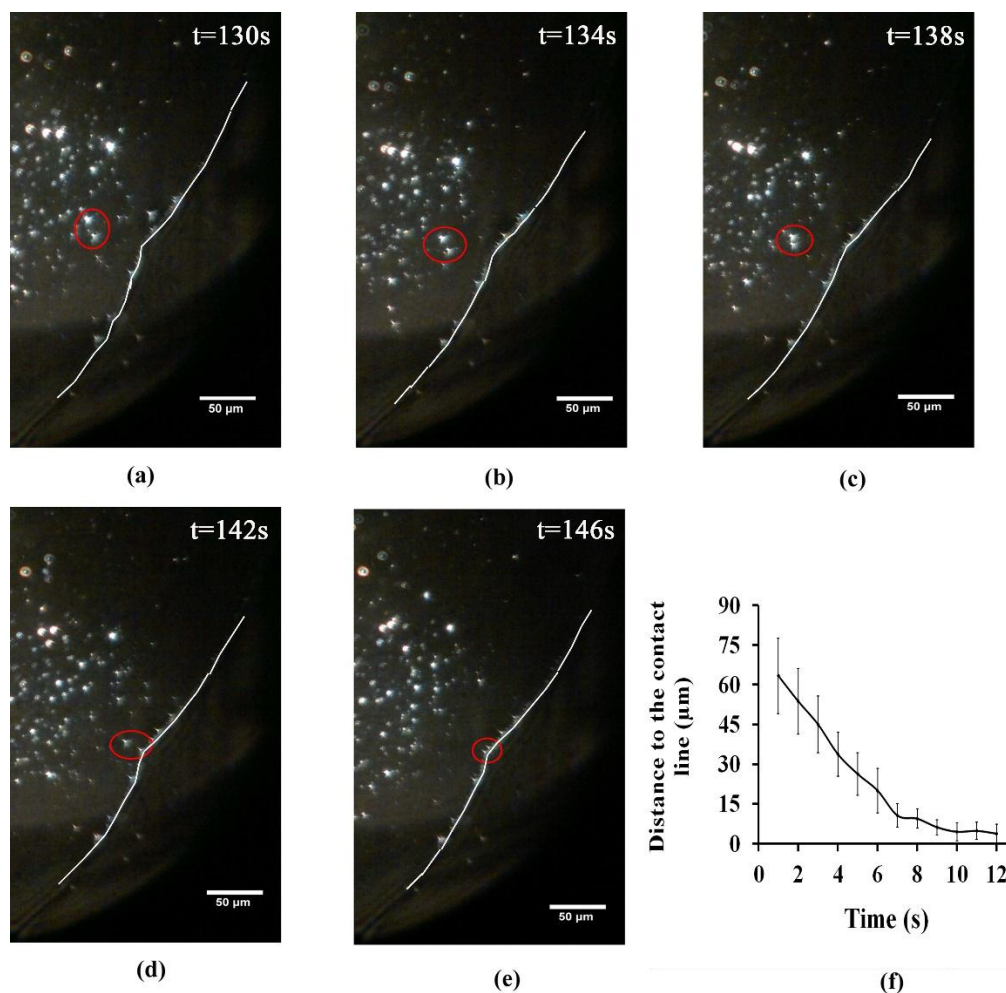


Figure 3.2: Sequential images [(a) to (e)] showing phage movement towards the contact line for diluted dialyzed phage (10^9 pfu/mL), and (f) illustrates phage distance to the contact lines vs time for the randomly selected phage nanoparticles near the contact line, within 3-5 min after droplet contact to the glass coverslip

The dominating forces, responsible for transporting nanoparticles towards the contact line, are induced by the combination of capillary flow and diffusion mechanisms. Shen et. al. [55], proposed two important time scales for the nanoparticles transportation near the contact line, in order to form a “coffee ring” structure. The first time scale is related to the diffusion-dominated transport mechanism of nanoparticles towards the contact line. The second time scale contributing towards the capillary flow mechanism [56, 57] (induced by droplet evaporation at a pinned contact line), is related to the time for the two adjacent nanoparticles near the contact line to meet each other. By comparing these two time scales it was shown that the velocity of nanoparticles diffusion towards the contact line was several times higher than the velocity of nanoparticles movement induced by capillary flow [55]. Accordingly, Figure 3.2-f shows that

randomly selected phage nanoparticles with various distances to the contact line (the vertical bars) are transported with higher velocities within the first 6 seconds time interval due to the diffusion-limited mechanism. However, their movements occurred at much lower velocities and in almost similar distances to the contact line within the next 6 seconds time interval, because the nanoparticle velocity influenced by the capillary flow is smaller than the diffusion velocity [55].

In order to find the trajectory of each moving objects, it was required to assess the location of the particle in each frame. For this purpose, mean-shift algorithm was used to locate the most likelihood region where the particle moves. Particle properties such as size and colour distribution have been considered to strengthen the tracking. It was assumed that the colour intensity of particle is changing with regard to 3D-Gaussian function. Therefore, mean-shift iteratively finds and refines the particle location considering the size and colour intensity profile in the particle. A flowchart detailing the algorithm developed for these experiments, using MATLAB software, is provided in Figure 3.3.

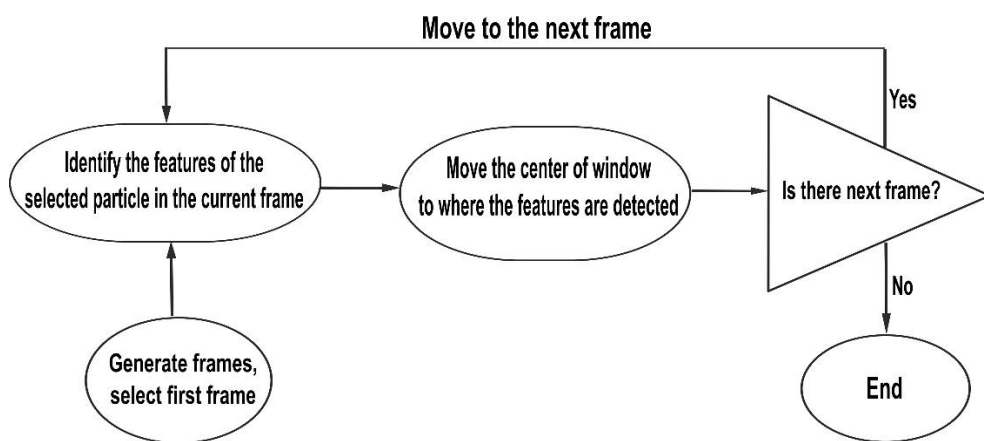


Figure 3.3: Flowchart describing the method for nanoparticle tracking using MATLAB software

Because the location of a particle is determined in each time frame, standard methods to calculate mean-squared displacement (MSD) could be used to analyse the trajectory of each particle. MSD may be considered as the squared distances during particle's oscillation in the position over an identified time interval (with certain length of Δt). Figure 3.4 shows the influences of salt ions and phage concentration on the mean-squared displacement of phage nanoparticles under conditions where the fluid motion is slow (as Movies S1 to S3). Time lags (τ) were determined as a function of certain length of time interval Δt , and the number of time intervals n , ($\tau=n\Delta t$). In this study, time lags of $\tau=5, 10$ and 50 were considered to analyse the MSD values and subsequently, diffusion coefficient for phage nanoparticles in each solution. For the duration of observation, increasing time lag, which will lead to increasing n , yields to more time points for accurate estimation of displacement. However, the results were accompanied with a larger variance with

increasing n (error bars in Figure 3.4-c), because the uncertainty of the particles position over larger n values increases as the reciprocal of the square root of displacements [45].

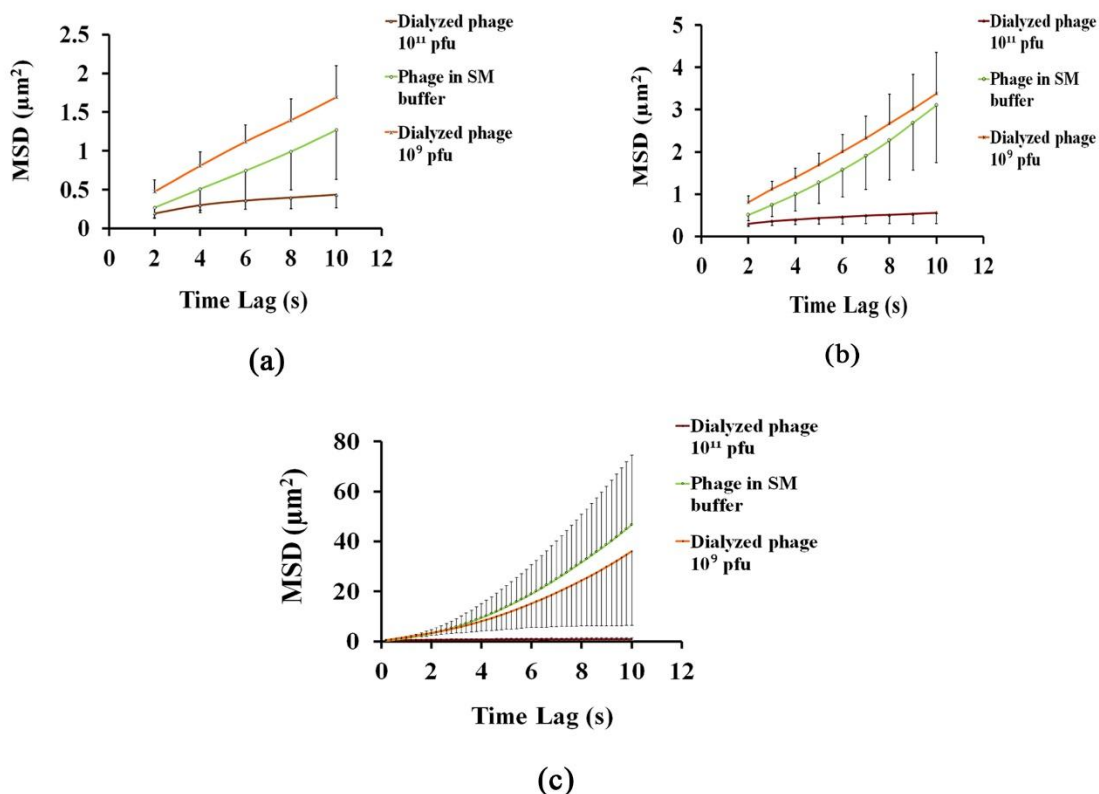


Figure 3.4: Mean square displacement of phage nanoparticles under different conditions with (a) $\tau=5$, (b) $\tau=10$, and (c) $\tau=50$

In order to analyse the diffusion coefficient of phage nanoparticles, the slope of the best fitted lines for each MSD curve, as the average diffusion coefficient, was obtained and compared with the standard diffusion coefficient of phage T4. The standard diffusion coefficient for *E. coli* bacteriophage T4 has been reported in the literature to be in the range of 4×10^{-8} to 8×10^{-8} cm^2/sec [52]; this value is highly dependent on phage concentration. However, it has been pointed out that the concentration of electrolyte has no significant effect on the diffusivity of phage T4 [53]. Table 3.1 presents the phage diffusion coefficients calculated for the various conditions used in this work.

Standard diffusion coefficient of phage T4, in water at 23 °C (10^8 to 10^9 pfu/mL) [52]	4×10^{-8} to 8×10^{-8} cm ² /sec
Average diffusion coefficient of phage in SM buffer (10^9 pfu/mL)	4.8×10^{-8} cm ² /sec
Average diffusion coefficient of phage, for concentrated phage suspension in water (10^{11} pfu/mL)	5.6×10^{-10} cm ² /sec
Average diffusion coefficient of phage, for diluted phage suspension in water (10^9 pfu/mL)	3.6×10^{-8} cm ² /sec

Table 3.1: Diffusion coefficient of phage T4 suspensions used in this study

Based on Table 3.1, the average diffusion coefficient of bacteriophages in SM buffer is within the range of standard diffusion coefficients for the same phage as reported in the literature. Hence, it can be interpreted that phage nanoparticles motion in SM buffer was dominated by random Brownian diffusion, and therefore, phage adsorption to the glass substrate is a diffusion-limited process [54]. However, deviation of phage diffusion coefficient from the standard value, for suspensions of diluted (10^9 PFU/mL) and concentrated (10^{11} PFU/mL) phages, suggests that the possibility of phage adsorption to the substrate, may influence the normal diffusive motion of nanoparticles, as well as on the final dried pattern.

3.3.2 *Analysing fluid flow through monitoring drying process and final dried patterns (macroscopic observations)*

The movies captured with the dark-field microscope showed nanoparticles motions inside the droplet, upon placing a droplet containing phage nanoparticles in contact with glass coverslips. The appearance of salt crystals was evident upon drying of the non-dialyzed suspension (Figure S) but the dialyzed suspensions did not exhibit salt crystals but rather exhibited patterns containing two main regions: boundary and inner part (Figure S).

The dynamic phage nanoparticle motion in the fluid flow was apparent in the captured video from drying process of dialyzed solutions with high and low concentrations. In the first 15 min, for the high concentration phage suspensions, and 9 min, in the case of the diluted phage suspensions, the movement of the phage nanoparticle presented an outward motion, following pinning-/de-pinning process and formation of repeated concentric rings (Movies S1 for higher phage concentrations and S5 for lower phage concentrations, Figure 3.5). The Pinning-/de-pinning process is an evaporation-driven effect and is the result of Stokes-Darcy transition (the two main physical laws governed the initial drying processes) [58, 59], which was directly observed for both high concentration (Movie S1) and diluted phage samples (Movie S4) through the jumps of contact line and variation in the contact line position. The process has been explained by deposition of particles at the contact lines during pinning process, following by contact line

jumps between pinning sites with droplet shrinkage, resulting in the formation of repeated concentric rings [60]. These observations confirm similar ones in a study on evaporation mechanism of rod-like viruses, reported in the literature [61]. Nevertheless, Moffat et. al [62], proved that the pinning step is not “absolute” and small contact line recession may occur during pinning process.

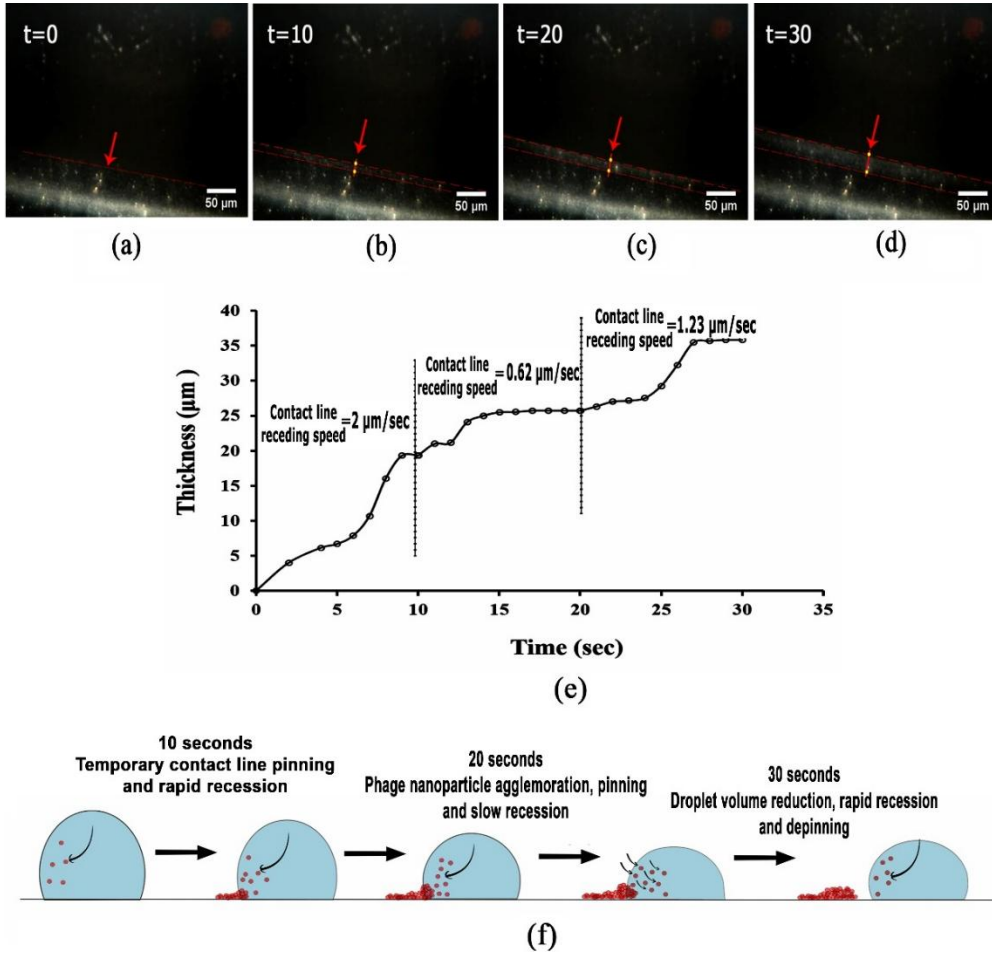


Figure 3.5: Sequential images derived from captured movies during drying of concentrated phage suspension, showing (a-d) concentric ring formation at 36% of drying process, during 30 secs in 10 secs intervals, using 20X objective, (e) the contact line receding speed and (f) schematic diagram of pinning-depinning process (the black arrows show the direction of phage nanoparticles motion towards the contact line during pinning and towards the centre of droplet during depinning processes).

Figure 3.5 (a-d) shows the formation of concentric ring at 36% of drying process of the high concentration phage suspension after 30 secs of drying. The variation of the receding contact line speed (slow or fast moving contact line) with variations in dried deposit from narrow ring to wide ring, has been discussed elsewhere through assessing the dynamics of contact line [62-64]. Moffat et. al [62], revealed

that for the solutions with higher nanoparticle concentrations, the accumulation of nanoparticles near the contact line, as the result of advection during evaporation, induced the viscosity at the contact line, and subsequently the dynamic pinning behaviour. Figure 3.5-e illustrates the average speed for the contact line receding of $2 \mu\text{m/s}$ for the first 10 secs, $0.62 \mu\text{m/s}$ for the second 10 secs, and $1.23 \mu\text{m/s}$ for the third 10 secs.

As shown in Figure 3.5-f, higher receding speed of contact line during the first 10 sec could be due to the high concentration of phage nanoparticles carried towards the contact lines at the droplet periphery (Movie S1 and arrows shown in Figure 3.5-f), leading to the so-called temporary contact line pinning [62], passing from one nanoparticle to the next. The reduced speed of contact line recession, observed at the second 10 sec period could be due to higher phage nanoparticle deposition, which prevents the contact line from receding and keeps the droplet at its contact area [63, 65]. Increasing the contact line speed in the third 10 secs, as the result of depinning process, is due to the continues evaporation of droplet at almost a constant contact area, followed by reduction of droplet volume that can exceed the contact line recession towards the centre, in order to reach a thermodynamic equilibrium state [66].

From the drying process movies, it was possible to observe and follow the complete drying process, for both diluted and concentrated phage suspensions. Upon the evaporation of phage droplet, it was observed that the motion of phage nanoparticles in the concentrated suspensions occurred in a more confined area (Movie S1) than for the diluted suspensions, consisting of more free spaces (Movie S4), leaving behind several distinct concentric coffee rings. On the contrary, the patterns formed after drying of phage nanoparticle suspension with low concentrations (Figure S), contained no distinct bands (coffee rings), as opposed to what could be observed for high phage concentration.

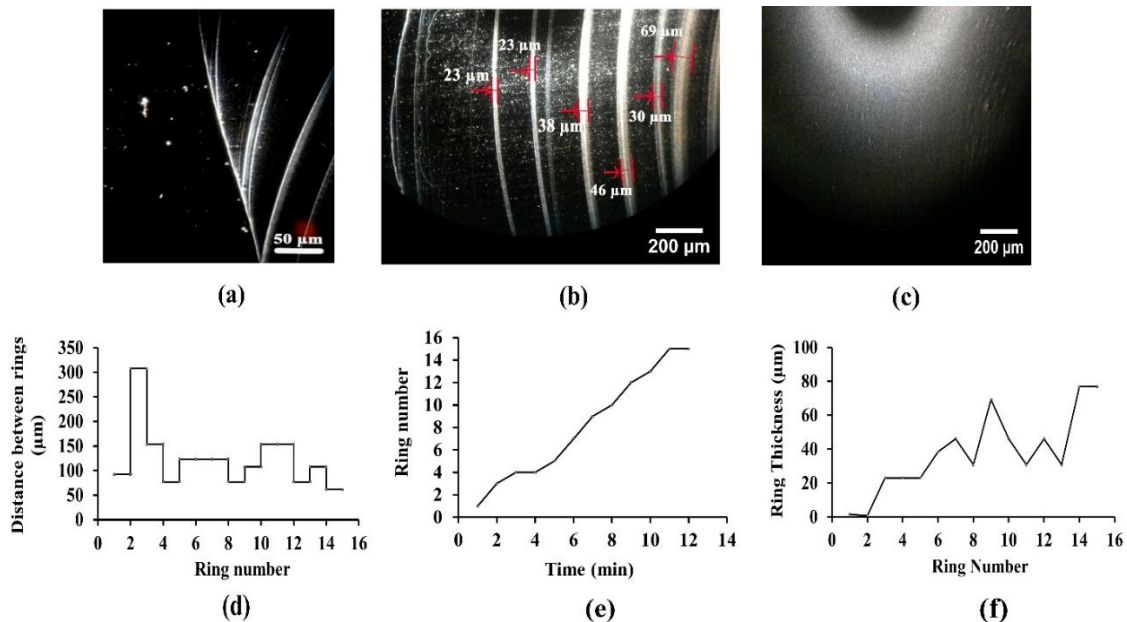


Figure 3.6. Patterns after drying of phage (dialyzed) with higher phage concentration (10^{11} PFU/ml). (a-b) Multiple coffee rings and (c) inner dried regions. The coffee rings thicknesses are pointed by arrows in (b). The characteristics of coffee rings formed for the concentrated dialyzed phage suspensions are shown as (d) distance between rings vs. ring number, (e) ring number vs. time, (f) ring thickness vs. ring number.

Figure 3.6 shows images of drying stages and the characteristic plots of multiple-ring formation, for concentrated phage suspension. For the solutions with high phage concentrations, increasing of phage nanoparticle concentration at the contact lines may result in the formation of a gel-like agglomeration in liquid-solid contact edges and consequently result in slow movement of gel-like phage agglomerates towards the centre of the droplet, during the de-pinning process (Movie S1). The solvent evaporation from such gel-like assemblies during their movement may induce the formation of highly dense inner contact regions [67].

Such behaviour was observed as the evaporative deposition of phage nanoparticles in the distinct contact rings (arrows in Figure 3.6-b), and 15 pinned contact rings were visualized from the drying process movies, during the early initial 13 min of evaporation. The observation showed that the contact rings were accumulated in one side of a droplet, while their ends joined together (Figure 3.6-a). It seems that the pinning-depinning process occurred on one side of the droplet edge, whereas the other side was pinned permanently, which is in contrast with most of the studies, expressing pinning-depinning process symmetrically, during evaporation of droplets with spherically symmetric configurations. Nevertheless, Sáenz et. al. [68], implied that the droplet geometry dictates the particle deposition and evaporative dynamics, in a way that a non-uniform coffee ring effect could be the result of non-uniform evaporation flux along the non-spherical droplet interface. The evaporation flux is larger at the corners than along the rest of the perimeter, leading to a preferential particle accumulation in these regions. Hence, such observations in this study may be due to the unintentional spreading of droplet with non-spherical geometry.

Figures 3.6 (d-f), illustrate the coffee ring characteristics for the concentrated phage suspension (without salt). As the droplet shrinks continuously, the thickness of contact rings increases due to the higher phage concentration at the centre, and consequently, the spacing between rings decreases.

Phage nanoparticles in the low-concentration suspension probably had enough free space to diffuse and recirculate towards the contact lines and backwards, within the droplet (Movie S2). Therefore, at the very initial stages of drying, they are arranged into closely packed particles in the contact lines as the result of both fluid flow and particle diffusive motion (Movie S4). Moreover, Kajiya et. al. [69], proved that the

concentration of particles near the contact line is quite large for the suspensions with both high and low colloid concentrations, which was due to the outward flow and was visible at the early moments of the drying process. As evaporation progressed, the flow velocity towards the contact line increased in order to replenish the evaporated liquid, while the droplet height was vanishing [70]. The decrease in liquid surface area transported the trapped diffusing particles from the air-liquid interface, towards the substrate surface. Increasing the particles density near the surface decreased their free motion and resulted in their deposition in thicker contact areas rather than the previously observed thinner ring-like structures previously observed (Figures S) [71]. Hence, the dried patterns of phage nanoparticles at the edges are not in the form of repeated contact rings (Figures S), as it was the case for the edge patterns observed for the concentrated dialyzed phage (Figure 3.6 (a-c)).

The inner structures of the dried patterns of both diluted and concentrated phage suspensions are quite different, representing an irregular disordered structures (Figure S) and a uniform pattern (Figure 3.6-d), respectively. The disordered irregular inner structures of dried patterns for diluted phage suspension, may be due to the non-uniform distribution and increasing the velocity of phage nanoparticles as the result of air invasion (entering of air to the droplet) [72, 73], at the final drying stage. Visualization of the final stage of evaporation, for suspensions with lower phage concentration, showed that the phage nanoparticles were entrapped as small or large clusters in the bulk flow and transported in the direction of air invasion (Movie S5). Therefore, phage nanoparticles were packed into a non-uniformed structure in the central part of the patterns. The non-uniform structure of suspensions at the final stage of drying, has also been observed by other authors [72, 74].

On the contrary, in the concentrated suspension, due to the confined diffusive motion of nanoparticles, phages were prone to be trapped by the surface and compacted at the centre of droplet/substrate interface since the initial stages of evaporation. Therefore, the formation of packed nanoparticles caused the nucleation of capillaries at the centre of the droplets [75]. Consequently, the thin film of liquid at the air-liquid interface in the final stage of drying was disrupted, as single capillary nucleation occurred inside the droplet and therefore the solution shrank from different directions (Movie S6).

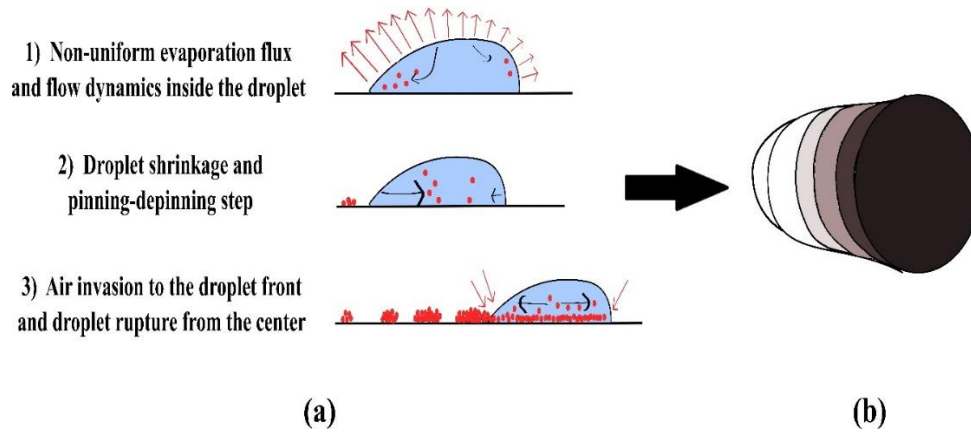


Figure 3.7: The schematic diagram of the drying process for concentrated dialyzed phage suspension, (a) the drying steps of droplet including: evaporation (formation of coffee rings and dense regions), and air invasion (formation of central area), (b) final dried patterns. Colour gradient represents different nanoparticle densities deposited onto the substrate, during the drying stages

Figure 3.7 illustrates a schematic diagram of the drying process for the high concentration phage suspension, according to the observations presented in Figure 3.6. Briefly, the phage nanoparticles deposited at the contact lines at the early stage of drying, due to the highest evaporation flux at the contact regions of the droplet. Increasing the non-uniform evaporation flux along the droplet surface enhanced the flow dynamic and radial velocity at greater distance from the droplet center. Hence, the accumulation of nanoparticles at the droplet-substrate interfaces, may sediment and pin the contact lines. At later time points of the evaporation, the bulk drop volume decreased, causing the nanoparticles flow toward the drop center and de-pinning of contact lines. The final seconds of evaporation was along with the air invasion to the droplet front, while the thin film of liquid at the air-liquid interface was ruptured from the center. The colour gradient in Figure 3.7-b represents the different phage densities deposited onto the glass coverslip during evaporation process. Phage deposition was observed to increase from the initial coffee rings towards the dense inner contact lines and inner area.

Finally, correlating the diffusion behaviour of phage nanoparticles from tracking results (Figure 3.4) to the images obtained after drying of phage suspensions (Figure 3.6 and Figure S) confirmed that deviation from normal diffusive motion, as the result of phage nanoparticle entrapment at the surface, influenced influencing the evaporation process and the dried patterns features.

Boulogne et. al.[51] stated that the drying of colloidal suspension is a competition between fluid flow causing the particles accumulation at the free surface, and the diffusive motion which smooths the concentration gradient. The formation of a skin at the surface of a drying film (as the result of fluid flow), or the consolidation in the bulk phase (due to the diffusive motion), can be distinguished through measuring

Peclet number. Hence, in future works, diffusion coefficient, film thickness and the evaporation rate, could be assessed in order to obtain the Peclet number as an index to distinguish between skin formation and consolidation in the bulk.

3.4 Concluding Remarks

Bacteriophage immobilization onto functional materials through evaporation is a simple, fast and effective method to develop a suitable bioactive material. Dark-field enhanced optical microscopy (CytoViva) was applied in this research to visualize and track phage nanoparticles movements in an aqueous liquid and observe their final assembly patterns after evaporation.

Phage arrangement on the surface originated from a competition between fluid flow and nanoparticle motion during evaporation. Assessing the fluid flow and phage motion during the drying process of aqueous solutions of phage suspension with different concentrations clarified the impact of parameters such as liquid salinity and phage concentration on the drying process and final dried patterns. It was found that thin distinguishable rings and a uniform inner pattern were formed at higher concentrations, while thicker contact regions at the edges as well as a disordered inner pattern have been observed for the lower concentrations.

Aside from the parameters investigated in this approach, there are still several other factors, such as pH, surface type and hydrophobicity, temperature and different salt type and concentrations that require further research to reach a thorough analysis of phage immobilization onto the surfaces.

Tracking of phage nanoparticles is an advanced capability of the technique proposed in this study that provides insights for inferring the phage-based structures under various conditions. That may be regulated. Calculation of phage nanoparticles diffusion coefficient through the tracking method and its comparison with the standard diffusion coefficient at the same temperature, may lead to define the phage adsorption process onto a substrate. A diffusion-limited adsorption can be attributed to a system with normal phage diffusive motion, while there is less phage entrapment by the substrate during evaporation. However, the effect of concentration on the diffusive motion of phage nanoparticles could result in the possibility of phage adsorption to the substrate, as well as on the final dried pattern.

The label-free technique introduced by this paper is a useful method for the in-situ study of both monitoring of the microscopic particles and the in-situ study of the self-assembly process. This technique has the advantage of being simple, without any laborious preparations, for repeatedly applying to track VNPs. Therefore, it can be extensively used for a range of practical applications based on phage templating. However, the results are still in the very early stage, therefore requiring further work to reach the full capacity of this technique.

Our tracking and self-assembly results provide new insights for tuning the self-assembly behaviour of viruses by manipulating the experimental conditions in order to fabricate the desired architectures. Comparison of viral and non-viral motion in a simulated designed environment to that of biological ones with the presented method, may help with the studies of gene and drug delivery for future works.

T4 Bacteriophage immobilization on substrates is widely investigated for the biosensor applications as well as formation of novel bioactive surfaces used for prevention of biofilm formation in medical applications. Patterned immobilization of T4 phages on top of surfaces may lead to better capture of pathogens in different applications.

Supplementary Materials: The following are available online at www.mdpi.com/link.

3.5 References:

1. Moghimian, P., et al., *Adsorption and self-assembly of M13 phage into directionally organized structures on C and SiO₂ films*. *Langmuir*, 2014. **30**(38): p. 11428-32.
2. Yoo, P.J., et al., *Spontaneous assembly of viruses on multilayered polymer surfaces*. *Nature Materials*, 2006. **5**: p. 234.
3. Lee, L.A., et al., *Assembly of Virus Particles and Virus-like Particles as Templates for Biomedical Applications*, in *Nanomaterials for Biomedicine*. 2012, American Chemical Society. p. 21-56.
4. Lin, Y., et al., *Layer-by-layer assembly of viral capsid for cell adhesion*. *Acta Biomaterialia*, 2008. **4**(4): p. 838-843.
5. Wang, L., et al., *Bottom-Up Synthesis and Sensor Applications of Biomimetic Nanostructures*. *Materials (Basel)*, 2016. **9**(1).
6. Lee, S.Y., J.S. Lim, and M.T. Harris, *Synthesis and application of virus-based hybrid nanomaterials*. *Biotechnol Bioeng*, 2012. **109**(1): p. 16-30.
7. Rink, V., et al., *Electrostatic conditions define the 2D self-assembly of tomato bushy stunt viruses on solid surfaces*. *Biointerphases*, 2017. **12**(4): p. 04e402.
8. Ahmed, S. and K.M. Ryan, *Centimetre scale assembly of vertically aligned and close packed semiconductor nanorods from solution*. *Chemical Communications*, 2009(42): p. 6421-6423.
9. Zanella, M., et al., *Self-assembled multilayers of vertically aligned semiconductor nanorods on device-scale areas*. *Adv Mater*, 2011. **23**(19): p. 2205-9.
10. Bigioni, T.P., et al., *Kinetically driven self assembly of highly ordered nanoparticle monolayers*. *Nature Materials*, 2006. **5**: p. 265.
11. Baker, J.L., et al., *Device-Scale Perpendicular Alignment of Colloidal Nanorods*. *Nano Letters*, 2010. **10**(1): p. 195-201.
12. Ma, H. and J. Hao, *Ordered patterns and structures via interfacial self-assembly: superlattices, honeycomb structures and coffee rings*. *Chemical Society Reviews*, 2011. **40**(11): p. 5457-5471.
13. Brezesinski, T., et al., *Evaporation-Induced Self-Assembly (EISA) at Its Limit: Ultrathin, Crystalline Patterns by Templating of Micellar Monolayers*. *Advanced Materials*, 2006. **18**(17): p. 2260-2263.
14. Josten, E., et al., *Superlattice growth and rearrangement during evaporation-induced nanoparticle self-assembly*. *Scientific Reports*, 2017. **7**(1): p. 2802.

15. Lee, S.-W., B.M. Wood, and A.M. Belcher, *Chiral Smectic C Structures of Virus-Based Films*. Langmuir, 2003. **19**(5): p. 1592-1598.
16. Wu, L., et al., *Electrospinning fabrication, structural and mechanical characterization of rod-like virus-based composite nanofibers*. Journal of Materials Chemistry, 2011. **21**(24): p. 8550-8557.
17. Joksimovic, R., et al., *Self-organized patterning through the dynamic segregation of DNA and silica nanoparticles*. Scientific Reports, 2014. **4**: p. 3660.
18. Kunstmann-Olsen, C., D. Belic, and M. Brust, *Monitoring pattern formation in drying and wetting dispersions of gold nanoparticles by ESEM*. Faraday Discussions, 2015. **181**(0): p. 281-298.
19. Lin, Y., et al., *Self-Assembly of Virus Particles on Flat Surfaces via Controlled Evaporation*. Langmuir, 2011. **27**(4): p. 1398-1402.
20. Zhang, X., A. Crivoi, and F. Duan, *Three-dimensional patterns from the thin-film drying of amino acid solutions*. Scientific Reports, 2015. **5**: p. 10926.
21. Goldsmith, C.S. and S.E. Miller, *Modern uses of electron microscopy for detection of viruses*. Clin Microbiol Rev, 2009. **22**(4): p. 552-63.
22. Isenbugel, K., Y. Gehrke, and H. Ritter, *Evaporation-driven self-assembly of colloidal silica dispersion: new insights on janus particles*. Macromol Rapid Commun, 2012. **33**(1): p. 41-6.
23. Goehring, L., W.J. Clegg, and A.F. Routh, *Plasticity and fracture in drying colloidal films*. Phys Rev Lett, 2013. **110**(2): p. 024301.
24. Negishi, M., et al., *Phase behavior of crowded like-charged mixed polyelectrolytes in a cell-sized sphere*. Phys Rev E Stat Nonlin Soft Matter Phys, 2011. **83**(6 Pt 1): p. 061921.
25. Fang, X., et al., *Drying of DNA Droplets*. Langmuir, 2006. **22**(14): p. 6308-6312.
26. Maheshwari, S., et al., *Coupling Between Precipitation and Contact-Line Dynamics: Multiring Stains and Stick-Slip Motion*. Physical Review Letters, 2008. **100**(4): p. 044503.
27. Zhang, L., et al., *Evaporative Self-Assembly from Complex DNA-Colloid Suspensions*. Langmuir, 2008. **24**(8): p. 3911-3917.
28. Fumagalli, L., et al., *Label-free identification of single dielectric nanoparticles and viruses with ultraweak polarization forces*. Nature Materials, 2012. **11**: p. 808.
29. Brandenburg, B. and X. Zhuang, *Virus trafficking – learning from single-virus tracking*. Nature reviews. Microbiology, 2007. **5**(3): p. 197-208.
30. Lakadamyali, M., et al., *Visualizing infection of individual influenza viruses*. Proc Natl Acad Sci U S A, 2003. **100**(16): p. 9280-5.
31. Ruthardt, N., D.C. Lamb, and C. Brauchle, *Single-particle tracking as a quantitative microscopy-based approach to unravel cell entry mechanisms of viruses and pharmaceutical nanoparticles*. Mol Ther, 2011. **19**(7): p. 1199-211.
32. Hsieh, C.-L., et al., *Tracking Single Particles on Supported Lipid Membranes: Multimobility Diffusion and Nanoscopic Confinement*. The Journal of Physical Chemistry B, 2014. **118**(6): p. 1545-1554.
33. Scherr, S.M., et al., *Real-Time Capture and Visualization of Individual Viruses in Complex Media*. ACS Nano, 2016. **10**(2): p. 2827-33.
34. Wang, S., et al., *Label-free imaging, detection, and mass measurement of single viruses by surface plasmon resonance*. Proceedings of the National Academy of Sciences of the United States of America, 2010. **107**(37): p. 16028-16032.
35. Faez, S., et al., *Fast, Label-Free Tracking of Single Viruses and Weakly Scattering Nanoparticles in a Nanofluidic Optical Fiber*. ACS Nano, 2015. **9**(12): p. 12349-12357.
36. Mitra, A., et al., *Nano-optofluidic detection of single viruses and nanoparticles*. ACS Nano, 2010. **4**(3): p. 1305-12.
37. Mitra, A., F. Ignatovich, and L. Novotny, *Real-time Optical Detection of Single Human and Bacterial Viruses Based on Dark-field Interferometry*. Biosensors & bioelectronics, 2012. **31**(1): p. 499-504.
38. Kukura, P., et al., *High-speed nanoscopic tracking of the position and orientation of a single virus*. Nature Methods, 2009. **6**: p. 923.

39. Klein, N.D., et al., *Dark Field Transmission Electron Microscopy as a Tool for Identifying Inorganic Nanoparticles in Biological Matrices*. Analytical Chemistry, 2015. **87**(8): p. 4356-4362.
40. Theoret, T. and K.J. Wilkinson, *Evaluation of enhanced darkfield microscopy and hyperspectral analysis to analyse the fate of silver nanoparticles in wastewaters*. Analytical Methods, 2017. **9**(26): p. 3920-3928.
41. Li, H., et al., *Direct observation of nanoparticle multiple-ring pattern formation during droplet evaporation with dark-field microscopy*. Physical Chemistry Chemical Physics, 2016. **18**(18): p. 13018-13025.
42. Enoki, S., et al., *Label-free single-particle imaging of the influenza virus by objective-type total internal reflection dark-field microscopy*. PLoS One, 2012. **7**(11): p. e49208.
43. Wan, X.-Y., et al., *Real-Time Light Scattering Tracking of Gold Nanoparticles- bioconjugated Respiratory Syncytial Virus Infecting HEp-2 Cells*. Scientific Reports, 2014. **4**: p. 4529.
44. Sambrook, J., Russell, J., *Molecular Cloning: A Laboratory Manual*. 2001: Cold Spring Harbor Laboratory Press: NY, USA.
45. Guo, P., et al., *Rapid and simplified purification of recombinant adeno-associated virus*. J Virol Methods, 2012. **183**(2): p. 139-46.
46. Bernhardt, S., *Mean-shift video tracking*. 2008, MATLAB Central File Exchange. Retrieved March 8, 2012.
47. Moon, J.-S., et al., *M13 Bacteriophage-Based Self-Assembly Structures and Their Functional Capabilities*. Mini-Reviews in Organic Chemistry, 2015. **12**(3): p. 271-281.
48. Yang, S.H., et al., *Assembly of bacteriophage into functional materials*. Chem Rec, 2013. **13**(1): p. 43-59.
49. Bodiguel, H. and J. Leng, *Imaging the drying of a colloidal suspension*. Soft Matter, 2010. **6**(21): p. 5451-5460.
50. Fan, F. and K.J. Stebe, *Assembly of colloidal particles by evaporation on surfaces with patterned hydrophobicity*. Langmuir, 2004. **20**(8): p. 3062-7.
51. Boulogne, F., F. Giorgiutti-Dauphine, and L. Pauchard, *Surface patterns in drying films of silica colloidal dispersions*. Soft Matter, 2015. **11**(1): p. 102-8.
52. Polson, A., *Diffusion constants of the E. coli bacteriophages*. Proc Soc Exp Biol Med, 1948. **67**(3): p. 294-6.
53. Polson, A. and C.C. Shepard, *On the diffusion rates of bacteriophages*. Biochimica et Biophysica Acta, 1949. **3**(Supplement C): p. 137-145.
54. Cookson, J.T. and W.J. North, *Adsorption of viruses on activated carbon. Equilibriums and kinetics of the attachment of Escherichia coli bacteriophage T4 on activated carbon*. Environ Sci Technol, 1967. **1**(1): p. 46-52.
55. Shen, X., C.-M. Ho, and T.-S. Wong, *Minimal Size of Coffee Ring Structure*. The Journal of Physical Chemistry B, 2010. **114**(16): p. 5269-5274.
56. Fischer, B.J., *Particle Convection in an Evaporating Colloidal Droplet*. Langmuir, 2002. **18**(1): p. 60-67.
57. Hu, H. and R.G. Larson, *Analysis of the Microfluid Flow in an Evaporating Sessile Droplet*. Langmuir, 2005. **21**(9): p. 3963-3971.
58. Kaplan, C.N., et al., *Dynamics of evaporative colloidal patterning*. Physics of Fluids, 2015. **27**(9): p. 092105.
59. Kaplan, C.N. and L. Mahadevan, *Evaporation-driven ring and film deposition from colloidal droplets*. Journal of Fluid Mechanics, 2015. **781**.
60. Rio, E., et al., *Moving Contact Lines of a Colloidal Suspension in the Presence of Drying*. Langmuir, 2006. **22**(7): p. 3186-3191.
61. Lin, Y., et al., *Self-assembly of rodlike bio-nanoparticles in capillary tubes*. Angew Chem Int Ed Engl, 2010. **49**(5): p. 868-72.

62. Moffat, J.R., K. Sefiane, and M.E.R. Shanahan, *Effect of TiO₂ Nanoparticles on Contact Line Stick–Slip Behavior of Volatile Drops*. The Journal of Physical Chemistry B, 2009. **113**(26): p. 8860-8866.
63. Li, Q., P. Zhou, and H.J. Yan, *Pinning–Depinning Mechanism of the Contact Line during Evaporation on Chemically Patterned Surfaces: A Lattice Boltzmann Study*. Langmuir, 2016. **32**(37): p. 9389-9396.
64. Baldwin, K.A. and D.J. Fairhurst, *Classifying dynamic contact line modes in drying drops*. Soft Matter, 2015. **11**(8): p. 1628-1633.
65. Zhang, J., F. Müller-Plathe, and F. Leroy, *Pinning of the Contact Line during Evaporation on Heterogeneous Surfaces: Slowdown or Temporary Immobilization? Insights from a Nanoscale Study*. Langmuir, 2015. **31**(27): p. 7544-7552.
66. Orejon, D., K. Sefiane, and M.E.R. Shanahan, *Stick–Slip of Evaporating Droplets: Substrate Hydrophobicity and Nanoparticle Concentration*. Langmuir, 2011. **27**(21): p. 12834-12843.
67. Tarasevich, Y.Y., I.V. Vodolazskaya, and O.P. Isakova, *Desiccating colloidal sessile drop: dynamics of shape and concentration*. Colloid and Polymer Science, 2011. **289**(9): p. 1015-1023.
68. Sáenz, P.J., et al., *Dynamics and universal scaling law in geometrically-controlled sessile drop evaporation*. 2017. **8**: p. 14783.
69. Kajiya*, T., D. Kaneko, and M. Doi, *Dynamical Visualization of “Coffee Stain Phenomenon” in Droplets of Polymer Solution via Fluorescent Microscopy*. Langmuir, 2008. **24**(21): p. 12369-12374.
70. Trantum, J.R., et al., *Cross-Sectional Tracking of Particle Motion in Evaporating Drops: Flow Fields and Interfacial Accumulation*. Langmuir, 2013. **29**(21): p. 6221-6231.
71. Li, Y., et al., *Rate-dependent interface capture beyond the coffee-ring effect*. Scientific Reports, 2016. **6**: p. 24628.
72. van der Kooij, H.M., G.T. van de Kerkhof, and J. Sprakel, *A mechanistic view of drying suspension droplets*. Soft Matter, 2016. **12**(11): p. 2858-2867.
73. van der Kooij, H.M., et al., *Coalescence, Cracking, and Crack Healing in Drying Dispersion Droplets*. Langmuir, 2015. **31**(15): p. 4419-28.
74. Marín, Á.G., et al., *Order-to-Disorder Transition in Ring-Shaped Colloidal Stains*. Physical Review Letters, 2011. **107**(8): p. 085502.
75. Eales, A.D., et al., *Evaporation of pinned droplets containing polymer – an examination of the important groups controlling final shape*. AIChE Journal, 2015. **61**(5): p. 1759-1767.

4. Chapter Four

Immobilization of Bacteriophages on glass and collagen surfaces: An approach to make antibacterial coatings

*Ima Ghaeli^{1,2,3}, Adam L.J. Olsson⁴, Natalie Fekete⁴, Nathalie Tufenkji⁴, Corinne A. Hoesli⁴,
Fernando J. Monteiro^{1,2,3}*

¹i3S-Instituto de Investigação e Inovação em Saúde, Universidade do Porto, Portugal

²INEB - Instituto de Engenharia Biomédica, Universidade do Porto, Porto, Portugal

³Faculdade de Engenharia, Universidade do Porto, Porto, Portugal

⁴Department of Chemical Engineering, McGill University, Montreal, QC, Canada H3A 0C5

Abstract

Biomaterials and medical device-associated infections as well as bacterial resistance to conventional antibiotics account for more than 60% of health care-associated infections that cost billions of dollars annually. The surface modification of biomaterial surfaces is a promising methodology to achieve antibacterial properties, as the bulk integrity of the material is kept unchanged. Hence, current work focuses on modifying the material surfaces and generating novel products in order to mitigate the bacterial adhesion to the surfaces as well as inhibit their growth in the media. Based on the therapeutic promise of bacteriophages used to control bacterial infections as an alternative route to the use of antibiotics, this work developed novel antibacterial surfaces through bacteriophage T4 immobilization. Such surfaces were shown to inhibit *Escherichia coli* bacterial growth in the medium and reduce biofilm formation. The inhibitory mechanism is shown to be obtained by the effect of immobilized phages killing the bacteria to prevent bacterial growth in the medium in the initial stages (12 hours) and reducing biofilm formation on substrates for longer periods (24 hours). The bioactivity lifetime of the produced surfaces was assessed through storage of phage immobilized surfaces for 1 and 7 days at room temperature under sterile conditions. Moreover, the bacteriophage stability on the material surfaces has been analyzed by incubation of phage immobilized materials under stirring at 37 °C, for 24 hours and 3 days culture medium without any bacteria inoculated. The phage stability analysis showed promising results for the phage-immobilized collagen surfaces.

Furthermore, the surface-modified biomaterials did not significantly affect mesenchymal cell viability and metabolic activity. The ability of this novel phage-immobilized surfaces to counteract biofilm formation and promote mesenchymal stem cell attachment makes it a suitable novel and cost effective antibacterial coating that can be used in medical applications.

4.1 Introduction

Biofilm formation on medical devices and biomaterial surfaces (e.g. catheters, prosthetic joints, mechanical heart valves, pacemakers, and contact lenses), is a major problem in hospital-associated infections, particularly in the context of increasing bacterial resistance to conventional antibiotics. Approximately 40-50% of prosthetic heart valve infections and 50-70% of catheter biofilm infections, are caused by bacteria that are known as antibiotic resistant bacteria in health care systems [1, 2]. Moreover, infections associated to implanted intravascular devices, caused by staphylococci, increased the health costs in US, from 4000\$ to 56000\$ for each infection, creating a burden on healthcare systems [3, 4]. Other complications include infections associated with orthopedic implants surgery (such as joint replacement,

hip and knee prostheses), with estimated costs of \$50,000 for each infection [5]. These latter infections are typically caused by polymicrobial pathogens including *staphylococci* (30-40%), *Staphylococcus aureus* (12-23%), and *streptococci* (9-10%) [6].

Biofilm formation starts with bacterial attachment to medical biodevice materials, which is followed by rapid growth and deposition of exopolymeric substances (EPS), as the components of the extracellular bacterial structures, forming a polymer matrix that maintains and protects the microorganisms within the produced biofilms [6, 7]. Biofilms are recalcitrant to antibiotic killing and therefore the best approach to control biofilm formation is preventing bacterial adhesion. As such, a smart approach to reduce microbial attachment to the surface is to engineer bactericidal surfaces.

Unlike traditional antibiotics, the high specificity of bacteriophages to the targeted hosts makes them highly suitable for antibacterial applications, particularly against antibiotic-resistant bacteria [8]. Bacteriophage indwelling materials and medical devices are characterized by a significant capacity to kill bacteria [9-12] and thereby provide pathways for developing novel healthcare methods to inhibit biofilm-mediated infections on implantable medical devices. Despite a number of studies published on the potential incorporation of bacteriophages into the medical devices, recent studies on immobilization techniques mostly focused on the phage orientation techniques, with highly controlled phage-surface interactions [13]. These studies indicate that designing stimuli-responsive bioactive surfaces using bacteriophages, with high bacterial capture capability, requires proper phage orientation on the surfaces [14] in such a way that phages heads are immobilized onto the surface, while the tails are free to capture bacteria.

The literature on phage encapsulation and immobilization shows that except for chemical modification of phage and substrate to facilitate chemical adsorption, the simplest immobilization methods include physisorption, electrostatic attachment and covalent bonding [15-21]. Physico-chemical characteristics of both medium and surface are important parameters for phage adsorption to the substrates and to control phage aggregation. Alterations of pH affect both phage and substrate charges. At elevated pH (~9), negatively charged carboxylic acid groups on phages can adsorb to positively charged surfaces. At lower pH values (~3), phages can easily adsorb by their covered H_3O^+ ions, to the negatively charged groups of the surfaces [22]. Moreover, surface physical characteristics, such as hydrophobicity and roughness, have proved to improve not only the filamentous phage attachment, but also their directional alignment so as to form a highly orientational substrate [23].

Besides controlled phage-surface interactions, phages at the liquid-air interface and in bulk fluid can be assembled in such a way that a layer of phages is transferred to the solid-liquid interface through various techniques such as Langmuir-Blodgett and air drying method [24-26]. In the air drying method, phage alignment and assembly on the surface are governed by an evaporation-driven mechanism [27, 28].

This work aims at developing an antimicrobial biocompatible coating for biomaterials through bacteriophage immobilization by air-drying method.

4.2 Materials and Methods:

4.2.1 Sample preparation

Bacteriophage T4 was obtained from the F Félix D'Herelle Reference Centre for Bacterial Viruses (Université Laval, Quebec, Canada), and *Escherichia coli* BL21 was purchased from Cedarlane (Cedarlane Corporation, Burlington, Ontario, Canada). Two cultures of *Escherichia coli* BL21 (5 mL each) were grown overnight in Lysogenic broth (LB) at 37 °C. The first 5 mL culture was added to 200 mL of sterile LB and incubated at 37 °C for 3 hours with shaking. The second 5 mL culture was inoculated with 100 µL of bacteriophage T4 stock isolated from *Escherichia coli* BL21, for 15 minutes at room temperature, and then added to the above-mentioned 3 hours incubated culture and shaken overnight at 37 °C.

For phage purification and propagation, the overnight cultures were centrifuged at 6000 rpm (RC-6, Sorvall) for 20 min, and the supernatant was recovered and sterile-filtered. The supernatant was treated with nuclease solutions (final concentration of 1 µg/mL, 30 min at room temperature), and subsequently mixed with 1M NaCl and PEG 8000 (10 v/w%) and stirring overnight at 4 °C to precipitate phage particles. The precipitated phage were spun down by centrifugation (14000 rpm, 10 °C, for 3 hrs). Finally, the phage suspension was purified using ultracel 100kDa filters (Amicon Ultra centrifugal filters, Millipore). The precipitated phage were re-suspended in SM buffer (containing 5.8 g/L NaCl, 120 mg/L MgSO₄, 50 mL of 1 M Tris-HCl, pH 8) and sterile filtered. This method resulted in a phage titer of 10¹⁰-10¹² PFU/mL. To determine the phage titer, ten-fold serial dilutions were prepared and after mixing with overnight host bacteria, the solutions were added to molten soft agar, which was spread over the plates. The plates were incubated overnight at 37 °C and the number of plaques were enumerated.

4.2.2 Phage-based materials

Type I collagen extracted from rat-tail tendons and solubilized in acetic acid solution (0.02 N) at a concentration of 4 g/L, was obtained from Laval University, Quebec, Canada [29]. The films were prepared through air drying of solutions at room temperature onto circular glass cover slides (Fisher) that had been previously cleaned with ethanol. Thereafter, phage liquids were air-dried onto bare glass cover slides (previously cleaned with ethanol) and collagen films, for overnight under sterile conditions in a biosafety cabinet.

4.2.3 Phage stability analysis

The stability of surface-immobilized phages was analyzed through incubation of surfaces with immobilized phages under shaking at 37 °C, for 24 hours in LB without any bacteria inoculated, and 3 days in cell culture medium without any cells. Phage release in LB and cell culture medium was assessed through phage titration, in order to measure the plaque forming units (pfu) per ml.

4.2.4 Antimicrobial properties of phage immobilized materials

The infectivity of phage immobilized materials was analyzed using disc diffusion method to visualize the lysis zone around the immobilized substrates. Phage dried substrates were laid on agar plates and following overnight incubation at 37 °C, lytic rings were observed by naked eyes.

4.2.5 Bacteria culture and antibacterial activity of materials

Incubated overnight *E. coli* cultures of 5 ml were diluted into 100 ml of LB. Phage immobilized samples were placed in 2 ml of diluted bacterial cultures, incubated and left shaking at 150 rpm, for 12 and 24 hours. Bacterial cultivability was measured by bacteria counting, through serial dilutions and plating on LB agar. The non-immobilized samples as well as culture media, were considered as controls. Each assessment was done in triplicate.

4.2.6 Bacterial adhesion to the surfaces

The phage immobilized materials were incubated in 2 ml of bacterial culture (10^6 CFU/mL), under 150 rpm agitation, for 24 hours. The overnight incubated surfaces were washed twice with deionized water and subjected to the live/dead bacterial staining solution for 15 min in the dark. The excess solution was then removed and the samples were placed on top of glycerol on microscope glass slides. Samples were then observed using a fluorescence microscope (Olympus IX71, Tokyo, Japan).

4.2.7 Storage effect:

The storage effect on phage activity was assessed by storage of phage immobilized substrates for a period of 7 days at room temperature. After exposing the materials to the *E. coli* culture, a quantitative biological assay was carried out by bacterial counting through serial dilutions and LB agar plating.

4.2.8 In vitro cytotoxicity

Frozen Mesenchymal stem cells kept in liquid nitrogen tank from 2008, were a gift from Professor Leask at McGill University. The thawed MSCs were cultured in high glucose DMEM supplemented with 10% FBS. The MSCs in their 7th passage were seeded onto the phage-based materials. The control wells contained the non-immobilized substrates, as well as the empty tissue culture polystyrene well (TCPS).

After incubating for 5 days, the samples were transferred separately to different plates for the Live/Dead viability, WST-1 and Immunofluorescence staining assays.

Cell viability was assessed via the WST-1 assay, based on cleavage of tetrazolium salts by mitochondrial dehydrogenase in viable cells. Therefore, after the incubation for 5 days in cell culture media, the cell-material complexes were incubated in the WST-1 solution for 2 hours in a humidified atmosphere (37 °C and 5% CO₂). The absorbance of formazan product derived from cell metabolism was measured at 420-480 nm (with maximum absorption at about 440 nm) using a TECAN Infinite M200 Pro microplate reader (TECAN group Ltd., Switzerland).

The Live/Dead viability assay (Invitrogen) was used to quantify cell death. Briefly, a solution of 150 µl stain containing calcein AM and ethidium homodimer-1 (EthD-1), was mixed with 150 µl culture medium, added to the cell-substrates complexes and kept under dark conditions for 30 min. After removing the staining solutions, the fluorescence data were measured by fluorescence microscopy (Olympus IX81, Tokyo, Japan), at 530 and 645 nm, for live and dead cells, respectively.

For the Immunofluorescence staining assay, the transferred samples, after incubation, were washed with PBS and the cells on the films were fixed with 4% paraformaldehyde for 15 minutes at room temperature. After washing samples with PBS, the cells on substrates were permeabilized with 0.1% Triton X 100 for 15 minutes. After blocking with Protein Block solution (Dako, Cedarlane) for another 15 min, samples were stained for actin using Phalloidin-TRITC at 1:200 dilution in Dako antibody diluent, for 1 hour at room temperature. Nuclei were then stained with 1 mg/mL 4',6-diamidino-2-phenylindole (DAPI, Sigma) diluted in PBS 1:1000. The stained samples were imaged on a fluorescence microscope system (Olympus IX81). DAPI, TRITC and FITC filters were used in addition to phase contrast for 10× and DIC for 40× and 60× objectives. Channel merger plugin in ImageJ software was applied for obtaining final images.

4.3 Results:

4.3.1 Immobilization of phages on glass coverslip

Drying, which induces self-assembly of phage colloidal solution, was used as a simple method to prepare a thin layer of phage nanoparticles on top of substrates to obtain antibacterial surfaces.

Based on an evaporation-driven mechanism, phage started to deposit onto the substrate from the droplet periphery while the solvent was evaporated at room conditions. As shown in Figure 4.1, the final dried patterns obtained after drying of phage suspension (10⁹ pfu/ml) on glass cover slide, has been visualized under a dark-field microscope. However, due to the opacity of collagen films, the dried patterns of phage suspension on top of collagen were not obvious under the microscope.

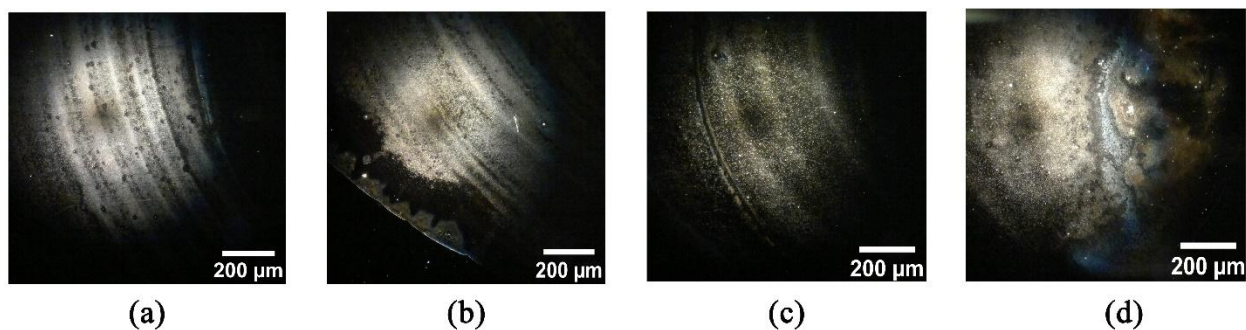


Figure 4.1: Patterns after drying of dialyzed phage droplet (10^9 pfu/ml) on glass cover slide, using darkfield microscope, (10× objective): (a-c) the edges of dried droplet, (d) the central part

Figure 4.1 represents the patterns of various areas of dried droplet. As it can be seen, phage nanoparticles deposited non-uniformly onto the glass cover slide, during evaporation. During evaporation procedure, the competition between evaporation rate and diffusion rate of nanoparticles, dictates the final dried patterns, in such a way that at slow evaporation rate, the diffusion rate of nanoparticles dominates and results to the diffusion-limited adsorption of phages [30, 31]. However, during drying process, several parameters such as particle interactions, mass and heat transfer during drying process, particle concentration, and surface hydrophobicity should be considered that may influence on the final dried patterns [32].

4.3.2 Antibacterial activity

The bioactivity of phage immobilized substrates has been assessed both visually and quantitatively, through incubating the substrates in the *E.coli* lawn (disc diffusion method) and suspension, respectively. The formation of a transparent ring-shaped zone around the phage immobilized substrates (after 1-day storage) on top of the lawns, is shown in Figure 4.2.

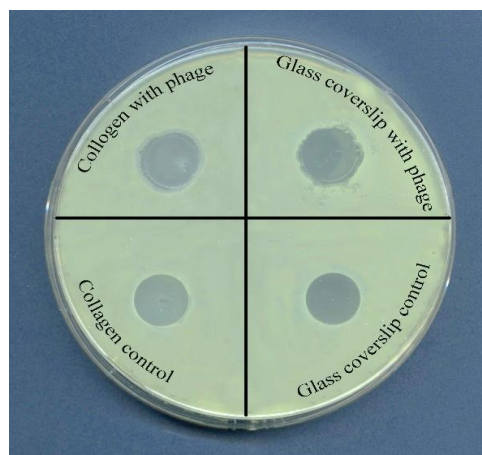


Figure 4.2: Lysis ring of phage immobilized collagen and glass coverslip, as well as the non-immobilized substrates

No clear zone could be observed around the non-immobilized substrates. Hence, the lysis rings around the samples with immobilized bacteriophages is due to the diffusion of phage particles through the bacterial laws, which demonstrates the antimicrobial activity of such surfaces.

As shown in Figure 4.3, the quantitative analysis of phage immobilized surface bioactivity has been assessed through planktonic growth of *E. coli* bacteria (cfu/ml) (with a defined initial concentration of $1.52E+07$ cfu/ml), in the presence of various substrates (phage immobilized and non-immobilized substrates), after 12 and 24 hours of incubation. The bacterial cultures in the individual polystyrene wells without materials, were used as the negative controls.

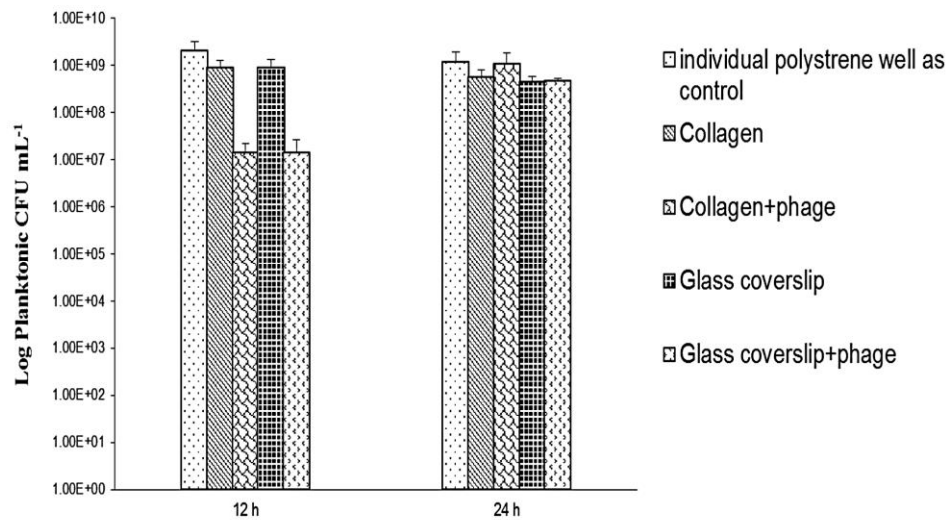


Figure 4.3: Antibacterial efficiency of substrates through *E. coli* planktonic growth analysis after incubation of surfaces for 12 and 24 hours (with the bacteria initial concentration of $1.52E+07$).

Generally, monocultures with *E. coli* bacteria reached maximum cell densities of 10^8 to 10^9 bacteria/ml within the first day [33]. As shown in Figure 4.3, within 12 hours, the maximum *E. Coli* cell densities were obtained for the control polystyrene culture wells. However, the planktonic *E. coli* growth was significantly inhibited by the substrates with immobilized phages within 12 hours of inoculation. Nevertheless, after 24 hours, maximum cell densities were obtained for all the samples, that may be due to the emergence of planktonic resistant cells to the phages [34] between 12 to 24 hours.

Besides the planktonic cell growth studies that might represent antibacterial activity of phage-immobilized substrates for short period of time (12 hours), the biofilm formation was assessed visually and quantitatively, using live/dead and crystal violet assays, respectively (Figure 4.4).

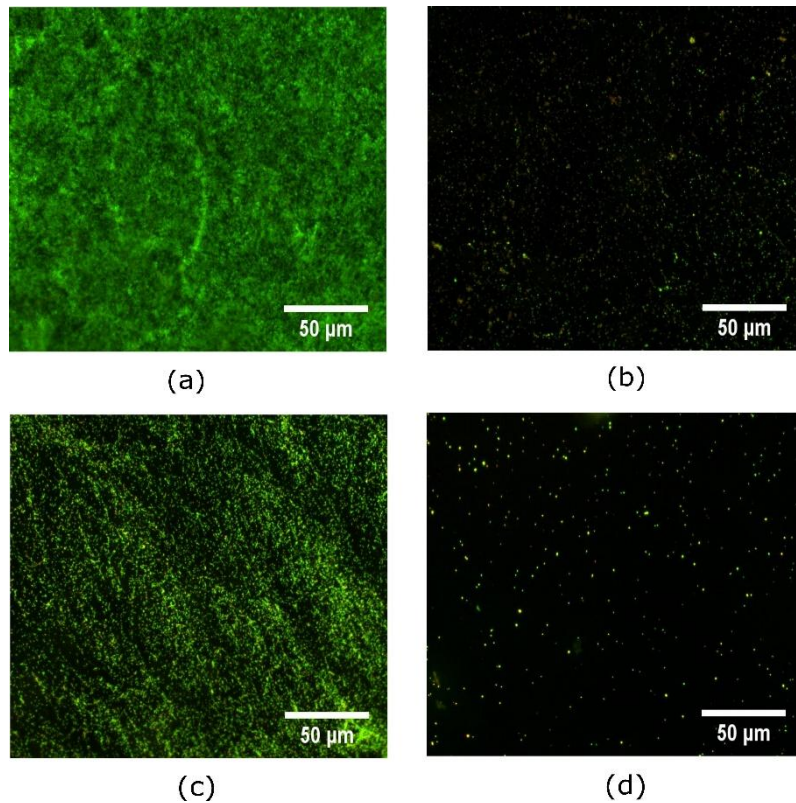


Figure 4.4: Visualization of biofilm formation onto surfaces after 24 hours (through Live/dead bacteria staining): (a) collagen, (b) phage-immobilized collagen, (c) glass cover slide, (d) phage-immobilized glass cover slide

As expected, collagen surfaces were conducive to biofilm attachment [33]. The fibril forming collagen I has influence on bacteria-protein interactions and biofilm formation [35]. As shown in Figure 4, the fluorescence microscopy analysis confirmed that the biofilm was significantly reduced on to the phage immobilized surfaces. The reduction of both planktonic bacteria after 12 hours and inhibition of biofilm formation after 24 hours, confirms the inhibitory effect of phage immobilized surfaces compared to the non-immobilized samples.

4.3.3 Phage stability and lysis analysis:

The stability of the immobilized phages was assessed by placing the test surfaces in bacteria medium without bacteria and MSC cell culture medium without cells. The concentration of released phages in the culture media has been measured after 3 days of incubation. Considering the initial phage concentration of $5.4E+10$ pfu/ml used for immobilization, a low amount of phage, $3.33E+04$ pfu/ml was released from collagen, and no phage was released from glass cover slides.

Based on these results and considering a low amount of phage release in the absence of bacteria, the immobilized surfaces were then incubated in the bacteria culture media, for 12 and 24 hours. The number of phage released after infection of the bacteria, has been shown in Figure 4.6.

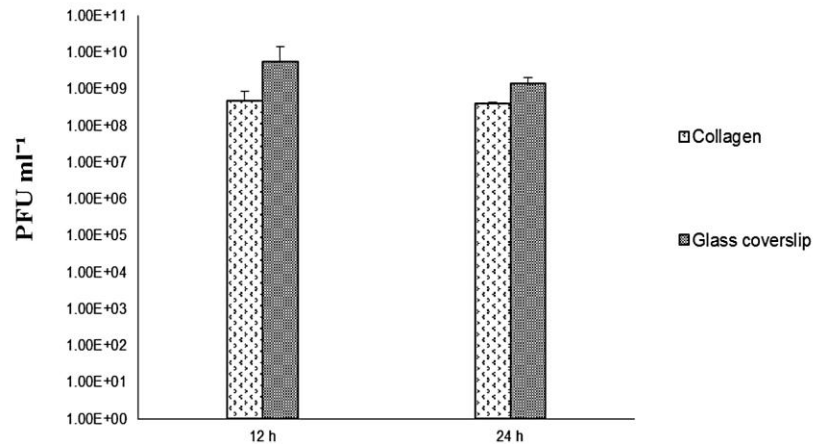


Figure 4.6: Phage concentration in the culture media after inoculation of immobilized surfaces for 12 and 24 hours (The initial phage concentration was 5.4E+10 pfu/ml)

The amount of produced progeny phage in the bacterial culture media after 12 and 24 hours of sample inoculations, is shown in Figure 4.6. It can be observed that after 12 hours of infection, there was a substantial burst of progeny phage with around 1E+08 pfu/ml. However, the amount of phage progeny after 24 hours increased to 1E+09 pfu/ml, illustrating the completion of the lysis cycle, as the bacteria growth reached a stationary phase, and the lack of nutrients in the environment decreased the ability to produce further phages. As above mentioned, there is no phage release from the surfaces in the media without bacteria. Hence, the existence of active phages in the inoculated media after bacterial infection is due to the production of progeny phages and independent of phage detachment from the substrates.

4.3.4 Storage effect on the phages infectivity

One of the important challenges in phage-based materials is the stability and activity of phages on biomaterials during storage time. It has been revealed that tailed phages, especially T4 phages, are the most resistant to storage [36]. The storage analysis of phage-immobilized materials may be useful for further industrial applications.

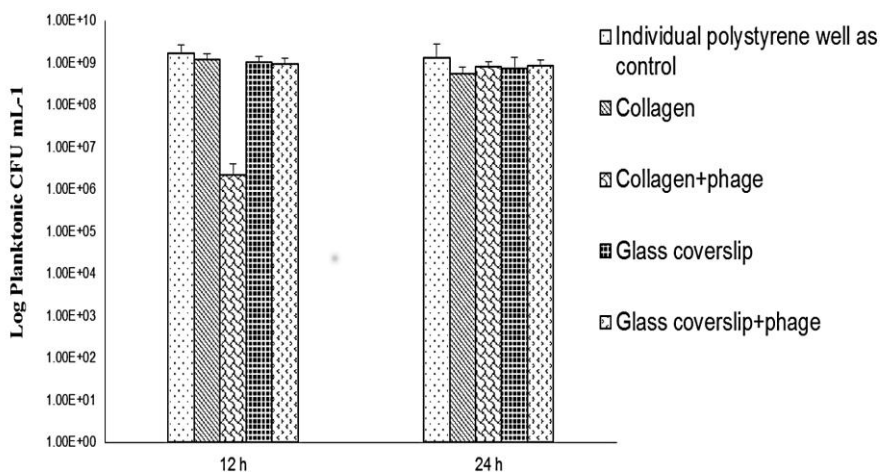


Figure 4.7: Storage effect (7 days storage at room temperature) on planktonic growth after incubation of surfaces for 12 and 24 hours (with the initial bacteria concentration of $1.27E+07$ cfu/ml).

As it can be observed in Figure 7, all the materials except phage-immobilized collagen, presented nearly similar planktonic growth after 12 and 24 hours of inoculation. This means that immobilized phages were not stable during storage, except on collagen.

A possible hypothesis for such observation may be the swelling behavior of collagen surface structure during drying of phage aqueous droplet that can enhance phage penetration to the three-dimensional network of the superficial triple helix collagen chains. The surface morphology of collagen coatings that was hydrated by water treatment, is expected to change during drying in ambient environment. The crystallinity of collagen surface was transformed to amorphous state after water treatment, and the triple helix of collagen changed to a highly hydrated state, through the formation of hydrogen bonds [37]. Meanwhile, strong covalent and electrostatic bonds may have been formed between collagen and phage head molecules. The natural drying process that gives rise to the compaction of the collagen flexible fibrous structure [37], may cause phage nanoparticles to be entrapped into the collagen chains, and therefore preserve phages from dehydration [38] by exposure to air along storage time. After being exposed to the aqueous bacteria culture, the compressed fibrils of collagen undergo osmotic swelling. Therefore, collagen fibers expand to recover their original state, while the encapsulated phages are exposed to the bacterial culture. Moreover, observation of a few phages released from collagen to the culture without bacteria, in the stability study, confirmed the encapsulation of phages in the collagen film. It has been shown that phage encapsulation can be a method for a long term storage of bacteriophages [39].

Phage progeny after inoculation of the immobilized samples in bacteria culture has been measured for 12 and 24 hours, and the results are presented in Figure 4.8.

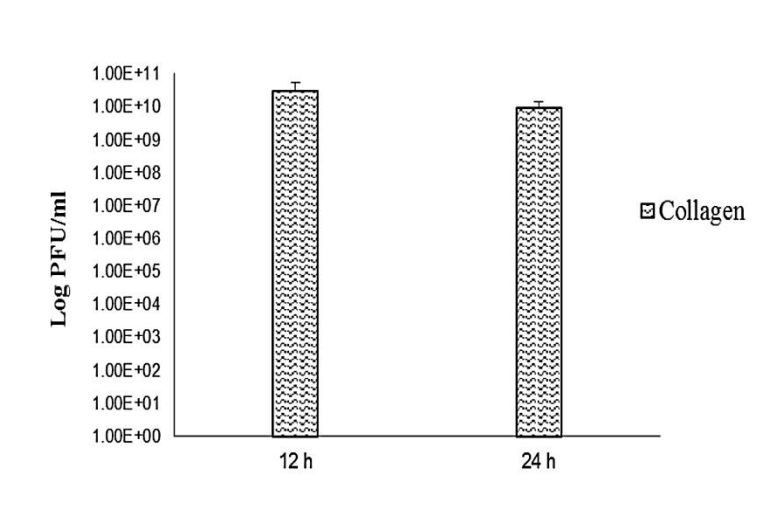


Figure 4.8: Storage effect on *E. coli* lysis after 12 to 24 hours of incubation in the presence of phage immobilized surfaces. The concentration of produced phages in the case of glass cover slide was zero

(The initial phage concentration on substrates was 5.4E+10 PFU/ml)

As shown in Figure 4.8, the concentration of produced phages is almost in the same range of the initial concentration used for phage immobilization onto the collagen surface, while no produced phages were observed in the inoculated media containing immobilized glass cover slide. Since phages are known to be damaged after exposure to dehydration, the minimum moisture content for phage lytic activity has been reported to be between 4-6% [38]. Therefore, the lack of phage progeny obtained after *E. coli* incubation with the glass cover slides could be explained by the loss of phage activity due to complete dehydration of bacteriophages during 7-days storage. However, the observed bioactivity of phage-based glass cover slide after 1 day storage may indicate the need for (4-6%) humidity to be retained in the phages, during short periods of storage.

4.3.5 Mammalian cell adhesion on the phage-based surfaces

Next, the potential cytotoxicity of the surfaces with immobilized phages towards mammalian cells was assessed using MSCs. As shown in Figure 4.9, both cell adhesion and growth showed different patterns during 2 days of culture, as observed via light microscopy.

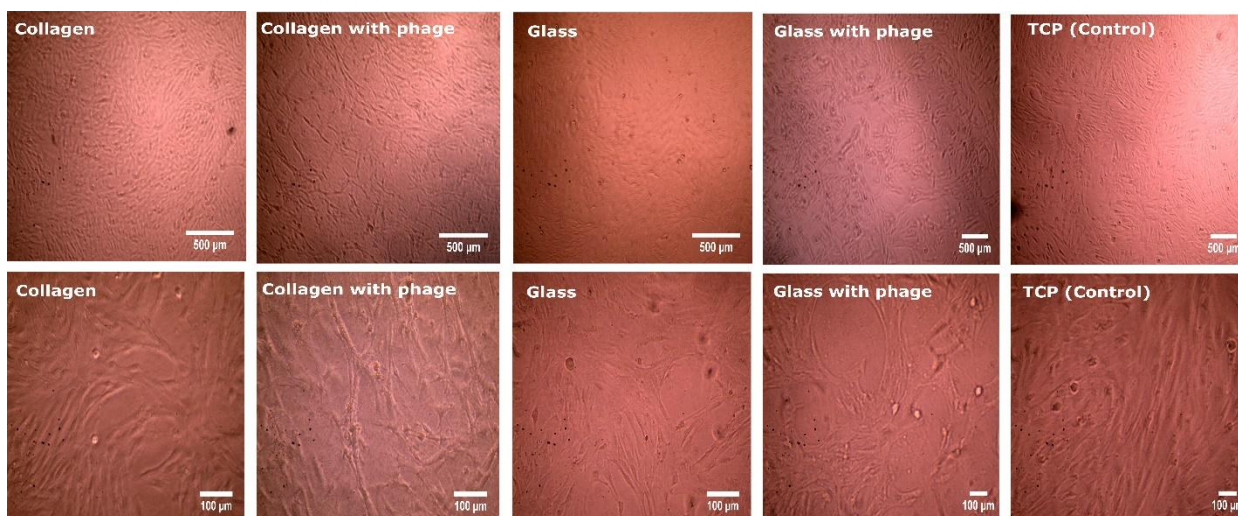


Figure 4.9: Morphologic characteristics of bone marrow-derived MSC proliferation on different surfaces during 2 days with 4× objective (upper row) and 10× objective (lower row)

Light microscopy (Figure 4.9) showed that cells deposited on collagen, phage-immobilized collagen and TCP substrates (tissue culture plates), were elongated. The elongated cells on collagen surface showed a tendency to form fused cell bundles that coursed through the surface in a more confluent organization, while the elongated cells on phage immobilized collagen formed a net-like structure containing spindle shaped cells with free spaces between the cell bundles, which distributed uniformly throughout the substrate. Cell morphology on glass cover slide presented spindle like morphology. However, the phage-immobilized substrates showed a non-uniform “storiform patterned” structure.

The cytocompatibility of treated and non-treated samples was evaluated by WST-1 and live/dead assays. As shown in Figure 4.10-a (WST-1 assay), after a 5 day culture period, the phage-immobilized substrates resulted in higher MSCs proliferation and viability compared to their non-treated controls. Moreover, collagen surfaces showed higher cell proliferation than glass cover slides. In addition, the results of viability analysis by the fluorescent intensity of live (with calcein AM stain)/dead cells (with EthD-1 stain), showed similar viable cells for the phage-based materials and for the untreated samples (Figure 4.10-b). The observed decrease in calcein fluorescence may lie in the fact that calcein AM has the capability to form complexes with divalent metallic ions, such as calcium and magnesium [40]. Therefore, at physiological pH, its fluorescence intensity may be quenched by the possible Mg^{+2} salt that still may be remaining in small amounts in the T4 phage solution after dialysis for 24 hours. It should also be mentioned that the sensitivity of calcein to the calcium and magnesium ions depends on the ion/calcein ratio, at physiological pH [41]; hence, to prove such assumption, the amount of remaining salts after dialysis procedure should be measured by the conductivity methods, in further studies.

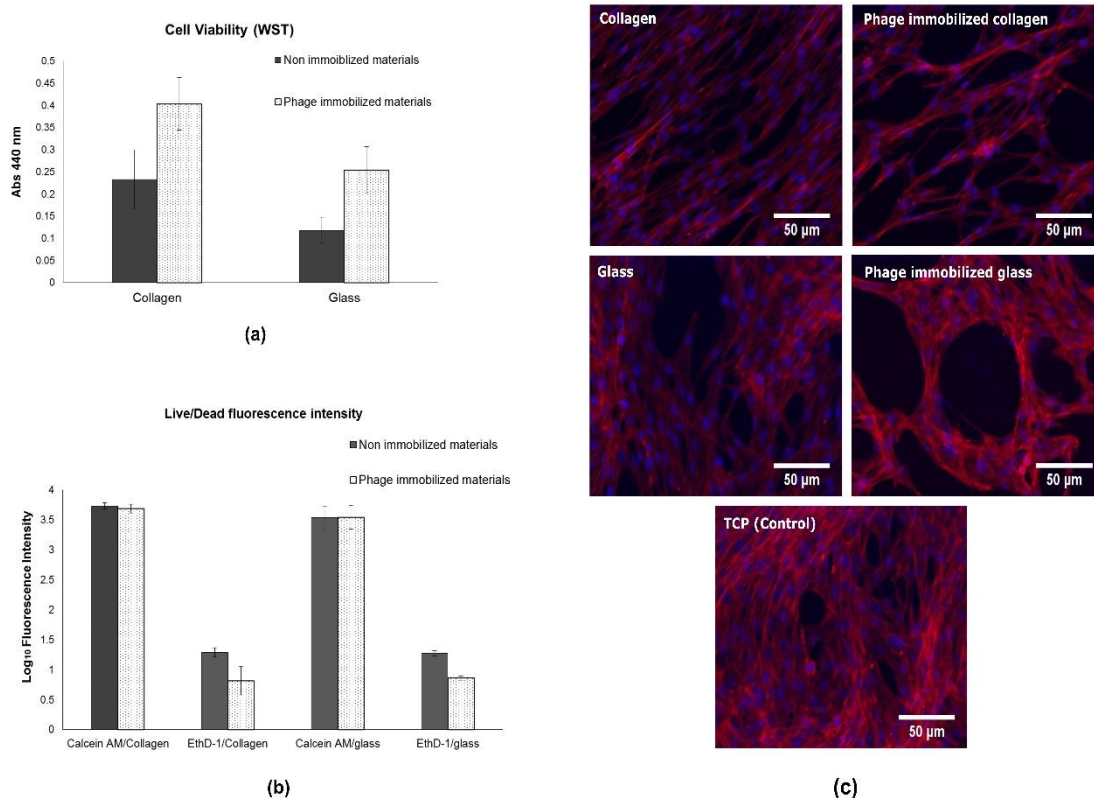


Figure 4.10: Cytocompatibility analysis of phage-immobilized and non-immobilized surfaces through (a) cell proliferation after 5 days of culture using WST-1 assay, (b) cell viability as the fluorescence intensity graph of Live/Dead staining after 5 days of culture (Live cells stained with calcein AM while dead cells stained with ethidium homodimer-1), (c) immunofluorescence images of cells following 5 days culture (F-actin labeled with phalloidin shown in red and nuclei stained with DAPI shown in blue).

We further confirmed the cell phenotypes by immunofluorescence analysis after 5 days of culture, as shown in Figure 4.10-c. The uniform distribution of elongated cells on collagen surfaces revealed a high density of nuclei, which may suggest the onset of osteogenic cell differentiation. In contrast, the cell morphology on phage immobilized collagen was observed as a network of bundle-like structures with the spaces empty in between, which is consistent with the light microscopy observations (Figure 4.9). Both collagen and immobilized collagen presented aligned F-actin bundles. However, cells on glass and immobilized glass surfaces showed a randomly spread morphology with dense F-actin networks. The morphology of MSCs proliferation on phage-immobilized samples may be due to the surface patterns formed as the result of phage deposition onto collagen surfaces during drying process.

It has been proved that the virus nanoparticles, depending on their shape, create topographical features onto the surfaces that can lead the osteogenic differentiation of MSCs [42]. As shown in Figure 4.1, the pattern formed through drying induced assembly of T4 phage nanoparticles onto the glass cover slides

represents different morphologies distributed over the entire surface, which may have influenced the MSCs adhesion and morphology, as shown in Figures 4.9 and 4.10-c. However, further studies are needed to analyze the phage dried patterns onto collagen for further interpretation of MSC proliferation and differentiation.

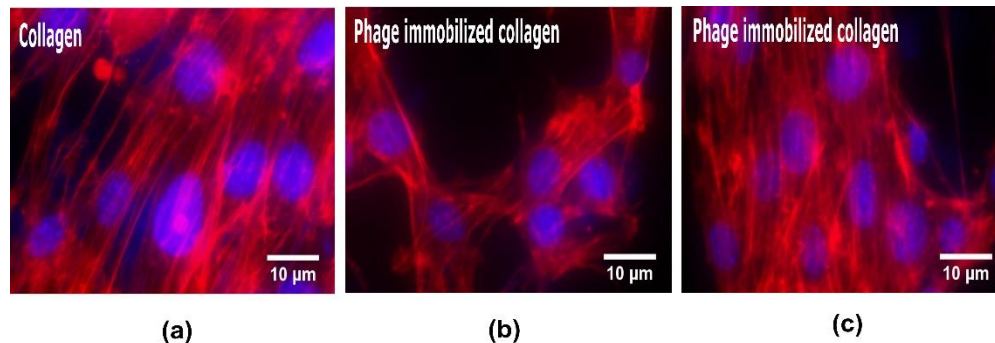


Figure 4.11: Actin cytoskeleton of MSCs on collagen and collagen-immobilized surfaces observed under 40× objective. F-actin and nuclei are stained with phalloidin (red) and DAPI (blue), respectively.

Higher magnification images of actin cytoskeleton on immobilized and non-immobilized collagen surfaces are shown in Figure 4.11. MSCs on collagen presented more ellipsoidal nuclei and an elongated cytoskeleton compared to cells on phage-immobilized collagen that presented more spheroidal nuclei. Moreover, the higher density of actin stress fibers observed in the cells cultured on the untreated collagen surface may represent higher cytoskeleton tension (Figure 4.11-a), while the cells on phage-immobilized collagen showed more evenly distributed actin filaments around the empty holes in net-like structure (Figure 4.11-b) and higher stress fibers (Figure 4.11-c) in the direction of elongated cell bundles.

4.4 Discussion

Phage immobilization may be a novel and successful strategy to control surface biofilm formation in biomedical applications. Phage immobilization helps to ensure that phages are retained near the surface, thus preventing their excessive waste.

In this research, drying-induced assembly, as a simple and cost effective method, has been applied to immobilize phages on surfaces. The immobilization procedure addressed by this study is not only simple and cost effective, but also could provide full surface coverage by bacteriophages (even if not in a uniform way). It should be noted that this method does not allow for controlling the amount of active phages immobilized on the material. However, high amounts of phages on the surface increase the possibility of larger numbers of phages being adsorbed to the surface in the right position.

The phage coating procedure used in this study improved the surface bioactivity against *E. coli*. This study showed that the use of phage-immobilized materials is efficient for inhibition of planktonic bacteria during short periods of up to 12 hours. The increase of planktonic bacteria for longer periods may be the result of phage-resistant bacteria emergence. However, the biofilm formation reduced significantly after 24 hours incubation of phage-treated substrates, illustrating the efficiency of the immobilization technique to prevent biofilm formation.

Even though the final results showed the inhibition of biofilm growth, there is still possibility of biofilm formation onto the surface during incubation. The reason for that is the capability of phages to kill the surface-attached bacteria, while the dead bacterial cells may deposit onto the surface. It has been reported that bacteria from the planktonic phase could form biofilm upon the layer of surface-associated dead bacteria [43]. Cerca et. al.[44], revealed that phage lysis capability is faster for planktonic cells than for bacterial cells in biofilm because the biofilm structure prevents easy access of phages to the bacteria in the initial layers. However, the observed biofilm inhibition after 24 hours of inoculation may be the result of phages weakly bound to the substrates that facilitate the removal of biofilms from the surface through washing steps.

In addition, this study assessed the effect of storage on phage stability (effect of the exposure time of dried phages to the environmental conditions), bearing in mind future industrial applications. As opposed to glass cover slide surfaces, the number of activated phages after inoculation of phage immobilized collagen for both 1-day and 7-days storage indicated that collagen was an adequate environment to maintain phage bioactivity over prolonged storage times in ambient conditions. The parameters that may contribute to the potential effect of collagen on preserving phage activity include the presence of positively charged groups that facilitates phage head stabilization during drying, and swelling effect of collagen helical chains on the surface, that may encapsulate some phages after the drying process, and limit the oxidative damage on phages.

Different MSC morphologies on treated and untreated surfaces illustrate the potential effect of phage immobilization for designing functional surfaces. How does phage nanoparticle immobilization onto the surfaces influence the MSC growth and possibly osteogenic differentiation? It is well known that the surface of biomaterials has an important role in governing MSC adhesion, proliferation and differentiation *in vitro* [45]. Generally, supermolecular assemblies of virus nanoparticles represent two or three dimensional organized architectures that enhance cell growth, spreading and proliferation. The controlled drying of virus nano-suspensions showed that the viruses formed multiple stripe patterns, and the cells tend to align in the same orientation of viruses [46]. Moreover, calcium mineralization during MSC growth on phage films, was 1.5 times more intense than in films without phages, proving the occurrence of MSC differentiation into the osteogenic phenotype [46]. Drying-induced virus assembly, resulting in various surface patterns

specially for the plane surface of glass cover slide, can be identified as an important factor to increase MSC adhesion and proliferation, likely due to the additional topographical changes through particle deposition and aggregation.

Furthermore, the small changes in surface hydrophobicity and roughness, can significantly influence the cellular behavior [47, 48]. Excessive cell attachment to the smooth substrates has been reported to inhibit osteogenic differentiation, while the weaker cell attachment to the rough surfaces increased the osteogenic differentiation [49]. Hence, the osteogenic appearance of cells on treated and untreated collagen surfaces may be the result of weak cell attachment, whereas the flatter and thicker cell phenotypes on treated and untreated glass cover slides may be the result of stronger cell adhesion. The weak cell attachment to their culture surfaces might increase their motility and facilitate the formation of aggregates, when compared to the stronger cell attachment, which is in line with mitigation of cell migration and differentiation.

Besides topographical features, the functional groups presented by the surface's topographical features can influence the MSC cell differentiation. Since the MSC differentiation is affected by chemical and biological signals, modifications of surfaces may influence their behavior. Surface functionalities such as -NH₂ and -COOH groups, existing in collagen molecules, are favorable for increasing MSC adhesion, proliferation and differentiation to osteogenic cell types, as confirmed by the higher content of mineralized calcium quantified after several days of cell culture [50, 51]. Therefore, inclusion of biological molecules onto the surfaces, as performed via bacteriophage immobilization to enhance the surface bioactivity, may alter the surface functional groups, and consequently, MSC behavior.

Furthermore, a susceptible senescent cell morphology could be observed for cells proliferating on phage-immobilized samples that should be assessed in more details [52].

4.5 Conclusion:

Aiming at providing a bioactive surface for phage therapy applications, this study showed an easy and novel method to successfully immobilize phages on glass surfaces with or without collagen coating. Drying-induced phage assembly used in this study, is a simple, single-step and cost effective method without requiring any chemical reagents, in which phage nanoparticles aggregation, as the result of evaporation-driven mechanism, generated ordered/disordered patterns onto the surfaces.

The results show that both collagen and glass cover slides are able to preserve the activity of immobilized phages after 24 hours storage at ambient conditions. The materials with immobilized phages not only inhibited the planktonic growth for 12 hours, but also significantly reduced biofilm growth after 24 hours. However, only collagen films were able to stabilize phages without bioactivity loss after 7 days of storage. The swelling behavior of collagen chains at the surface during phage drying process may be an

influential parameter on entrapment and preservation of phage activity after 7 days storage that has been proved through phage release from collagen surfaces in an aqueous environment.

In addition, the cyto-compatibility results showed that the phage immobilized materials can provide “smart” antibacterial surfaces for tissue engineering applications with the capability to reduce biofilm formation and to enhance the possibility of osteogenic differentiation of MSCs. However, more detailed experiments are needed to confirm this hypothesis. The parameters influencing MSC behavior could be surface topographical characteristics and functional groups that should be further studied in detail to better understand the effects of phage-modified surfaces on MSC adhesion and differentiation.

1. Agarwal, A., K.P. Singh, and A. Jain, *Medical significance and management of staphylococcal biofilm*. FEMS Immunol Med Microbiol, 2010. **58**(2): p. 147-60.
2. Diekema, D.J., et al., *Survey of infections due to Staphylococcus species: frequency of occurrence and antimicrobial susceptibility of isolates collected in the United States, Canada, Latin America, Europe, and the Western Pacific region for the SENTRY Antimicrobial Surveillance Program, 1997-1999*. Clin Infect Dis, 2001. **32 Suppl 2**: p. S114-32.
3. Maki, D.G., D.M. Kluger, and C.J. Crnich, *The risk of bloodstream infection in adults with different intravascular devices: a systematic review of 200 published prospective studies*. Mayo Clin Proc, 2006. **81**(9): p. 1159-71.
4. Uckay, I., et al., *Foreign body infections due to Staphylococcus epidermidis*. Ann Med, 2009. **41**(2): p. 109-19.
5. T., S., *The economic impact of infected joint arthroplasty*. Orthopedics, 1995. **18**(9): p. 871-873.
6. Pandey, R., A.R. Berendt, and N.A. Athanasou, *Histological and microbiological findings in non-infected and infected revision arthroplasty tissues. The OSIRIS Collaborative Study Group. Oxford Skeletal Infection Research and Intervention Service*. Arch Orthop Trauma Surg, 2000. **120**(10): p. 570-4.
7. Pavithra, D. and M. Doble, *Biofilm formation, bacterial adhesion and host response on polymeric implants--issues and prevention*. Biomed Mater, 2008. **3**(3): p. 034003.
8. Pearl, S., et al., *Nongenetic Individuality in the Host-Phage Interaction*. PLoS Biology, 2008. **6**(5): p. e120.
9. Markoishvili, K., et al., *A novel sustained-release matrix based on biodegradable poly(ester amide)s and impregnated with bacteriophages and an antibiotic shows promise in management of infected venous stasis ulcers and other poorly healing wounds*. Int J Dermatol, 2002. **41**(7): p. 453-8.
10. Curtin, J.J. and R.M. Donlan, *Using bacteriophages to reduce formation of catheter-associated biofilms by Staphylococcus epidermidis*. Antimicrob Agents Chemother, 2006. **50**(4): p. 1268-75.
11. Fu, W., et al., *Bacteriophage cocktail for the prevention of biofilm formation by Pseudomonas aeruginosa on catheters in an in vitro model system*. Antimicrob Agents Chemother, 2010. **54**(1): p. 397-404.
12. Carson, L., S.P. Gorman, and B.F. Gilmore, *The use of lytic bacteriophages in the prevention and eradication of biofilms of Proteus mirabilis and Escherichia coli*. FEMS Immunol Med Microbiol, 2010. **59**(3): p. 447-55.
13. Hosseinidou, Z., A.L.J. Olsson, and N. Tufenkji, *Going viral: Designing bioactive surfaces with bacteriophage*. Colloids and Surfaces B: Biointerfaces, 2014. **124**: p. 2-16.

14. Dixon, D.V., Z. Hosseinidoust, and N. Tufenkji, *Effects of environmental and clinical interferents on the host capture efficiency of immobilized bacteriophages*. Langmuir, 2014. **30**(11): p. 3184-90.
15. Pearson, H.A., et al., *Phage-bacterium war on polymeric surfaces: can surface-anchored bacteriophages eliminate microbial infections?* Biomacromolecules, 2013. **14**(5): p. 1257-61.
16. Esteban, P.P., A.T.A. Jenkins, and T.C. Arnot, *Elucidation of the mechanisms of action of Bacteriophage K/nano-emulsion formulations against S. aureus via measurement of particle size and zeta potential*. Colloids and Surfaces B: Biointerfaces, 2016. **139**: p. 87-94.
17. Esteban, P.P., et al., *Enhancement of the antimicrobial properties of bacteriophage-K via stabilization using oil-in-water nano-emulsions*. Biotechnol Prog, 2014. **30**(4): p. 932-44.
18. Liana, A.E., et al., *Adsorption of T4 bacteriophages on planar indium tin oxide surface via controlled surface tailoring*. Journal of Colloid and Interface Science, 2016. **468**: p. 192-199.
19. Steinmetz, N.F., et al., *Layer-by-layer assembly of viral nanoparticles and polyelectrolytes: the film architecture is different for spheres versus rods*. Chembiochem, 2008. **9**(10): p. 1662-70.
20. Korehei, R. and J.F. Kadla, *Encapsulation of T4 bacteriophage in electrospun poly(ethylene oxide)/cellulose diacetate fibers*. Carbohydr Polym, 2014. **100**: p. 150-7.
21. Bean, J.E., et al., *Triggered Release of Bacteriophage K from Agarose/Hyaluronan Hydrogel Matrixes by Staphylococcus aureus Virulence Factors*. Chemistry of Materials, 2014. **26**(24): p. 7201-7208.
22. Jeon, D.-Y., et al., *Controlled surface adsorption of fd filamentous phage by tuning of the pH and the functionalization of the surface*. Journal of Applied Physics, 2011. **109**(6): p. 064701.
23. Moghimian, P., et al., *Adsorption and Self-Assembly of M13 Phage into Directionally Organized Structures on C and SiO₂ Films*. Langmuir, 2014. **30**(38): p. 11428-11432.
24. Guntupalli, R., et al., *Phage Langmuir monolayers and Langmuir-Blodgett films*. Colloids Surf B Biointerfaces, 2011. **82**(1): p. 182-9.
25. Lin, Y., et al., *Self-assembly of virus particles on flat surfaces via controlled evaporation*. Langmuir, 2011. **27**(4): p. 1398-402.
26. Wargacki, S.P., B. Pate, and R.A. Vaia, *Fabrication of 2D ordered films of tobacco mosaic virus (TMV): processing morphology correlations for convective assembly*. Langmuir, 2008. **24**(10): p. 5439-44.
27. Lin, Y., et al., *Self-Assembly of Rodlike Bio-nanoparticles in Capillary Tubes*. Angewandte Chemie International Edition, 2010. **49**(5): p. 868-872.
28. Rong, J., et al., *Oriented cell growth on self-assembled bacteriophage M13 thin films*. Chemical Communications, 2008(41): p. 5185-5187.
29. Rajan, N., et al., *Preparation of ready-to-use, storable and reconstituted type I collagen from rat tail tendon for tissue engineering applications*. Nat Protoc, 2006. **1**(6): p. 2753-8.
30. Josten, E., et al., *Superlattice growth and rearrangement during evaporation-induced nanoparticle self-assembly*. Scientific Reports, 2017. **7**(1): p. 2802.
31. Noguera-Marin, D., et al., *Impact of the collective diffusion of charged nanoparticles in the convective/capillary deposition directed by receding contact lines*. Eur Phys J E Soft Matter, 2016. **39**(2): p. 20.
32. Bishop, K.J., et al., *Nanoscale forces and their uses in self-assembly*. Small, 2009. **5**(14): p. 1600-30.
33. Birkenhauer, E., S. Neethirajan, and J.S. Weese, *Collagen and hyaluronan at wound sites influence early polymicrobial biofilm adhesive events*. BMC Microbiol, 2014. **14**: p. 191.
34. Pires, D., et al., *Use of newly isolated phages for control of Pseudomonas aeruginosa PAO1 and ATCC 10145 biofilms*. Res Microbiol, 2011. **162**(8): p. 798-806.
35. Chagnot, C., et al., *In vitro colonization of the muscle extracellular matrix components by Escherichia coli O157:H7: the influence of growth medium, temperature and pH on initial adhesion and induction of biofilm formation by collagens I and III*. PLoS One, 2013. **8**(3): p. e59386.

36. Ackermann, H.-W., D. Tremblay, and S. Moineau, *Long-term bacteriophage preservation*. WFCC Newsletter, 2004. **38**: p. 35-40.
37. Kim, C.-L. and D.-E. Kim, *Self-healing Characteristics of Collagen Coatings with Respect to Surface Abrasion*. Scientific Reports, 2016. **6**: p. 20563.
38. Puapermpoonsiri, U., S.J. Ford, and C.F. van der Walle, *Stabilization of bacteriophage during freeze drying*. Int J Pharm, 2010. **389**(1-2): p. 168-75.
39. Ma, Y., et al., *Microencapsulation of Bacteriophage Felix O1 into Chitosan-Alginate Microspheres for Oral Delivery*. Applied and Environmental Microbiology, 2008. **74**(15): p. 4799-4805.
40. Tiktopulo, E.I. and A.V. Kajava, *Denaturation of type I collagen fibrils is an endothermic process accompanied by a noticeable change in the partial heat capacity*. Biochemistry, 1998. **37**(22): p. 8147-52.
41. Thanh Thuy, D., et al., *Determination of traces of calcium and magnesium in rare earth oxides by flow-injection analysis*. Analytica Chimica Acta, 1994. **295**(1): p. 151-157.
42. Metavarayuth, K., et al., *Virus Nanoparticles Mediated Osteogenic Differentiation of Bone Derived Mesenchymal Stem Cells*. Advanced Science, 2015. **2**(10): p. 1500026-n/a.
43. Chiang, W.-C., et al., *Silver-Palladium Surfaces Inhibit Biofilm Formation*. Applied and Environmental Microbiology, 2009. **75**(6): p. 1674-1678.
44. Cerca, N., R. Oliveira, and J. Azeredo, *Susceptibility of Staphylococcus epidermidis planktonic cells and biofilms to the lytic action of staphylococcus bacteriophage K*. Lett Appl Microbiol, 2007. **45**(3): p. 313-7.
45. Anderson, H.J., et al., *Mesenchymal Stem Cell Fate: Applying Biomaterials for Control of Stem Cell Behavior*. Frontiers in Bioengineering and Biotechnology, 2016. **4**: p. 38.
46. Zhao, X., Y. Lin, and Q. Wang, *Virus-based scaffolds for tissue engineering applications*. Wiley Interdiscip Rev Nanomed Nanobiotechnol, 2015. **7**(4): p. 534-47.
47. McMurray, R.J., et al., *Nanoscale surfaces for the long-term maintenance of mesenchymal stem cell phenotype and multipotency*. Nat Mater, 2011. **10**(8): p. 637-644.
48. Hao, J., et al., *Mechanobiology of mesenchymal stem cells: Perspective into mechanical induction of MSC fate*. Acta Biomater, 2015. **20**: p. 1-9.
49. Mendonca, D.B., et al., *Titanium surface topography affects collagen biosynthesis of adherent cells*. Bone, 2011. **49**(3): p. 463-72.
50. Phillips, J.E., et al., *Human mesenchymal stem cell differentiation on self-assembled monolayers presenting different surface chemistries*. Acta Biomater, 2010. **6**(1): p. 12-20.
51. Somaiah, C., et al., *Collagen Promotes Higher Adhesion, Survival and Proliferation of Mesenchymal Stem Cells*. PLOS ONE, 2015. **10**(12): p. e0145068.
52. Schallmoser, K., et al., *Replicative senescence-associated gene expression changes in mesenchymal stromal cells are similar under different culture conditions*. Haematologica, 2010. **95**(6): p. 867-74.

5. Chapter Five

Antibacterial properties of phage-immobilized collagen/silk fibroin biocomposites

*Ima Ghaeli^{1,2,3}, Adam L.J. Olsson⁴, Natalie Fekete⁴, Nathalie Tufenkji⁴, Corinne A. Hoesli⁴,
Fernando Jorge Monteiro^{1,2,3}*

¹i3S-Instituto de Investigação e Inovação em Saúde, Universidade do Porto, Portugal

²INEB - Instituto de Engenharia Biomédica, Universidade do Porto, Porto, Portugal

³Faculdade de Engenharia, Universidade do Porto, Porto, Portugal

⁴Department of Chemical Engineering, McGill University, Montreal, QC, Canada H3A 0C5

Abstract

Implant-associated infection is the most common complication in orthopaedics, needing expensive and long-term treatment. Designing an anti-infection coating for implants which could prevent the surface from biofilm formation and enhance the activity of mesenchymal stem cells (MSCs), would be of great importance. The objective of this study was to produce an antibacterial coating by immobilizing phage T4 into biocomposites containing silk fibroin and collagen with various mixing ratios. The antibacterial activity of the materials stored at room temperature under sterile conditions for 24 hours, was analyzed against *E. coli* by plate culture and biofilm formation. We also investigated the cytotoxicity of the materials in MSCs cultures.

The antibacterial results indicated significant *E. coli* planktonic reduction for all the phage-immobilized materials, within 12 hours. The viability and proliferation of MSCs revealed that the phage-immobilized exerted increased cell growth.

5.1 Introduction

Biofilm formation on implant surfaces is a major problem in orthopaedic surgeries and difficult to destroy, requiring another surgery to remove implant and implementing long-term antibiotic treatment [1, 2]. On the other hand, the emergence of antibiotic-resistant bacteria reduced the efficiency of traditional antibiotic treatments. Engineering of bactericidal coatings containing biomaterials is a preventive method to protect surfaces from contamination by preventing biofilm formation [3].

Silk-based coatings with promising structural and mechanical features have been reported as new options for regenerative medicine including bone, skin, tendon, eye, ligament and cartilage regeneration. The degradation time of silk fibroin biomaterials could be changed from days to years, based on the crystalline content of silk fibroin [4, 5]. However, similarly to other biomaterials, silk biomaterials are prone to infections and biofilm formation [6] which is a disadvantage for using them as implant coatings.

Combination of silk material with other biomaterials such as chitosan [7] and antibacterial agent [8, 9] could provide a durable infection prevention capability and impose biocompatibility to prevent the second surgery. The antibacterial activity of silk fibroin has been mostly reported through its drug delivery characteristics [10-15]. Designing an interpenetrating network (IPN) in which the silk fibroin chains undergo conformational transition from random coil to beta sheets, could induce drug delivery. Crystallized silk fibroin in blend systems allows for controlled drug release [16]. Moreover, conjugation with natural polymers such as collagen may enhance the cytocompatibility of the mixtures, due to the presence of integrin binding motifs (RGD) [17].

In the present study, phage immobilized SF/collagen blend films were investigated as potential coatings with antibacterial properties. In order to obtain highly antibacterial coatings (with the aim of targeting antibiotic resistant bacteria), T4 phages have been used as fighting microbial viruses [18] that target host bacteria, inject their genomes, reproduce inside the host bacteria and disrupt the host membrane, while releasing their progeny. The phage immobilization method was a non-specific binding through evaporation method.

5.2 Materials and methods:

5.2.1 Phage propagation and purification

Two cultures of *Escherichia coli* BL21 (5 mL each) were grown overnight in Luria broth (LB) at 37 °C. The first 5 mL culture was added to 200 mL of sterile LB and incubated while shaking for 3 hours. The second 5 mL culture was inoculated with 100 µL of bacteriophage T4 stock isolated from *Escherichia coli* BL21, for 15 minutes at room temperature, and then added to the above-mentioned 3 hours incubated culture and shaken overnight at 37 °C.

For purification and propagation of phages, the overnight cultures were centrifuged at 6000 RPM (RC-6, Sorvall) for 20 min, and the supernatant was recovered and sterile-filtered. The supernatant was treated with nuclease solutions (final concentration of 1 µg/mL, 30 min at room temperature). and subsequently mixed with 1M NaCl and PEG 8000 (10 v/w%) and stirring overnight at 4 °C to precipitate phage particles. The precipitated phages were spun down by centrifugation (14000 RPM, 10 °C, for 3 hrs). Finally, the phage suspension was purified using ultracel 100k filters (Amicon Ultra centrifugal filters, Millipore). The precipitated phages were re-suspended in SM buffer (containing 5.8 g/L NaCl, 120 mg/L MgSO₄, 50 mL of 1 M Tris-HCl, pH 8) and sterile filtered. This method resulted in a phage titer of 10¹⁰-10¹² PFU/mL. To determine the phage titer, ten-fold serial dilutions were prepared and after mixing with overnight host bacteria, the solutions were added to molten soft agar, which was spread over the plates. These were incubated overnight at 37 °C and the number of plaques was enumerated. To remove excessive salt, bacteriophage suspension was dialyzed against distilled water for 24 hrs (MWCO: 14000), followed by sterile filtration and phage titer count.

5.2.2 Phage-based materials

Type I collagen extracted from rat-tail tendons and solubilized in acetic acid solution (0.02 N) at a concentration of 4 g/L, was obtained from Laval University, Quebec, Canada [19].

B. mori silk fibroin was prepared initially by degumming process through boiling silkworm cocoons in Na₂CO₃ solution at 1 g/L for 30 min at 85 °C. This procedure was repeated twice and finally the cocoons

were boiled in distilled water for 30 min in order to separate the glue-like sericin from fibroin. After adequate washing with distilled water, the obtained silk fibroin fibers were dried at room temperature. Finally, silk fibroin agglomerates were milled to facilitate their dissolution process. Dissolution of prepared silk fibroin was performed in solution of ternary solvent containing $\text{CaCl}_2:\text{CH}_3\text{CH}_2\text{OH}:\text{H}_2\text{O}$ (1:2:8 molar ratio), at 85 °C in order to obtain the final concentration of 10% (w/v%). The final solution was dialyzed against distilled water for 72 hours to yield the RSF solution. After measuring the concentration of dialyzed phages, the solution was diluted with distilled water in order to achieve the concentration of 4 g/L.

Collagen/silk fibroin mixtures have been prepared by simply mixing the two solutions of the same concentration, with Col/SF ratios of 100/0, 75/25, 50/50, 25/75 and 0/100.

The films were prepared through air drying of solutions at room temperature onto circular glass cover slides (Fisher) that had been previously cleaned with ethanol. Thereafter, filtered dialyzed phage liquids were spread onto bare glass coverslip (previously cleaned with ethanol) to cover the whole glass area (for 8 mm diameter of the substrate, 180 μl solution was used), allowing to be dried for overnight, under sterile conditions in a biosafety cabinet.

5.2.3 *In vitro* antibacterial properties

Inhibition zone: The inhibition zone was determined through soft agar overlay assay, in which a 5 ml of *E. coli* overnight culture was laid over a standard LB plate. Thereafter, immobilized and non-immobilized samples were placed on the prepared plates and incubated overnight, at 37 °C. The inhibition zones were visualized by formation of lytic rings.

Counting planktonic bacteria: The *in vitro* antibacterial activity of phage-immobilized samples was done through inoculating immobilized and non-immobilized samples in 2 ml of 1:100 diluted overnight *E. coli* bacteria culture, for 12 and 24 hours. *E. coli* planktonic growth has been measured through serial dilutions and LB agar plating. Non-immobilized samples as well as culture media in polystyrene well plates without samples, were used as controls. Each assessment was done in triplicate.

Biofilm formation: The immobilized samples inoculated in bacterial culture overnight were thoroughly washed twice with deionized water and exposed to live/dead bacterial staining solution for 15 min in the dark. The solution in excess was then removed and the samples were placed on the top of glycerol on microscope glass slides and were observed using a fluorescence microscope.

5.2.4 *Cytocompatibility of phage-immobilized surfaces*

Cell culture: Mesenchymal stem cells (provided by McGill University) were cultured in high glucose DMEM supplemented with 10% FBS and incubated at 37 °C and 5% CO_2 . Cultured cells at their 7th passage were trypsinized, harvested and seeded onto the phage-immobilized samples. Non-immobilized materials

and polystyrene well-plate without materials were considered as controls. After 5 days culture, samples were transferred to other plates for Live/Dead viability, WST-1 and immunofluorescence staining assays.

Cell proliferation assay (WST-1): After 5 days samples incubation, they were incubated in WST-1 solution for 2 hours in a humidified atmosphere (37 °C and 5% CO₂). Afterwards, absorbance at 420-480 nm (with maximum absorption at about 440 nm) was recorded using a microplate reader.

Cell viability assay: The viability assay was evaluated by Live/Dead assay containing calcein AM and ethidium homodimer-1 (EthD-1) stains. Hence, 150 µl of staining solutions were added to the 150 µl culture medium and added to the cell-substrates complexes after incubation and kept under dark conditions for 30 min. Fluorescent data from live and dead cells were measured at 530 and 645 nm, respectively.

Cell spreading and samples morphology: Samples, after 5 days incubation in cell culture medium, were washed with PBS, fixed with 4% paraformaldehyde for 15 min at room temperature and permeabilized with 0.1% Triton for another 15 min. Phalloidin-TRITC and DAPI staining were used to stain the actin filaments and nuclei, respectively. The stained samples were imaged on a spinning disk confocal system (Olympus 1×81). DAPI, TRITC and FITC filters were used in addition to phase contrast for 10× and DIC for 40× and 60× objectives. ImageJ software was applied for analysis and comparison of samples.

5.3 Results:

5.3.1 Antibacterial activity of immobilized and non-immobilized surfaces

The antibacterial activity of phage-immobilized materials was examined against *E. coli* bacterial strains. The inhibition zone is shown in Figure 5.1.

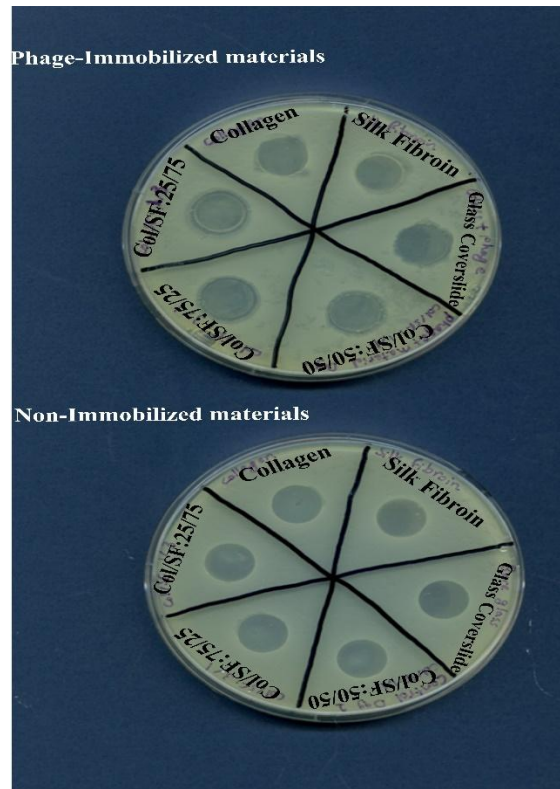


Fig 5.1: The inhibition zone of phage-immobilized and non-immobilized materials

The inhibition zones, as clearer parts surrounding the phage-immobilized samples, indicate that the immobilized materials possess antibacterial activity, while the non-immobilized materials present no inhibitory effect.

Inhibition of planktonic growth of *E. coli* was assessed by putting in contact the immobilized and non-immobilized substrates with the bacterial culture medium, and measuring the amount of planktonic cells after 12 and 24 hours. The controls were bacteria culture in the polystyrene wells without immobilized surfaces.

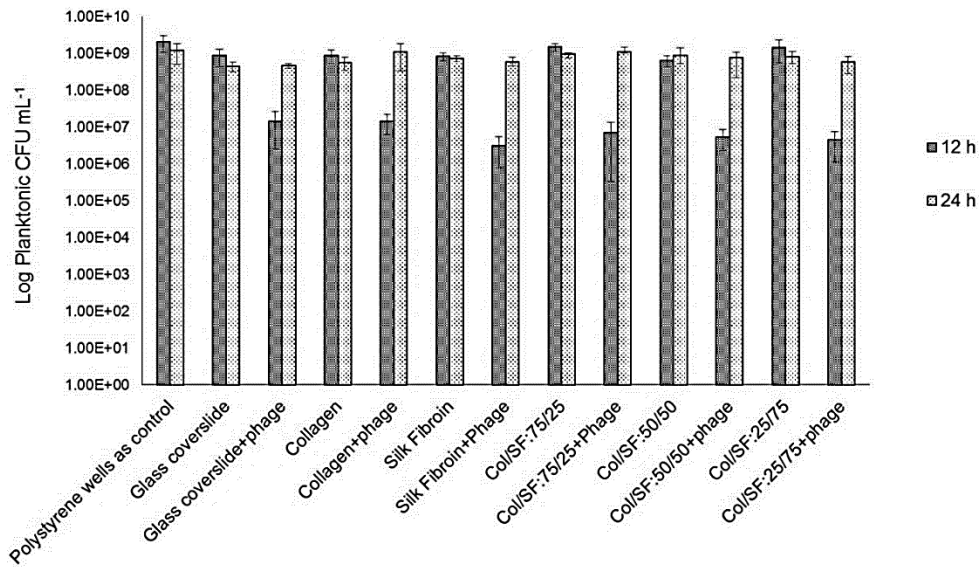


Fig 5.2: Planktonic growth of materials after 12 and 24 hours incubation in *E.coli* bacterial culture

As shown in figure 5.2., all phage-immobilized materials show lower amount of bacteria concentration than the non-immobilized materials, within 12 hours, with the lowest amount for phage-immobilized silk fibroin. However, all materials almost reach to the highest amount of planktonic growth in the media, similarly to polystyrene wells (control), after 24 hours. One hypothesis for the higher amount of planktonic growth after 24 hours than after 12 hours, may be the sedimentation of bacterial dead cells to the surfaces, acting as a novel surface for biofilm growth.

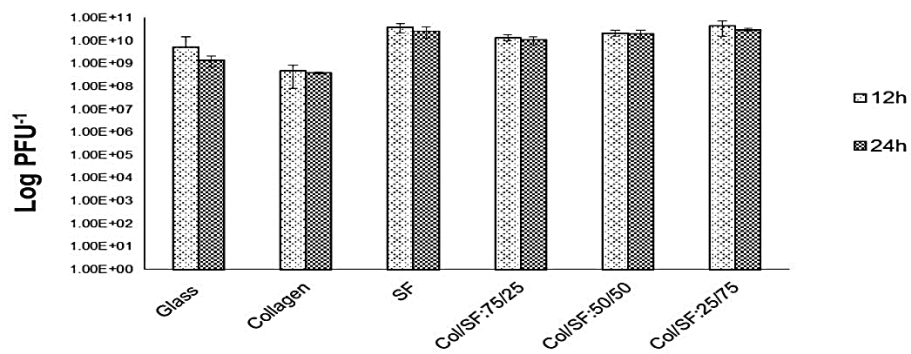


Fig 5.3: Phage progeny after incubation of phage-immobilized materials with *E.coli* bacterial culture for 12 and 24 hours

Figure 5.3 shows the analysis of phage progeny growth in the media after bacterial killing (using $5.4E+10$ as the initial dried concentration). Phage-immobilized collagen represented the lowest amount of

phage progeny in the media, which could result from less amount of planktonic cells being killed by immobilized phages, as shown in Figure 5.2.

On the contrary, silk fibroin represented higher phage progeny in the media, showing better bioactivity of phage-immobilized silk fibroin than other immobilized materials. It seems that the collision rate of planktonic bacteria with immobilized phage on silk fibroin is higher than the biofilm growth rate, resulting to lower planktonic growth and higher phage progeny in the media than that for phage immobilized collagen.

Differences between planktonic growth and phage progeny in the media with phage-immobilized collagen and phage-immobilized silk fibroin, may be due to the differences between biofilm growth rate onto each surfaces and proper collision rate of planktonic cells with immobilized phages that may be investigated in more details in future.

It should be noted that phage release analysis based on incubation of phage-immobilized materials in bacteria culture media without bacteria, showed no phage release from silk fibroin, compared to $3.33\text{E}+04$ pfu ml^{-1} phage release from collagen, after 3 days. Hence, the interaction of phages with silk fibroin chains is stronger than with collagen.

The blends showed almost similar trends of planktonic growth and phage progeny to the phage-immobilized silk fibroin, illustrating that silk fibroin structure has a dominant role in phage immobilizing mechanism and surface bioactivity. However, a comprehensive study should be carried out in the future in order to understand the hydrophobic/hydrophilic domains as well as negative/positive surface charges in the blends that may influence phage immobilization as well as final bacterial adhesion.

Besides planktonic growth, biofilm formation onto the materials has been analyzed for phage-immobilized collagen, silk fibroin, collagen/silk fibroin: 50/50 and glass coverslip.

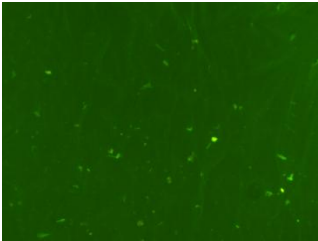
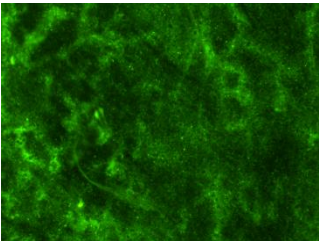
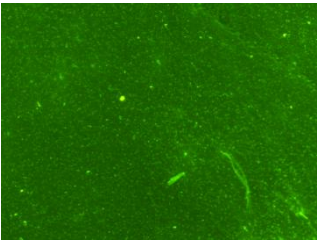
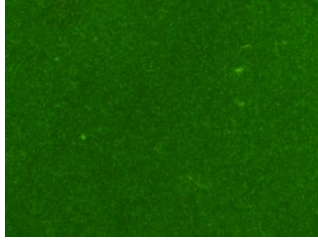
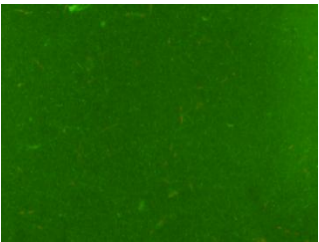
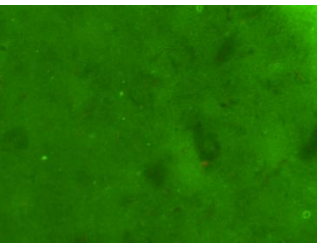
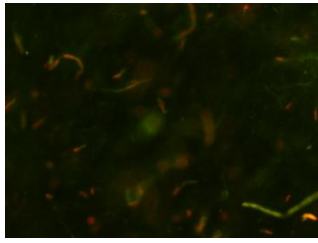
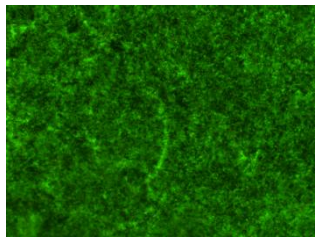
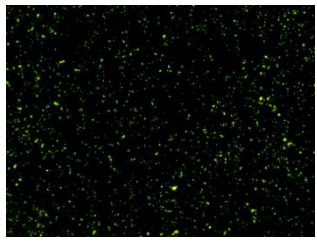

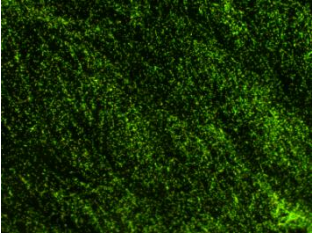
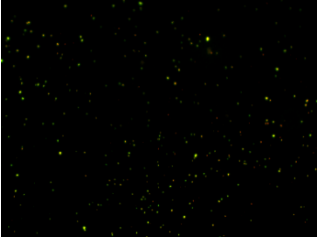
	Pure material	Biofilm on material	Biofilm on phage immobilized materials
RSF			
RSF/Col: 50/50			
Collagen			
Glass coverslip			

Fig 5.4: Biofilm formation onto phage-immobilized materials after 24 hours of inoculation

As shown in figure 5.4, the interaction of life/dead staining with silk fibroin and blend surfaces influences the background color, making it difficult to analyze the biofilm formation onto these surfaces. However, comparing with raw materials, it could indicate that phage-immobilized collagen, silk fibroin and glass coverslip show almost no biofilm formation, while the biofilm formation onto phage-immobilized RSF/Col:50/50 is not obvious.

5.3.2 *In vitro* cytocompatibility

The morphological changes of MSCs after growth on the materials are shown in Figure 5.5, with cytoskeleton pictured in red and nuclei in blue.

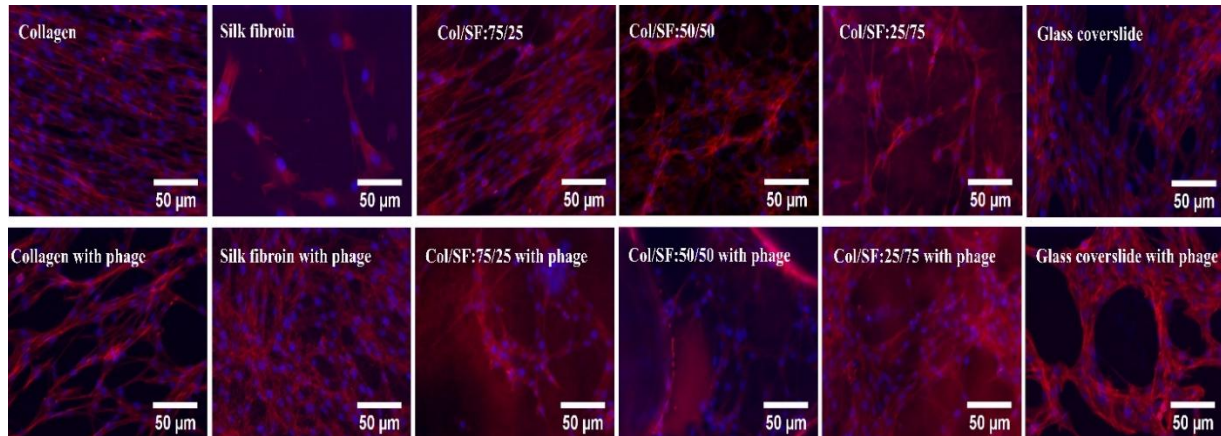


Fig 5.5: Cytoskeletal analysis on phage-immobilized and non-immobilized surfaces. Cytoskeleton stained with FITC conjugated phalloidin (red) and nucleus stained with DAPI (blue)

As shown in figure 5.5, cells on collagen and col/SF:75/25, were distributed as an elongated network, while on silk fibroin a few cells were stretched and no cellular connection could be observed. A stretched and interconnected cellular network on col/SF:50/50 and a laterally extended interconnected cellular network on col/SF:25/75, could be observed. MSC cultured on glass coverslips generated stretched interconnected networks. MSCs cultured on all phage-immobilized materials represented stretched and interconnected cellular network, with more elongated morphology on phage-immobilized collagen. The observed morphological changes for phage-immobilized silk fibroin and col/SF:25/75 exhibited a uniform population of stretched and laterally extended interconnected network structures.

The proliferation of MSCs on materials has been assessed through cell viability and Live/Dead staining assays after 5 days of culture.

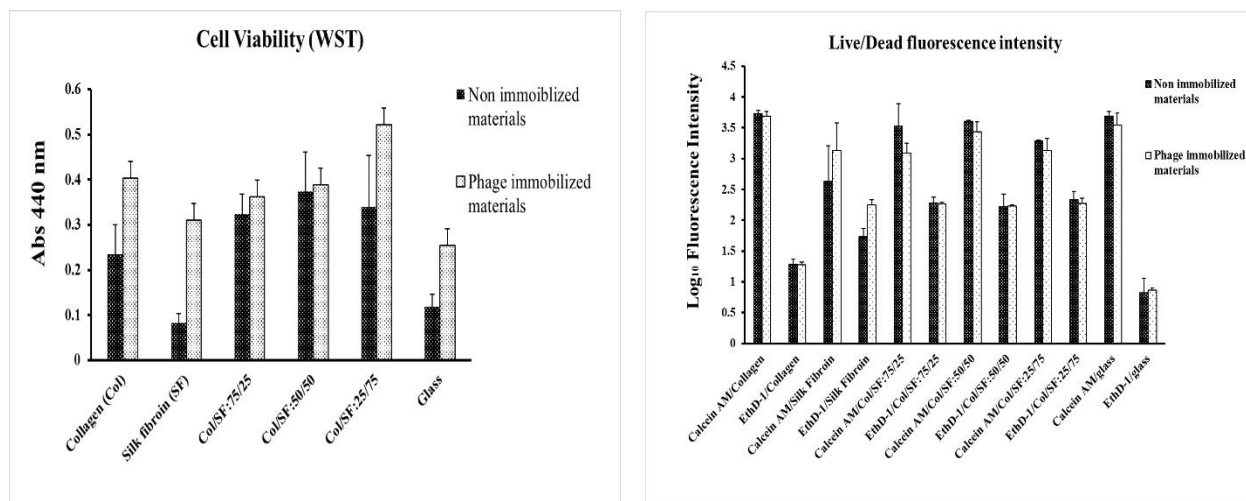


Fig 5.6: WST-1 and live/dead assays allowed to analyze the cell proliferation on the various materials

The results of live/dead tested cells showed the lowest fluorescence intensities for dead cells and highest amount for living cells on immobilized and non-immobilized collagen and glass coverslip surfaces. Higher amount of dead cells and lower difference between fluorescence intensities of living and dead cells were found for silk fibroin and mixtures, exhibiting the possible influence of silk fibroin on cell toxicity. Fluorescence intensity of live cells for phage-immobilized materials, except for silk fibroin, is lower than the corresponding non-immobilized materials, which could be due to the existence of small amount of divalent salt ions (Mg^{+2}). The possible remaining amount of divalent ions in T4 phage solution after dialysis, resulted in the quenching of fluorescence intensity of calcein AM, through complexes formation [20]. However, the fluorescence intensity of live cells increased for phage-immobilized silk fibroin, which could be due to the less intense effect of salt ions on complex formation with calcein AM.

In order to determine the cell proliferation trend on the materials, WST-1 method was applied. The results of cell viability assay (Figure 5.6) suggest an increased cell proliferation on all the phage-immobilized materials. However, the difference between cell proliferation on phage-immobilized and non-immobilized silk fibroin is the highest, showing the influence of phage on enhancement of MSC proliferation on silk fibroin. Moreover, phage-immobilized col/SF:25/75 presented the highest MSCs proliferation, suggesting this material as presenting the highest ability for MSC growth and proliferation.

5.4 Discussions:

Implant-associate infections present a substantial economic burden in healthcare systems, resulting in the need for a second surgical procedure [21]. Adhesion mechanism of pathogens to the surfaces is a complex procedure, influenced by different parameters such as substrate (hydrophobicity and charge), pH,

temperature, and surface charge of bacteria (under various conditions of pH and ionic strength) [22-24]. This present study introduces antibacterial silk-based coatings with the potential to reduce site infections.

Silk fibroin contains two major proteins with hydrophobic and hydrophilic regions. Moreover, silk fibroin has two types of structures, silk I, soluble in water with α -helix conformation and silk II, insoluble in water with β -sheet structure. The soluble silk fibroin in its solvent, becomes insoluble once casted and dried, due to the increasing of β -sheet structure. Furthermore, the random coil structure of silk fibroin in its soluble form, transforms to β -sheet upon gelation. Blending with other polymers in critical ratios, may change the structure of silk fibroin, enhancing its β -sheet formation [16] and having influence on bacterial cells adhesion and biofilm formation [25].

Bacterial adhesion and biofilm formation strongly depend on the substrate surface charge. High positive charges at the substrate enhance the negative bacterial attachment and biofilm growth. Rather than electrostatic interaction, the hydrophobic interaction between bacterial cells and a polymeric substrate has been identified as another important parameter in bacterial attachment and consequent biofilm formation. It has been revealed that moderate hydrophobicity and surface charge between -3 and +15 mV, could induce the microbial attachment and biofilm growth [25]. Hence, electrostatic and van der Waals strengths between substrate and bacterial cells should be analyzed to understand the reason behind biofilm formation on each substrate.

The hydrophobicity and surface charge have influence not only on bacterial growth, but also on phage stabilization and consequently surface bioactivity. It has been proved that surfaces with higher hydrophilicity may provide a mobile layer on which phage nanoparticles can move and re-align to interact with bacteria. Hence, the interaction of phage nanoparticles with negative and/or positive charges of amino acids existing in the hydrophilic domains of the substrates, may enhance the longevity of bioactive surfaces [26].

While drying phage solutions onto silk fibroin surfaces, water from phage solution penetrates inside the multiblock structure of silk fibroin (containing amorphous-crystalline block proteins [27]), acting as plasticizer through hydrogen bonding, and enhancing the mobility of amorphous and crystalline domains [28]. It has been proved that the components with molecular weight lower than that of silk fibroin tend to interact with beta-sheet domains of silk fibroin while the extent of immobilization depends on the strength of molecule and silk fibroin interactions [29]. Hence, phage nanoparticles may move between both amorphous and crystalline domains, establishing ionic bonds with the amino acid groups and being stabilized between chains after complete drying of the phage solutions, when the silk fibroin chains finally self-assemble with higher beta-sheet contents [27, 28]. After re-hydration while exposing to the bacterial medium, the silk fibroin chains move again and phage nanoparticles are exposed to planktonic cells.

Phage binding efficiency, rate of phage exposure to the bacterial culture and consequent phage-bacteria collisions and bacteria-surface interactions are the supposed parameters resulting to the extent of surface bioactivity. Rate of phage exposure to bacteria culture depends on the optimum amount of phage immobilized onto the surface in order to provide the highest bioactivity. Higher phage immobilization is desirable for higher bacterial capture, however, too high phage density onto the surface may cause phage inactivation through blockage of phage tails [30]. After initial inoculation of bacteria by immobilized phages, the produced progeny phages are released to the medium. The progeny phage-bacterial collisions happen at random Brownian motion and the adsorption rate increases with increasing both bacterial and phage concentrations [31]. These parameters should be analyzed, thoroughly, in order to form surfaces with higher bioactivity.

Cytotoxicity and MSCs morphology on the prepared bioactive surfaces were analyzed. Both collagen and silk fibroin support the actin stress and MSCs differentiation. However, surfaces with higher amount of collagen exhibited a highly elongated cellular network, while silk fibroin and mixtures with higher amount of silk fibroin represented a more laterally extended network. Moreover, phage immobilized materials showed higher cell proliferation than the non-immobilized ones, indicating the influence of immobilized phages on cell proliferation and growth. The lowest amount of cell viability as well as highest amount of dead cells for silk fibroin materials, indicate that silk fibroin alone has the lowest biocompatibility amongst all the tested materials.

5.5 Conclusion

In this study, silk fibroin, collagen and their mixtures with different ratios were successfully produced and immobilized by bacteriophages. The prepared phage-based materials exhibited an effective antibacterial activity against *E. coli*, through appearance of inhibition zones after 24 hours, as well as significant planktonic reduction compared to non-immobilized materials, within the first 12 hours. Phage progeny growth in the bacterial media was significant within 12 and 24 hours. The planktonic growth reached the highest level after 24 hours, which could be due to the sedimentation of bacteria dead bodies onto the surfaces after the initial 12 hours, resulting in biofilm formation within 24 hours. Phage immobilization enhanced MSCs growth and proliferation on all the samples, indicating that phage nanoparticles on the material surfaces increased their biocompatibility.

5.6 References

1. Nowakowska, J., et al., *Antimicrobial properties of 8-hydroxyserrulat-14-en-19-oic acid for treatment of implant-associated infections*. Antimicrob Agents Chemother, 2013. **57**(1): p. 333-42.
2. Zimmerli, W., A. Trampuz, and P.E. Ochsner, *Prosthetic-joint infections*. N Engl J Med, 2004. **351**(16): p. 1645-54.
3. Darouiche, R.O., *Device-associated infections: a macroproblem that starts with microadherence*. Clin Infect Dis, 2001. **33**(9): p. 1567-72.
4. Horan, R.L., et al., *In vitro degradation of silk fibroin*. Biomaterials, 2005. **26**(17): p. 3385-93.
5. Numata, K. and D.L. Kaplan, *Silk-based delivery systems of bioactive molecules*. Adv Drug Deliv Rev, 2010. **62**(15): p. 1497-508.
6. Jao, D., X. Mou, and X. Hu, *Tissue Regeneration: A Silk Road*. Journal of Functional Biomaterials, 2016. **7**(3): p. 22.
7. Cai, Z.-x., et al., *Fabrication of Chitosan/Silk Fibroin Composite Nanofibers for Wound-dressing Applications*. International Journal of Molecular Sciences, 2010. **11**(9): p. 3529-3539.
8. Bai, L., et al., *Surface modification and properties of Bombyx mori silk fibroin films by antimicrobial peptide*. Applied Surface Science, 2008. **254**(10): p. 2988-2995.
9. Fei, X., et al., *Green Synthesis of Silk Fibroin-Silver Nanoparticle Composites with Effective Antibacterial and Biofilm-Disrupting Properties*. Biomacromolecules, 2013. **14**(12): p. 4483-4488.
10. Kundu, J., et al., *Silk fibroin nanoparticles for cellular uptake and control release*. International Journal of Pharmaceutics, 2010. **388**(1-2): p. 242-250.
11. Lammel, A.S., et al., *Controlling silk fibroin particle features for drug delivery*. Biomaterials, 2010. **31**(16): p. 4583-91.
12. Wenk, E., et al., *Silk fibroin spheres as a platform for controlled drug delivery*. J Control Release, 2008. **132**(1): p. 26-34.
13. Srisuwan, Y., et al., *Preparation of Eri silk fibroin and gelatin blend film loaded chlorhexidine using as model for hydrophilic drug release*. Natural Science, 2012. **4**(7 (Jul 2012)): p. 454-460.
14. Zhang, Z., et al., *Electrophoretic deposition of tetracycline modified silk fibroin coatings for functionalization of titanium surfaces*. Applied Surface Science, 2014. **303**: p. 255-262.
15. Calamak, S., et al., *Ag/silk fibroin nanofibers: Effect of fibroin morphology on Ag⁺ release and antibacterial activity*. European Polymer Journal, 2015. **67**: p. 99-112.
16. Dyakonov, T., et al., *Design and Characterization of a Silk-Fibroin-Based Drug Delivery Platform Using Naproxen as a Model Drug*. Journal of Drug Delivery, 2012. **2012**: p. 10.
17. Bierbaum, S., et al., *Modification of Ti6AL4V surfaces using collagen I, III, and fibronectin. II. Influence on osteoblast responses*. J Biomed Mater Res A, 2003. **67**(2): p. 431-8.
18. Pearson, H.A., et al., *Phage-bacterium war on polymeric surfaces: can surface-anchored bacteriophages eliminate microbial infections?* Biomacromolecules, 2013. **14**(5): p. 1257-61.
19. Rajan, N., et al., *Preparation of ready-to-use, storable and reconstituted type I collagen from rat tail tendon for tissue engineering applications*. Nat Protoc, 2006. **1**(6): p. 2753-8.
20. *Indicators for Ca²⁺, Mg²⁺, Zn²⁺ and other metal ions*, in *Molecular Probes Handbook*. Life Technologies: New York.
21. Schierholz, J.M. and J. Beuth, *Implant infections: a haven for opportunistic bacteria*. J Hosp Infect, 2001. **49**(2): p. 87-93.
22. Simoes, L.C., M. Simoes, and M.J. Vieira, *Adhesion and biofilm formation on polystyrene by drinking water-isolated bacteria*. Antonie Van Leeuwenhoek, 2010. **98**(3): p. 317-29.
23. Donlan, R.M., *Biofilms: microbial life on surfaces*. Emerg Infect Dis, 2002. **8**(9): p. 881-90.
24. Palmer, J., S. Flint, and J. Brooks, *Bacterial cell attachment, the beginning of a biofilm*. J Ind Microbiol Biotechnol, 2007. **34**(9): p. 577-88.
25. Kaushik, S., et al., *Thin films of silk fibroin and its blend with chitosan strongly promote biofilm growth of Synechococcus sp. BDU 140432*. J Colloid Interface Sci, 2016. **479**: p. 251-9.

26. Khan MF, et al., *Low Discrimination of Charged Silica Particles at T4 Phage Surfaces*. Biosens J, 2015. **4**(125).
27. Hu, X., et al., *Microphase Separation Controlled β -Sheet Crystallization Kinetics in Fibrous Proteins*. Macromolecules, 2009. **42**(6): p. 2079-2087.
28. Hu, X., et al., *Regulation of silk material structure by temperature-controlled water vapor annealing*. Biomacromolecules, 2011. **12**(5): p. 1686-96.
29. Pritchard, E.M., et al., *Review physical and chemical aspects of stabilization of compounds in silk*. Biopolymers, 2012. **97**(6): p. 479-98.
30. Olsson, A.L.J., A. Wargenau, and N. Tufenkji, *Optimizing Bacteriophage Surface Densities for Bacterial Capture and Sensing in Quartz Crystal Microbalance with Dissipation Monitoring*. ACS Applied Materials & Interfaces, 2016. **8**(22): p. 13698-13706.
31. Lenski, R.E., *Dynamics of Interactions between Bacteria and Virulent Bacteriophage*, in *Advances in Microbial Ecology*, K.C. Marshall, Editor. 1988, Springer US: Boston, MA. p. 1-44.

6. Chapter Six

General conclusion and perspectives

The objective of this work was to develop a new antimicrobial coating for biomedical implants. The rising risk of infections following the implantation of biomedical implants, increases the necessity of antibacterial surfaces. However, the emergence of antibiotic resistant bacteria, as one of the biggest challenge in the healthcare system, have attracted the worldwide attention towards using bacteriophages.

Most of this work was done at INEB-Instituto Nacional de Engenharia Biomédica, Porto, Portugal. To acquire specialized techniques, I also worked in Brazil (UNICAMP, Campinas), Canada (McGill University) and Poland (Nicolaus Copernicus University, Toruń). Please refer to my CV.

Part 1

In the first part of the experimental work, the method for mixing two biomaterials of collagen and silk fibroin has been explained, considering the preservation of both biomaterials natural structures. I have analyzed methods for mixing two biomaterials of collagen and silk fibroin, with the aim of preserving the natural structures of both biomaterials. In this part:

- 1) The phase behavior of collagen/silk fibroin through viscosimetry analysis has been assessed. The boundary of miscibility/coacervate/precipitate of the mixtures was obtained through a ternary phase diagram.
- 2) The physicochemical properties of mixture have been assessed through circular dichroism (CD) for the mixture solutions and differential scanning calorimetry (DSC), Fourier transform infrared spectroscopy (FTIR), scanning electron microscopy and contact angle for the biocomposite films.

Results and conclusions part 1:

A basis for promising novel method has been developed in order to produce collagen/silk fibroin bio-composite film, to be used for a wide range of biopharmaceutical applications, from drug delivery to wound healing. Concretely, the following results was obtained:

1) obtaining a one-phase mixture before dialysis procedure through applying ternary solvent as the third component in the mixtures.

2) representing the influence of divalent calcium ions in ternary solvent on enhancement of ionic strength of the mixtures before dialysis. It has been demonstrated that the one phase mixtures can be acheived before dialysis and through applying ternary solvent as the third component in the mixtures, and the mixtures with different ratios have been obtained using ternary phase digram. The existance of divalent calcium ions in ternary solvent increases the ionic strength of the mixtures through enhancing the attraction forces between oppositely charged residues on the polymer chains. However, salt diffusion through dialysis procedure resulted to the coacervation or precipitation that could be due to the conformational changes of protein structures.

3) verifying the transition of random coil structure of silk fibroin to beta sheet formation through CD analysis for solutions after dialysis, and DSC and FTIR after film formation.

4) Representing the influence of silk fibroin beta sheet on tunable properties of bio-composite films by varying the blend ratios, and through SEM, contact angle and DSC assessment.

Part 2

Further investigations were focused on antibacterial properties of the mixture coatings. In this study, T4 bacteriophages have been used as the antibacterial agents and were applied to the surfaces through evaporation procedure. The drying procedure has been visualized through Darkfield enhanced optical microscopy (Cytoviva), through which phage nanoparticle movements have been tracked, the fluid motion and the final assembly patterns have been observed. A label-free technique to track phage nanoparticles in an aqueous solution, could be obtained, while the influence of parameters such as phage concentration or salt ions on phage motion or adsorption to the surface has been analyzed.

Results and conclusions part 2:

The results showed that evaporation as a simple and cost effective technique, could produce various features from phage nanoparticles onto the surface, that depends on the phage concentration and salt existance.

The outcomes revealed that tracking of phage nanoparticles through this study could provide insights for inferring the phage-based structures under various conditions.

Part 3

In the last part of this work, the antibacterial efficiency against *E. coli* with initial concentration of 10^7 CFU/ml and cytocompatibility of phage-immobilized surfaces using mesenchymal stem cells, were investigated.

Results and conclusions part 3:

- Non-immobilized substrates by themselves have shown planktonic growth for 12 and 24 hours of incubation, suggesting that the materials surfaces are prone to bacterial infections.
- The phage-immobilized substrates have shown promising results of inhibiting the planktonic growth within a specific period of time. Phage-immobilized substrates have shown to inhibit the planktonic growth within 12 hours, while after 24 hours, the planktonic proliferation increased for all the samples.
- The storage effect that has been assessed for the immobilized-materials have shown that only phage-immobilized collagen represented the antibacterial activity within 12 hours of inoculation, while all other substrates showed high amounts of planktonic growth after 12 and 24 hours, illustrating the instability of immobilized phages during storage. A possible hypothesis that may explain the stability of phage-immobilized collagen during storage, is the collagen swelling behaviour that could cause the phage encapsulation.
- The cytocompatibility assays through MSCs culture, showed increased cell proliferation on phage-immobilized materials. The highest difference level between immobilized and non-immobilized materials could be obtained for silk fibroin, showing the influence of phage on the enhancement of MSC proliferation.
- The cytoskeletal analysis of immobilized substrates, illustrates various cell morphology on each substrate, with more elongated morphology for phage-immobilized collagen.